**INTERIM REPORT**
PARTS I, II AND III
The Study of Space Communications Spread Spectrum Systems

REPORT 89-1

PREPARED FOR THE DEPARTMENT OF COMMUNICATIONS
UNDER DSS CONTRACT NO. 36001-8-3528/01-SS


Department of Electrical Engineering
Queen's University at Kingston
Kingston, Ontario, Canada

LKC
TK
5103.45
.S888
1989
c.2

**INTERIM REPORT**
PARTS I, II AND III
The Study of Space Communications Spread Spectrum Systems

REPORT 89-1

PREPARED FOR THE DEPARTMENT OF COMMUNICATIONS
UNDER DSS CONTRACT NO. 36001-8-3528/01-SS

Industry Canada
Library - Queen
MAR 18 2013
Industrie Canada
Bibliothèque - Queen

TK
5102.5
S488
1989
S-Gen

# SAW BASED JOINT GROUP

# DEMODULATION OF FSK AND DPSK SIGNALS

by

Peter McLane

Peter Traynor

INTERIM REPORT

PART I

DSS CONTRACT NO. 36001-8-3528/01-SS

Department of Electrical Engineering

Queen's University

Kingston, Ontario, Canada

March 27, 1989

TABLE OF CONTENTS

LIST OF FIGURES

SAW Based Joint Group Demodulation
of FSK and DPSK Signals
DSS Contract 36001-8-3528/01-SS

Interim Report
Part I

Peter McLane and Peter Traynor
Department of Electrical Engineering
Queen's University, Kingston, Ontario

## ABSTRACT

We present some aspects of the performance analysis of a SAW-based receiver that can jointly demodulate group FSK and DPSK signals. The DPSK demodulation is based on Fourier transforming a hop length DPSK signal which has synchronization advantages over a symbol based transform based demodulator in EHF Satcom systems. Since group based FSK demodulation by SAW devices is relatively well known the report concentrates on the DPSK section of the joint demodulation. We show that rectangular windows are best for the DPSK demodulator considered. However, adjacent channel interference and spectral domain truncation are two sources of significant performance degradation in the joint demodulation receiver. It is believed that this performance loss can be overcome by using bandwidth efficient modulations like CPFSK.

# SAW Based Joint Group Demodulation of FSK and DPSK Signals
DSS Contract 36001-8-3528/01-SS

Interim Report
Part II

Peter McLane and Peter Traynor
Department of Electrical Engineering
Queen's University, Kingston, Ontario

## 1. INTRODUCTION

A SAW based processor, capable of the joint group demodulation of FSK and PSK signals is proposed. FSK modulation will be used for low data rate (voice band), while PSK is used at a T1 data rate. A brief description of this processor is given. Earlier work on the contract [1] has considered windowing [2] in the group FSK demodulation of low data rate users. As well, experiments have been performed at CRC [3], that consider both inter-user interference and jamming. The processor is intended for possible application in the on-board demodulation of frequency dehopped signals in the Canadian EHF Satcom program. This program has reached an industrial phase and most proposals involve individual FSK and DPSK SAW based demodulation on-board the satellite. A key synchronization parameter for the EHF Satcom system is the rate of frequency hopping which we assume is of the order of 20 khops/sec. A group demodulator for joint detection of FSK and DPSK signals that requires only hop-length synchronization on-board the satellite has been presented by Felstead [4]. Note that the DPSK system, at medium data rate, is a slow hopping system.

The central theme of our study is a performance analysis of Felstead's joint demodulation system. The major goals are as follows:

(i) to determine the optimum window for the DPSK detection in the presence of Gaussian noise, inter-user interference, dehopping errors and timing offsets;

(ii) to provide a symbol timing strategy for the DPSK demodulation that works from the word synchronization provided by the hop synchronization system; and

(iii) to provide an approximate communication theory basis for the SAW based DPSK demodulator and from this to derive both M-C-M and C-M-C realizations of Felstead's joint FSK and DPSK SAW-based receiver.

Our study will concentrate on the DPSK aspects of the joint demodulation approach. This is because the FSK aspects have previously been treated in references [1-3].

Simulations of the DPSK demodulator have been performed with the intent of examining the effect of windowing on this branch of the demodulator (it has been shown [1],[2] that for practical FSK demodulation windowing of the transform is required). Simulated outputs are included, as are some conclusions regarding choice of optimum window for this demodulator. In addition, some C-M-C structures are presented that can cope with separate window functions in the FSK and PSK parts of the joint demodulator.

Our interim report will concentrate on certain aspects of Goals (i) and (iii) mentioned above. The communication theory model of SAW-based receivers will appear in Peter Traynor's M.Sc. thesis. To date, the work on this closely follows reference [8]. Regarding Goal (i) our model and software are in place to do an analysis of the bit-error-rate. This uses the basic theory of [5] and closely follows McLane's analysis [6] of windowed DPSK receivers where the satellite processor's integration time is on a symbol basis rather than a frequency hop time basis. Such an integration time puts severe constraints on the synchronization system of the overall EHF Satcom system, and is one of the reasons for considering Felstead's system for performance analysis.

## 2. DEMODULATOR STRUCTURE

Demodulation of the low data rate signals (M-ary FSK) is based on Fourier transform techniques. A Fourier transform (FT) is performed over the hop period of the signal ($T_H$= hop period in this case) and a decision based on the amplitude of the power spectrum is made. Medium data rate DPSK demodulation is performed on $\xi$-symbol length blocks of data where $\xi$ DPSK symbols occur per frequency hopping interval. The data is DPSK modulated and users are separated via FDMA on the uplink.

A block diagram of Felstead's [4] joint demodulator is presented in Figure 1. Note that joint FSK/DPSK demodulation is possible in the receiver structure in Figure 1. The FSK and DPSK signals are separated in frequency using FDMA. Thus the SAW-based FT will produce the FSK signals in time preceding the DPSK if the FSK signals occupy the higher frequency band. Thus the switch in Figure 1 is moved to A as the DPSK signals start to come out of the SAW-based Fourier transformer. To start the next hop interval the switch in Figure 1 is moved back to B to process the FSK signals.

In both cases a transform is performed over a time interval of length $T_H$. For DPSK this results in the Fourier spectrum of $\xi$-symbols, centred about each users carrier frequency and this is also shown in Figure 1. Assuming we have N DPSK users, this FT is separated into N time sections and is then inverse transformed to produce a version of the input DPSK data.

### 2.1 PROCESSOR STRUCTURE

A structure capable of performing the FSK and PSK demodulation is shown in Figure 2. It may be possible, however, to reduce the number of SAW devices by using equivalent configurations. The two expanders in Figure 2 must be ping-pong controlled and are required for a 100% duty cycle. In this respect the possibility of sharing SAW devices between a parallel group of demodulators in a multi-beam operation must also be considered. Note that individual window functions are possible in the FSK and DPSK portions of the receiver processor. This is important because, as this report demonstrates, the windowing requirements of the FSK and DPSK data are vastly different.

## 3. SYSTEM SIMULATION

Simulation of SAW FT devices has been performed using a FFT. That is, the continuous chirp FT performed by these devices has been modelled with a discrete Fourier Transform. A standard 2048 point FFT algorithm was used. Two types of discrepancy between the discrete FT and the SAW based FT can arise from this approximation. These discrepancies are:

1. Alaising errors occur due to the periodic extension of the input signal.

2. The finite number of samples in the FFT.

The effects of alaising are reduced to negligible levels by a sufficiently high sampling frequency. The second effect is also reduced by using a large number of samples.

## 3.1 SAW SIMULATION ASPECTS

Some assumptions were required to model the basic characteristics of the SAW devices. In particular, it was assumed that a 20 MHz bandwidth is available for the high data rate users. Since the forward transformation must sweep this entire bandwidth in a hop period ($T_H$), the choice of $T_H$ determines the dispersive slope of the SAW devices that are used. Here, $T_H$= 50 μsec is assumed, so this slope is μ = 400 KHz/μsec. A 2048 pt. FFT is used in our model, with a 40 MHz sampling frequency. Because only the positive portion of the FFT spectrum is considered as the SAW output, no significant alaising effects have been noted.

The bandwidth over which the inverse transform is performed depends on the frequency separation between carrier frequencies. In the simulation it is assumed that the inverse Fourier transform (IFT) is performed over the frequency range $f_{c_i} - \frac{\Delta f}{2} \leq f \leq f_{c_i} + \frac{\Delta f}{2}$ where Δf is the frequency separation of the carrier frequencies $f_{c_i}$ (i = 1,2).

By assuming 50 symbols/hop, the signalling period becomes 1μsec. A carrier separation of Δf = 5 MHz, thus, corresponds to a scaled separation of $\Delta f = \frac{5}{T}$, while Δf = 2 MHz corresponds to $\Delta f = \frac{2}{T}$. Note that Δf is also the bandwidth over which the IFT is performed and because the dispersive slope of the SAW's is the same for this transformation as it was in the forward case, each TDMA time slot will

be of duration $\frac{\Delta f}{\mu} = \tau$. Note, as well, that a 100% duty cycle over $T_H$ and $\tau$ are assumed for the FT and IFT processors, respectively.

## 3.2 SIMULATION RESULTS

A digital computer simulation program has been written to model the case of DBPSK for the receiver in Figure 1. That is, the FFT of one or two DBPSK signals, separated via FDMA, is computed. The individual transforms are then truncated in frequency and the inverse FFT is determined. Sources of error are then the truncation in the frequency domain and the presence of an interfering user.

We discuss a number of cases below. Later in section 4 we show how the average bit error rate can be computed from our simulation results through use of the basic mathematical theory in reference [5].

Figures 3(a) and 3(b) show the binary random signals used as input to the simulation. We have included a random 50 symbol sequence per hop period.

Figures 4(a), 4(b) and 4(c) illustrate 3 of the Kaiser-Bessel windows studied with varying $\alpha$ values which is the window parameter. The window in Figure 4(c) represents the most severe window.

Figures 5(a) and 5(b) show, respectively, the FFT output and IFT output for a two user system with $\Delta f = \frac{5}{T}$ and one of the users idle (that is there is no ACI).

It is worth making note of the time scales at this point. In Figures 1 and 2, the time scales are given as fractions of the hop period $T_H$. In Figures such as 3(a), where the FFT output is given, only the first half (0, 0.5) of this is considered as part of the SAW processor output. So the interval 0 to 0.5 represents $T_H$, and since $\mu T_H$ = 20 MHz, this same interval represents the bandwidth available to the data rate users. The time scale on the TDMA outputs is given as a fraction of $\tau = \frac{\Delta f}{\mu}$.

Note from Figure 5 that even with no interfering user present, the time-division multiplexed output is not an absolute replica of the original sequence. The ripple which is present at each discontinuity is known as Gibbs phenomena and is a result of truncating (time gating) the transformation to $\left[-\frac{\Delta f}{2}, + \frac{\Delta f}{2}\right]$ before the IFT operation. This ripple will be smoothed by the integrator in the integrate and dump DBPSK receiver but it may have an impact on performance. Also truncation of the frequency processing interval for the inverse FFT will result in a loss of signal energy.

Figures 6(a) and 6(b) represent the situation when both users are active and the frequency separation between users is 5/T. Upon comparison with Figure 5(a) and 5(b) we conclude that ACI is very small for the 5/T frequency separation.

Figures 7(a) and 7(b) represent the time domain signal for user one and the ACI it generates in user two's time slot. The frequency separation is 2/T, the frequency separation that was used in [7] and studied in [6]. Note that considerable pulse distortion exists. This is due to the fact that approximately 7/T Hz is required to represent 99% of the energy in a DBPSK signal [9]. Truncating the frequency function to 2/T represents a loss in energy of the DBPSK input signal. It appears that a frequency separation of 2/T will result in a 1 to 2 dB loss in error performance. This is because approximately 80% of the signal energy is confirmed to the [-2/T,2/T] Hz frequency interval with DBPSK signals having rectangular pulse shaping. Use of CPFSK signals [10] represent smoother phase modulated signals where a large percentage of the signal energy is confirmed to [-2/T, 2/T] Hz and these signals will perhaps give improved performance. This improvement is unknown at this time as CPFSK signals can have modest performance in differential detection receivers [10].

The spectral result for two users separated by 2/T Hz is given in Figure 8(a). Figure 8(b) represents the time domain output for two equal power users separated by 2/T Hz but with use of the window in Figure 4(a) ($\alpha$ = .25). Figure 8(c) is for almost the same situation as now the interfering user is 9dB more powerful than the reference user. Figure 9 shows the same situations as Figure 8 but now the window in

Figure 4(c) ($\alpha$ = 1.0) is used. Note that this window severely distorts the first 10 and last 10 bits of the 50 bit sequence.

From these illustrations it seems that windowing does not have a significant effect on ACI. To elaborate on this point compare the ACI present in figure 10(b) with that shown in figure 7(b). Figure 10 presents the reference plus equal power interference signal for the $\alpha$ = 1 window. Note that the only effect the windowing has had on the ACI is to create the same envelope that would exist over the signal. However, it is clear from Figure 8 that ACI is a problem for the 2/T frequency separation. We note that [9] use of a CPFSK signal will result in a more compact power spectrum than for a DBPSK signal and thus should lessen the ACI problem that is clear from Figure 8.

Mathematically, the fact that hop length windowing is not effective in suppressing ACI may be explained as follows. The Fourier transform of the windowed signal is

$$F.T.\{w(t)f(t)\} = F.T.\{w(t)\} * F.T.\{f(t)\} \qquad (1)$$

where

w(t) is the windowing function

f(t) is a waveform of $\xi$=50 binary symbols

* implies convolution.

The $F.T.\{f(t)\}$ has the same spectral characteristics of a fast hopped PCM spread spectrum signal. In particular, because a rectangular waveform was used, nulls will occur in the spectrum at intervals of $\frac{1}{T}$, where $\frac{1}{T}$ is the symbol rate. In contrast, $F.T.\{w(t)\}$ will have its first null at $\frac{1}{50T}$ for a rectangular window. The Fourier transforms of a rectangular and $\alpha$ = 1.0 Kaiser-Bessel window are shown in figures 11(a) and 11(b). Because of the relatively narrow width of these transformed windows, they act as impulse function relative to F(f). Equation (1), then, can be re-written as

$$F.T.\{w(t)\} * F.T.\{f(t)\} \approx \delta(t) * F.T.\{f(t)\}$$
$$= F.T.\{f(t)\} = F(f).$$

From this analysis it seems that the rectangular windows will be optimum. All other windows yield an SNR penalty with no ACI reduction.

## 4. BIT ERROR RATE ANALYSIS

To set the scene for the error analysis consider the integrator output for one of the ideal pulses in Figure 3(a). Let the constant integrator output voltage be x and assume the $E_b/N_0$ ratio is $\rho$. Next the integrator outputs for the 50 pulses in Figure 5b will be computed and their loss or gain relative to x will be determined. The relative value will be denoted by $\lambda_i$, i = 1, ..., 50. We then perturb $\rho$ by $\lambda_i^2$ to get 50 values of $\rho_i$. The bit error rule formula for DBPSK will depend on only the pair $(\rho_i, \rho_{i+1})$, i = 1, 2, ..., 49. As such 49 bit error rate values can be computed. Then the 49 values can be averaged to then give the average bit error rate. In addition, dehopping offsets and timing offsets will introduce phase effects and such can also be treated using the theory from [5].

## 5. CONCLUSION AND FUTURE STUDIES

Based on our interim studies we have two major conclusions:

(i) Windowing on a hop basis is not effective in slow hopped systems, including the present DBPSK, medium data rate system.

(ii) For a user frequency spacing of 2/T Hz, where T is the symbol interval, use of DPSK with rectangular pulse shapes will lead to a 1 to 2 dB performance loss due to the truncation of the received signal spectrum. Signals with improved spectral concentration of energy should have improved performance. This is a form of providing windowing but in the transmitter rather than the receiver.

(iii) ACI is a problem for a 2/T frequency separation between users that is not solved through hop length windowing; signals with

improved spectral concentration can also provide a solution to this ACI problem

Our future work will consider:

(i) the computation of the average bit error rate for the interesting situations presented herein and for DQPSK modulation;

(ii) the consideration of using pulse shaping in the transmitter for medium data rate signals to hopefully improve performance;

(iii) the development of a symbol timing strategy that use the accurate frequency hop timing signals that are available in the EHF Satcom System; and

(iv) the further development of a simple SAW communication theory model with the purpose of developing both C-M-C and M-C-M realizations of the joint FSK/DPSK Felstead receiver for later laboratory experiments.

REFERENCES

[1] Patrick Ma, "On Frequency Offsets in Windowed Reception of Frequency Dehopped M-ary FSK Signals for Multi-user Systems", Proceedings MILCOM'84, Los Angeles, Ca., October 1984.

[2] L.S. Metzger, D.M. Boroson, J.J. Urhan, "Receiver Windowing for FDM MFSK Signals", IEEE Trans. Comm., vol. COM-27, pp. 1519-1526, Oct. 1979.

[3] E.B. Felstead, J.L. Pearce and D.L. Selin, "A Saw-Based Demodulator for Multi-User Dehopped M-Ary FSK Signals", CRC Report 1392, Communications Reseph Centre, Dept. of Communications, Ottawa, Ont., June 1985.

[4] E.B. Felstead, "Synchronization and Processing of Uplink Higher Data Rate Signals for Canadian EHF Milsatcom Concept", Private Communication.

[5] R.F. Pawula, S.O. Rice and J.H. Roberts, "Distribution of the Phase Angle Between Two Vectors Perturbed by Gaussion Noise", IEEE Trans. on Comm., Vol. COM-30, pp. 1828-1841, Aug. 1982.

[6] P.J. McLane, "Performance of Windowed Reception for D-QPSK in Multi-User Systems", Report, DSS Contract 0ST85-00190, April 2, 1986.

[7] DSS file 065T-36001-4-1868. Comdev Report "Spacecraft Signal Processor Broadband Unit, Final Report".

[8] M. Jack, P. Grant, J. Collins, "The Theory, Design, and Applications of Surface Acoustic Wave Fourier-Transform Processors". Proceedings of the IEEE, vol. 68, No. 4, pp. 450-468, April 1980.

[9] F. Amoroso, "The Bandwidth of Digital Data Signals", IEEE Communications Magazine, Vol. 18, No. 6, pp. 13-24, November 1980.

[10] G.B. Boudreau and P.J. McLane, "Differential Detection of Duobinary CPFSK", IEEE Trans. Comm., Vol. COM-35, pp. 181-184, Feb. 1987.

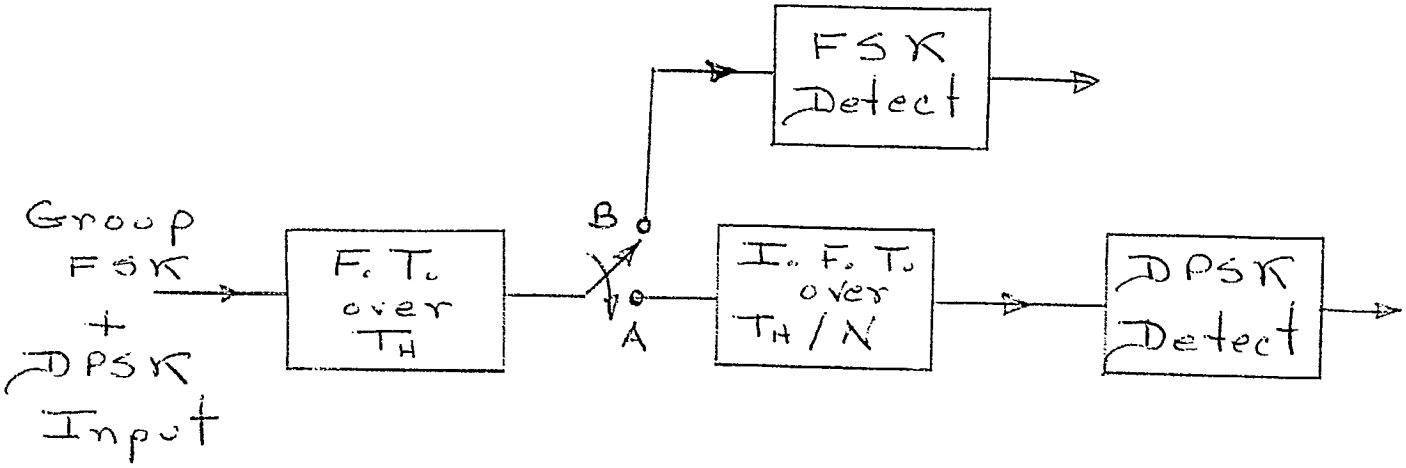


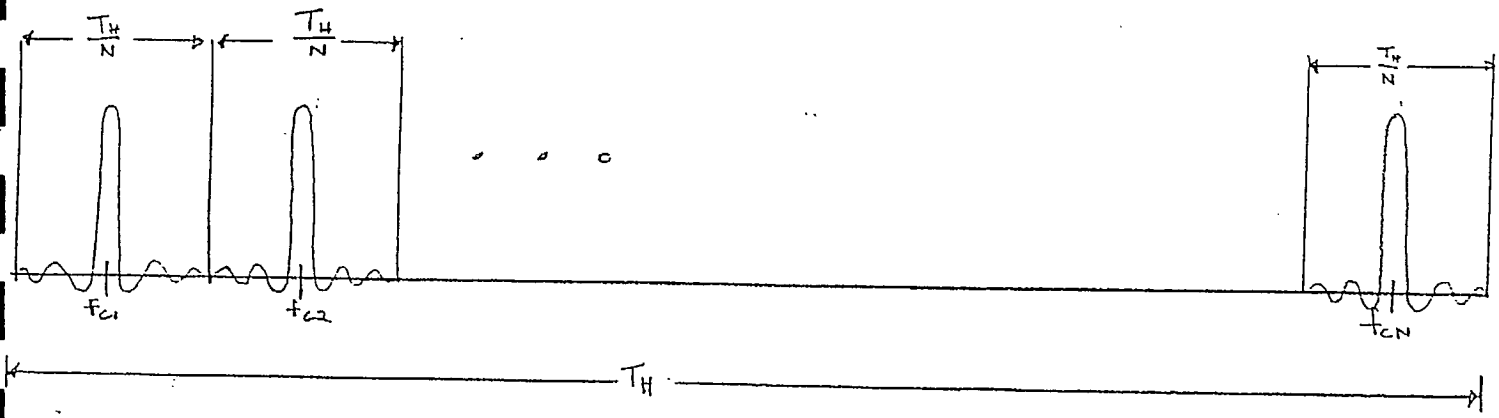


Figure 1:(a) Felstead's joint SAW-based FSK and DPSK receiver.

(b) The DPSK signal spectrum at point A.

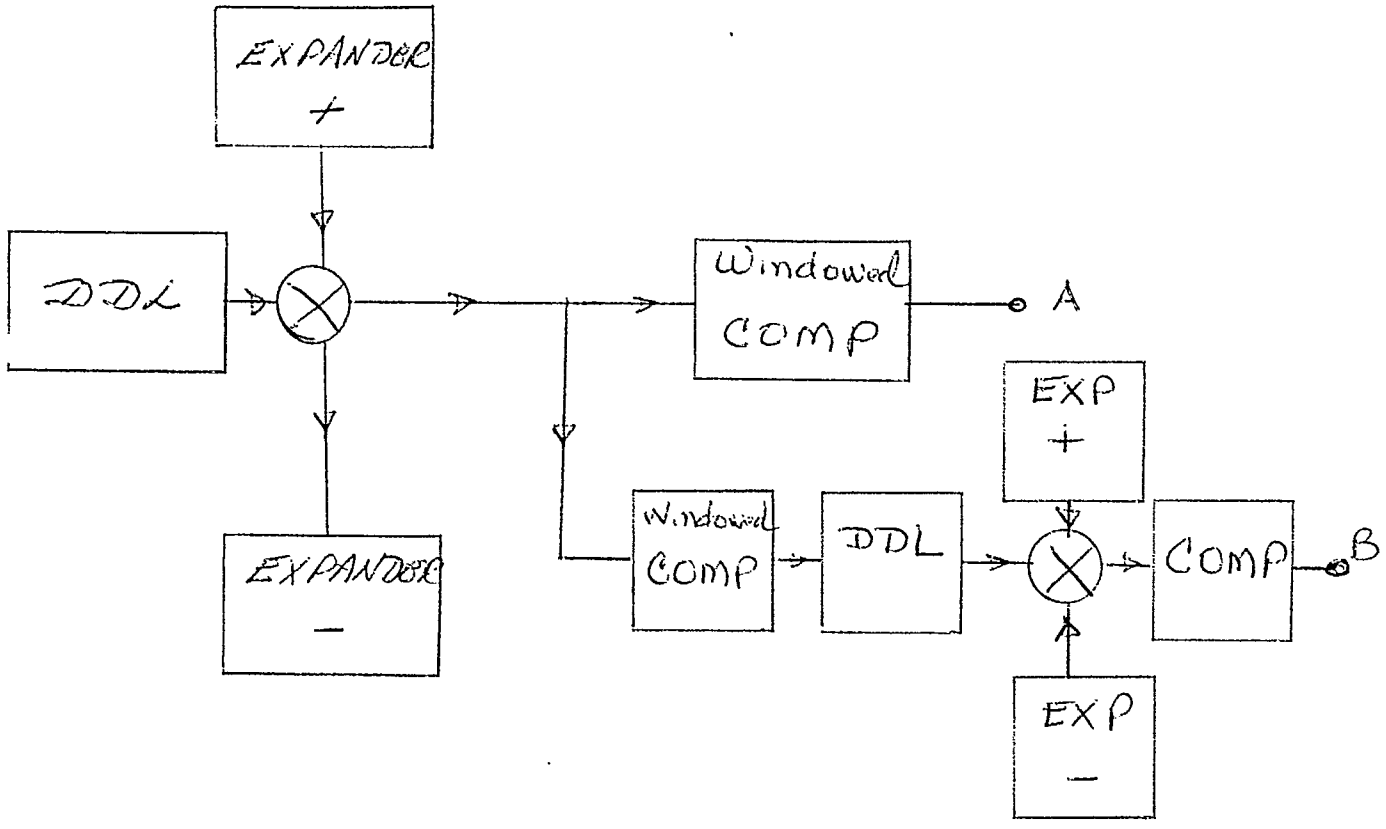


DDL = Dispersive Delay Line
COMP = Compressor
EX = Expander
A = To FSK Detector
B = To DPSK Detector

Figure 2: A Saw-based realization with separate FSK and DPSK window operations for the receiver of Fig. 1.

Figure 3 (a) 50 bit input sequence for the reference user
(b) 50 bit input sequence for the interfering user

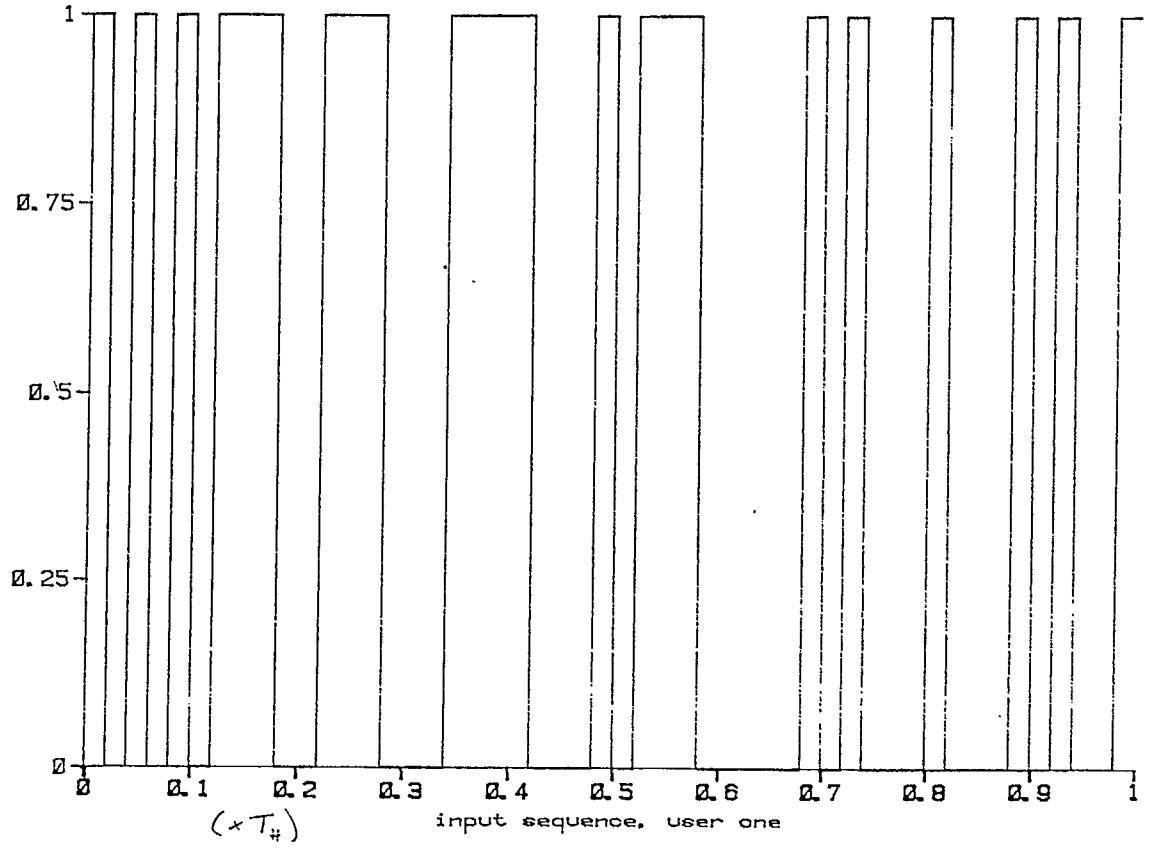


3a

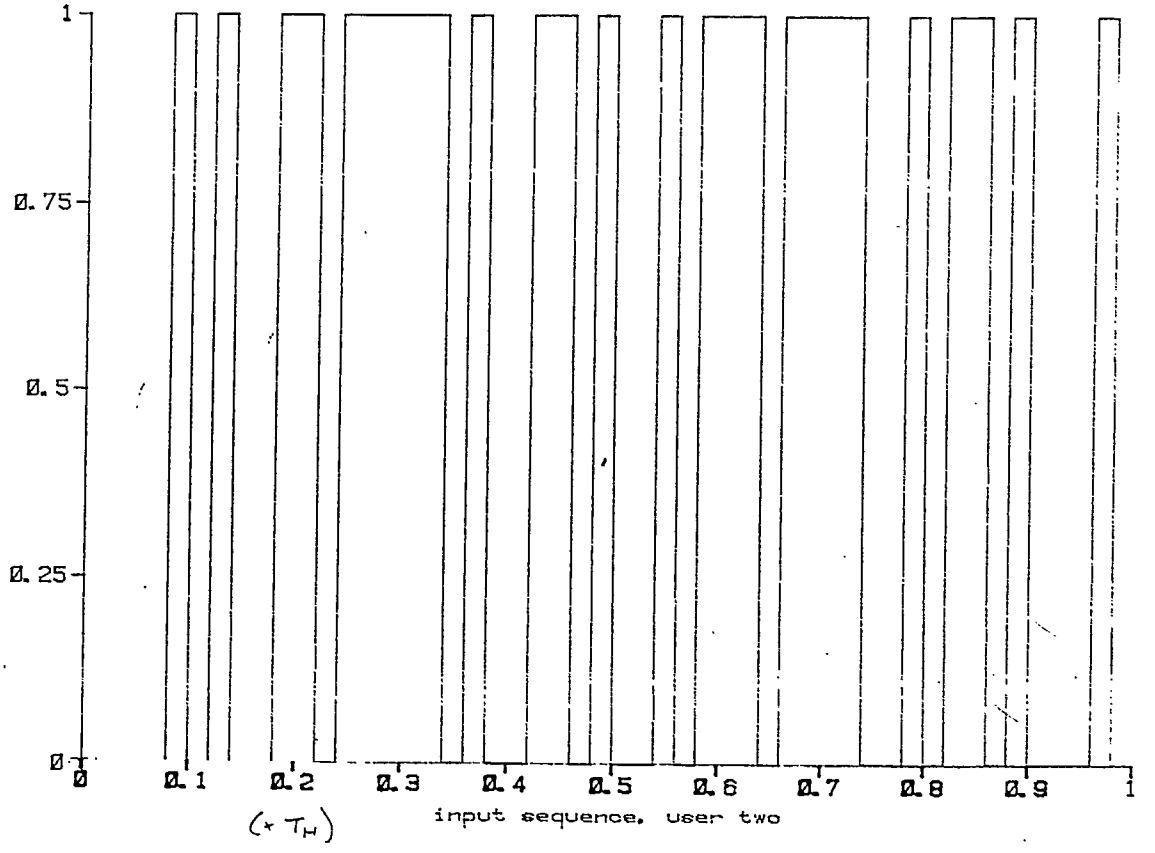


3b

14

4a

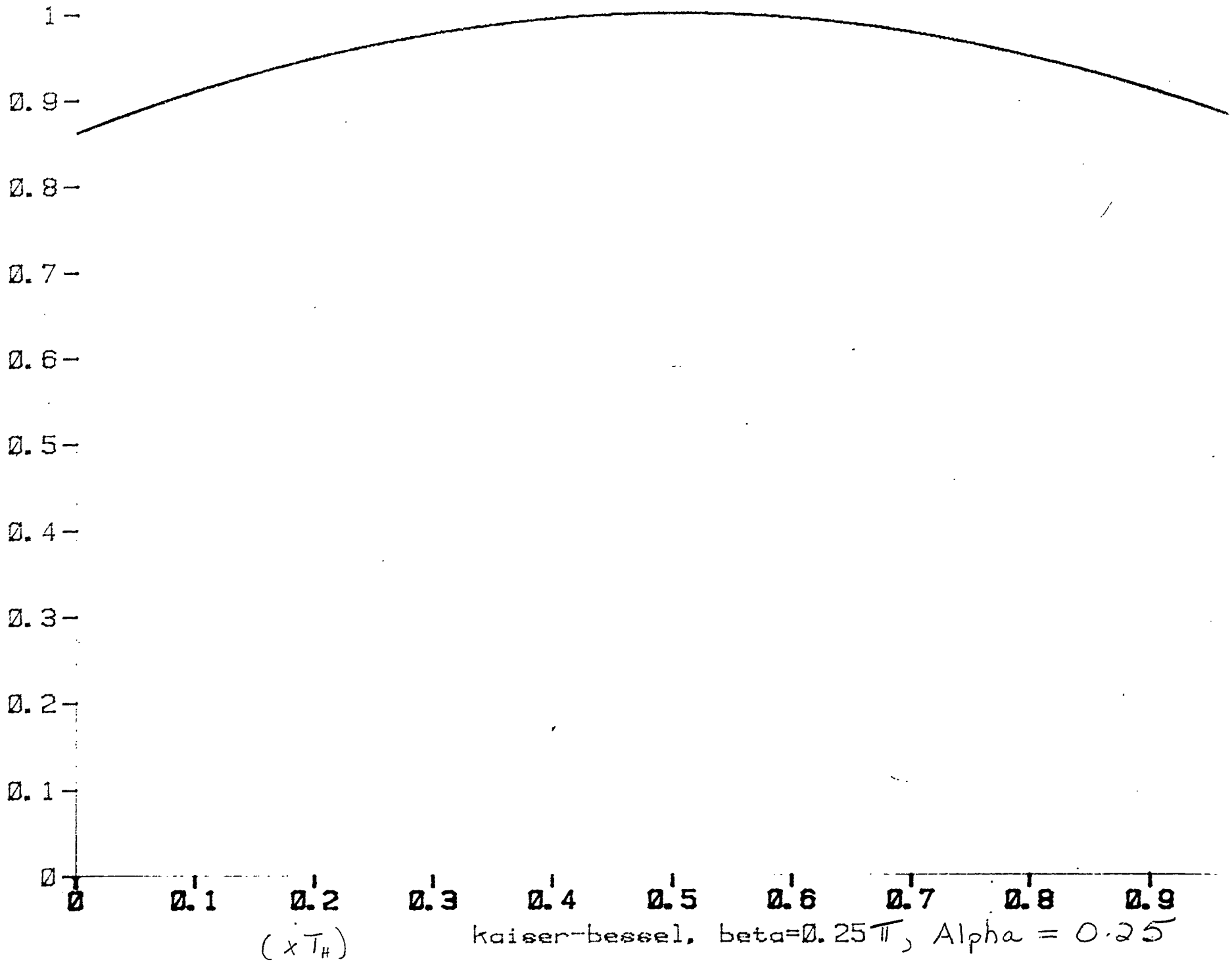
1
0.9
0.8
0.7
0.6
0.5
0.4
0.3
0.2
0.1
0
0
0.1
0.2
0.3
0.4
0.5
0.6
0.7
0.8
0.9
(x T_H)
kaiser-bessel, beta=0.25π, Alpha = 0.25

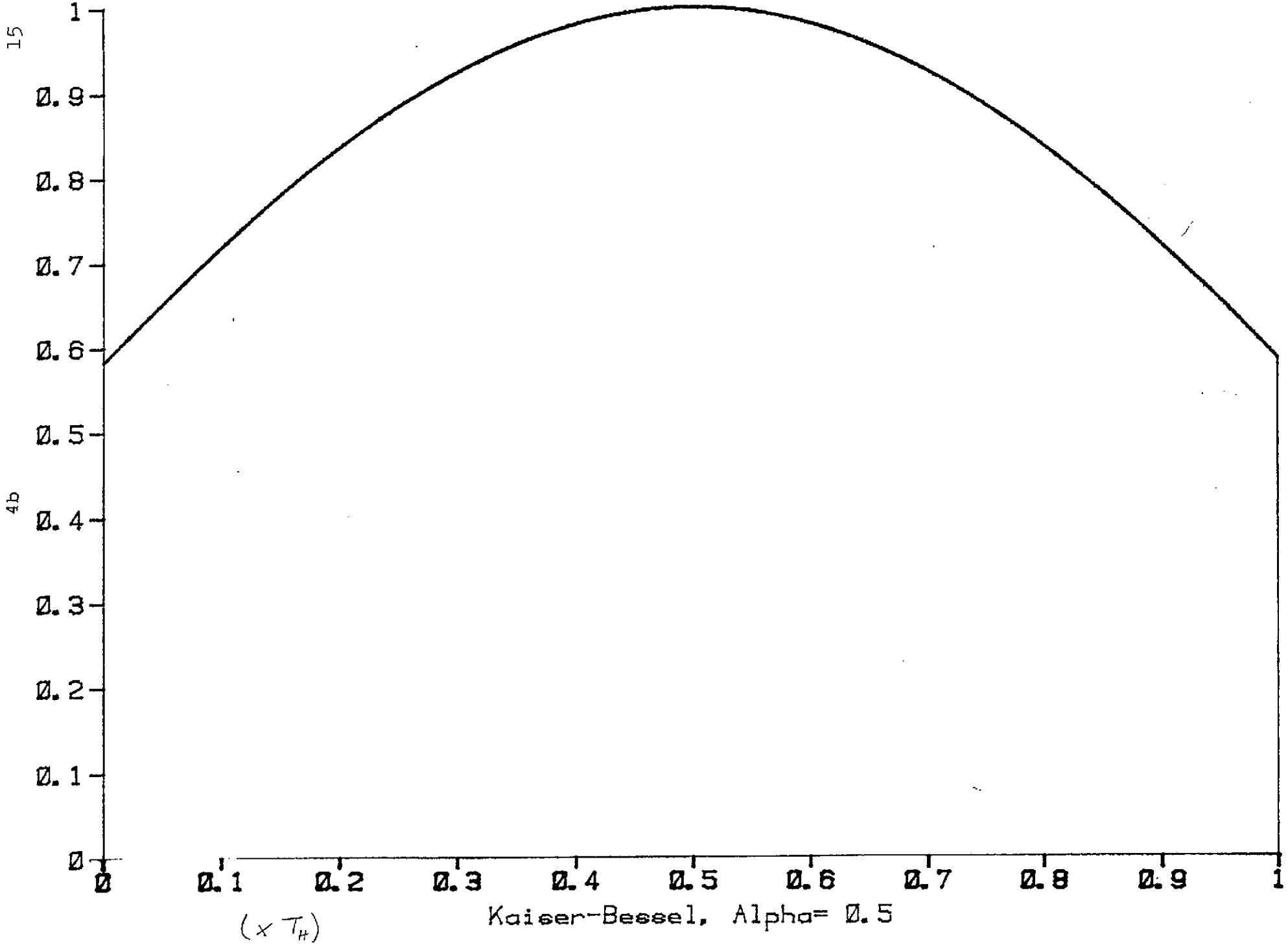
15
1
0.9
0.8
0.7
0.6
0.5
4b
0.4
0.3
0.2
0.1
0
0
0.1
0.2
0.3
0.4
0.5
0.6
0.7
0.8
0.9
1
(x $T_H$)
Kaiser-Bessel, Alpha= 0.5

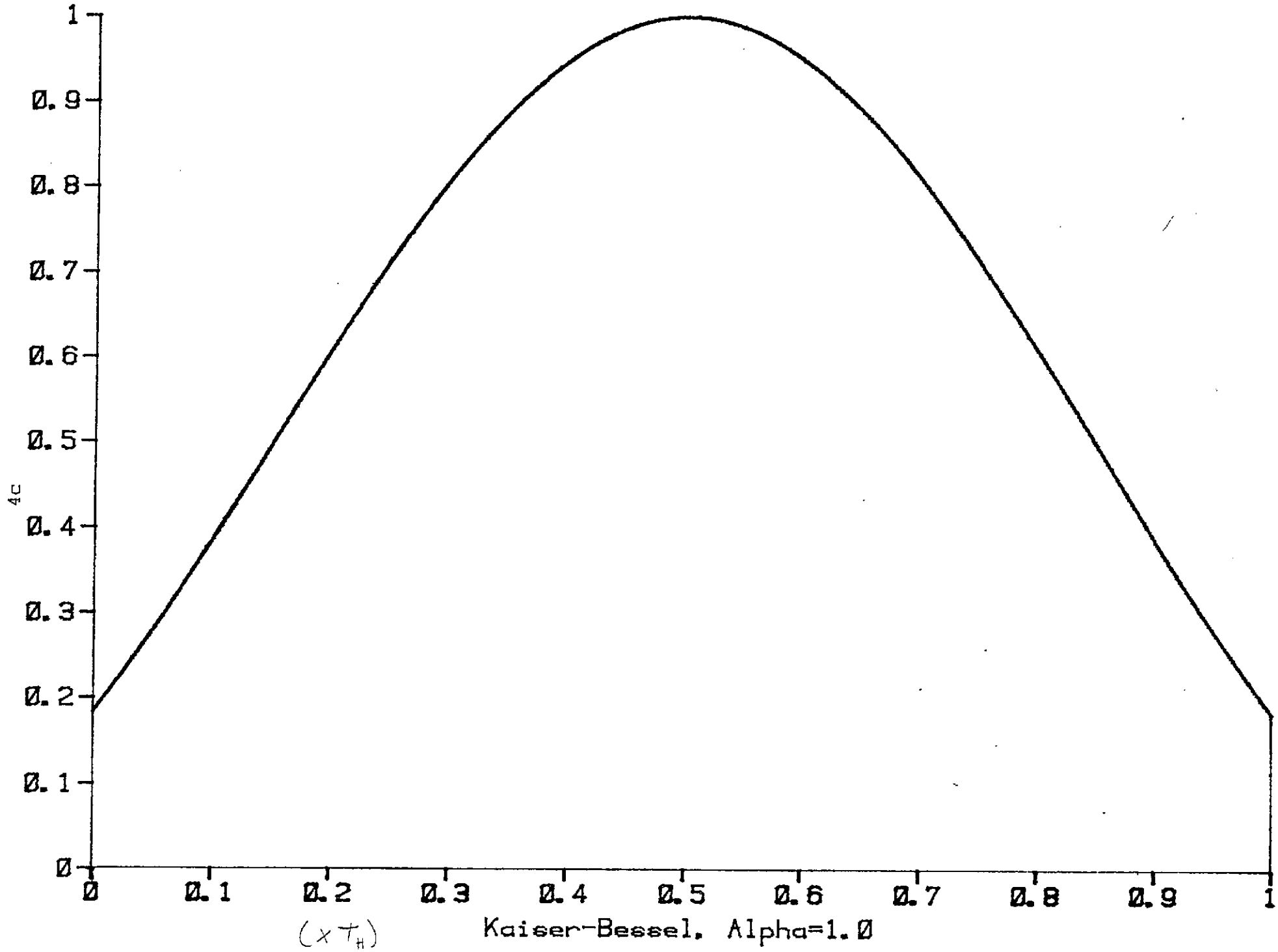
1
0.9
0.8
0.7
0.6
0.5
0.4
0.3
0.2
0.1
0
4c
0
0.1
0.2
0.3
0.4
0.5
0.6
0.7
0.8
0.9
1
(x T_H)
Kaiser-Bessel, Alpha=1.0

Figure 5: Spectral and time output from the computer simulation for no interfering user

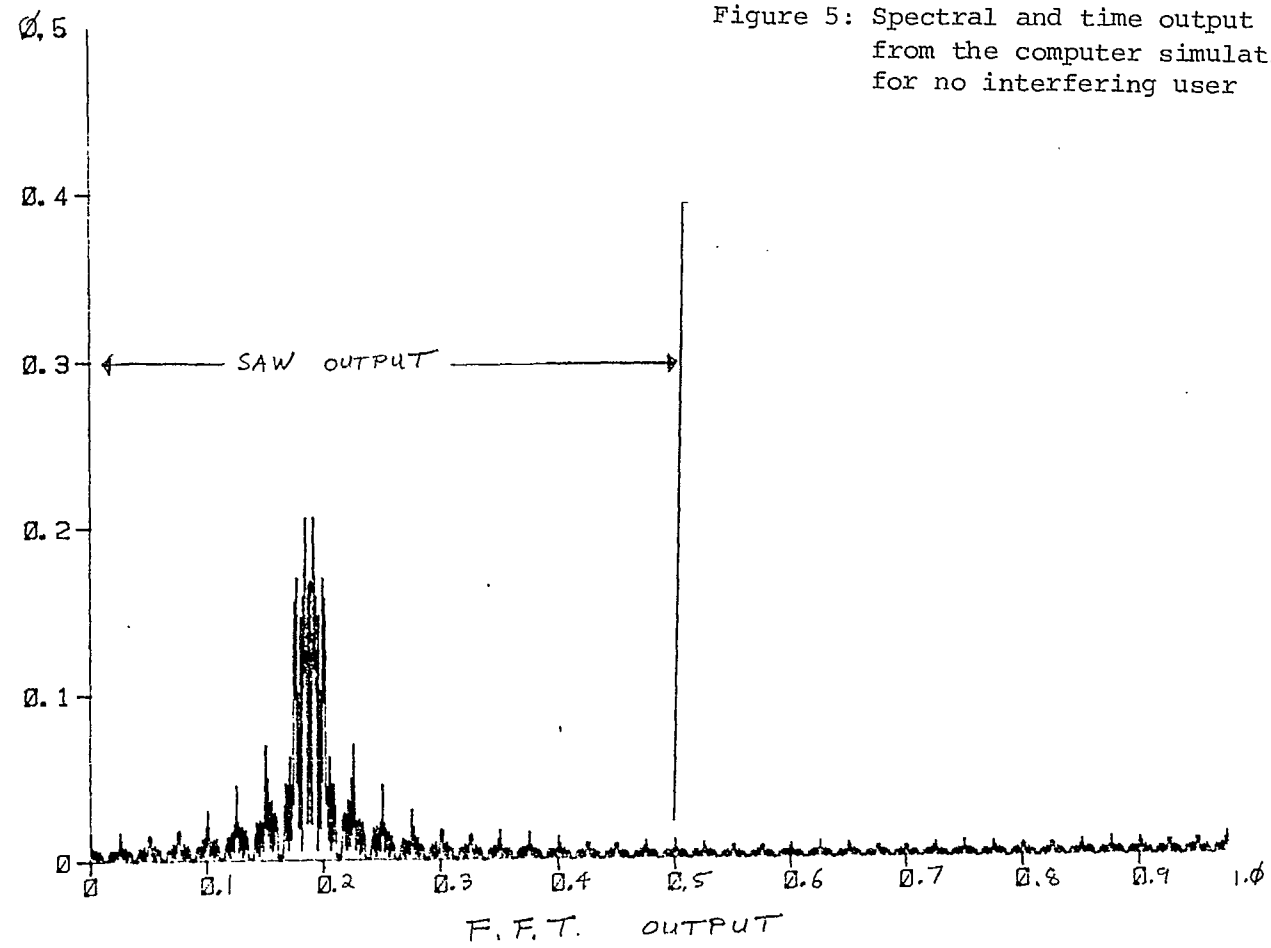


5a

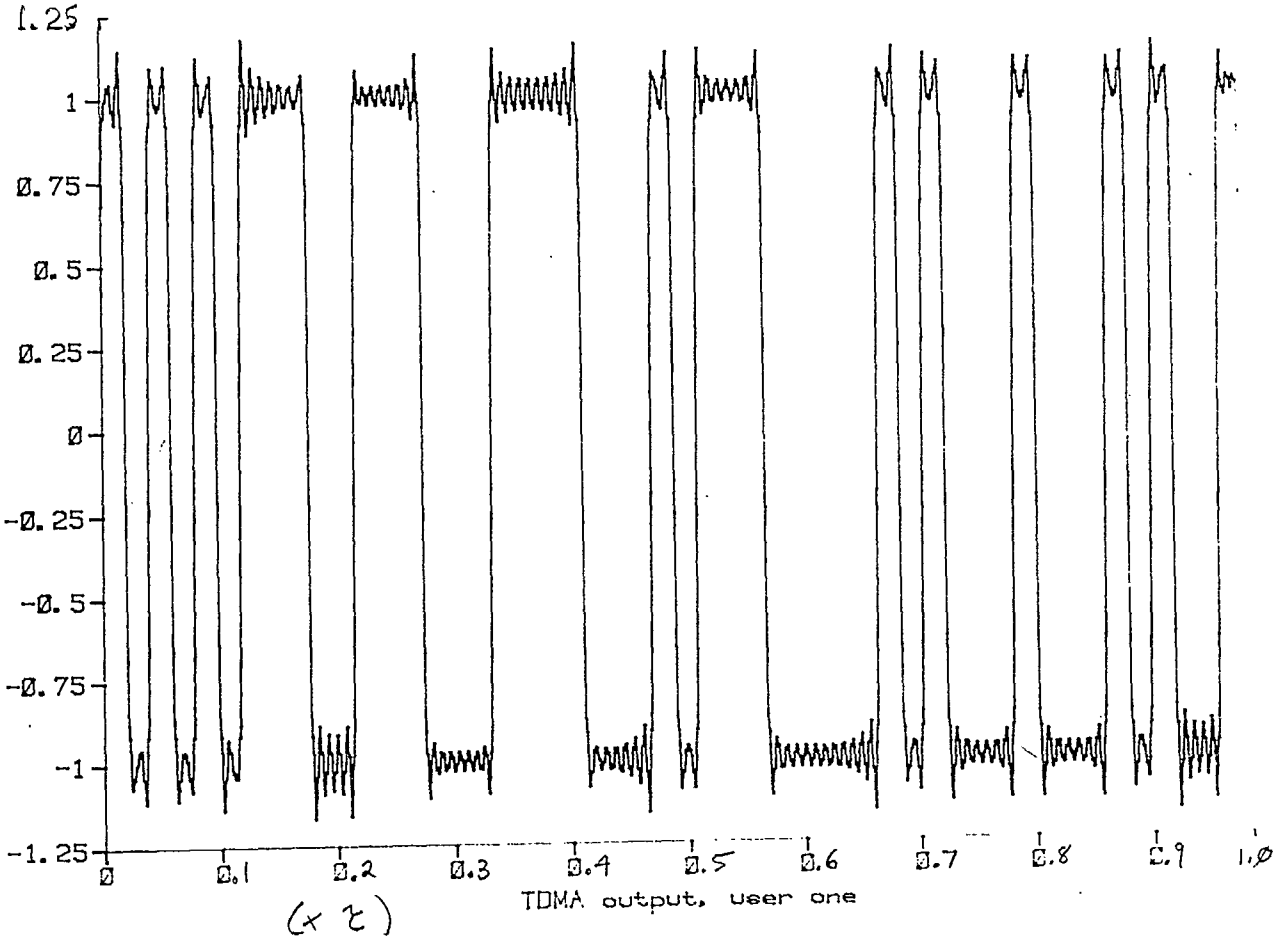


5b

Figure 6: Spectral and time output for two users with a frequency separation of 5/T

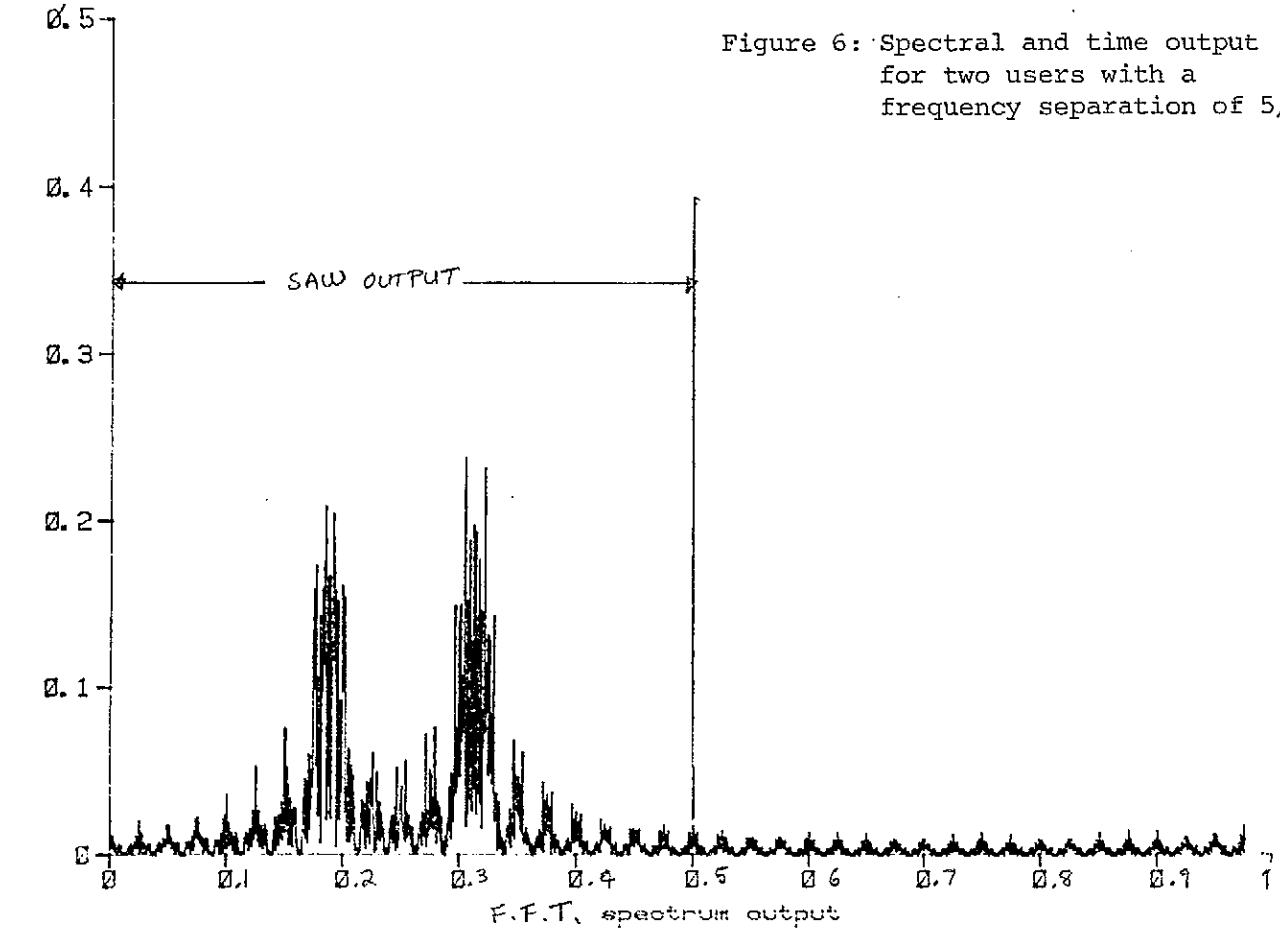


6a

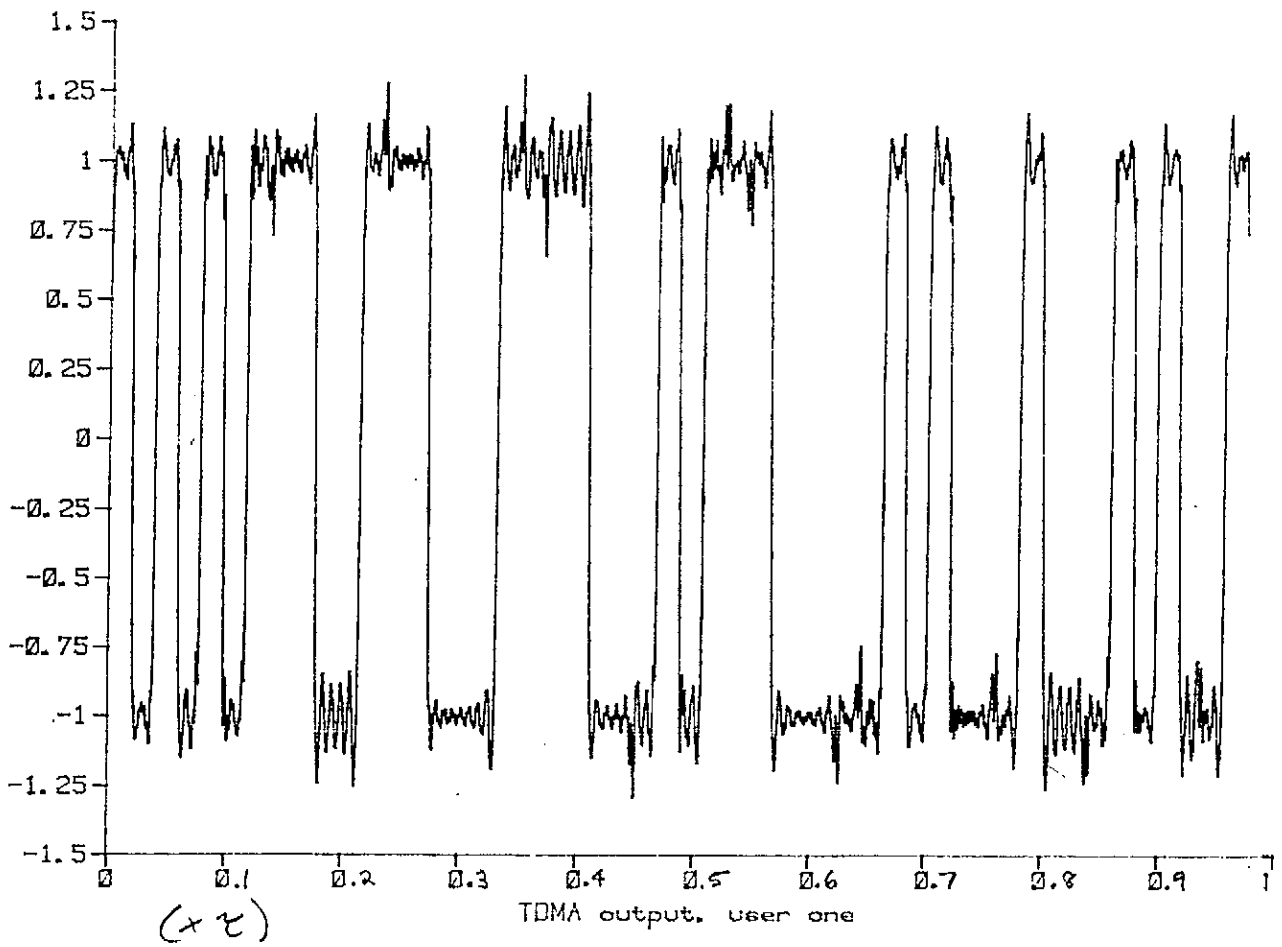


6b

Figure 7: Reference and interfering user time domain outputs for a frequency separation of 2/T

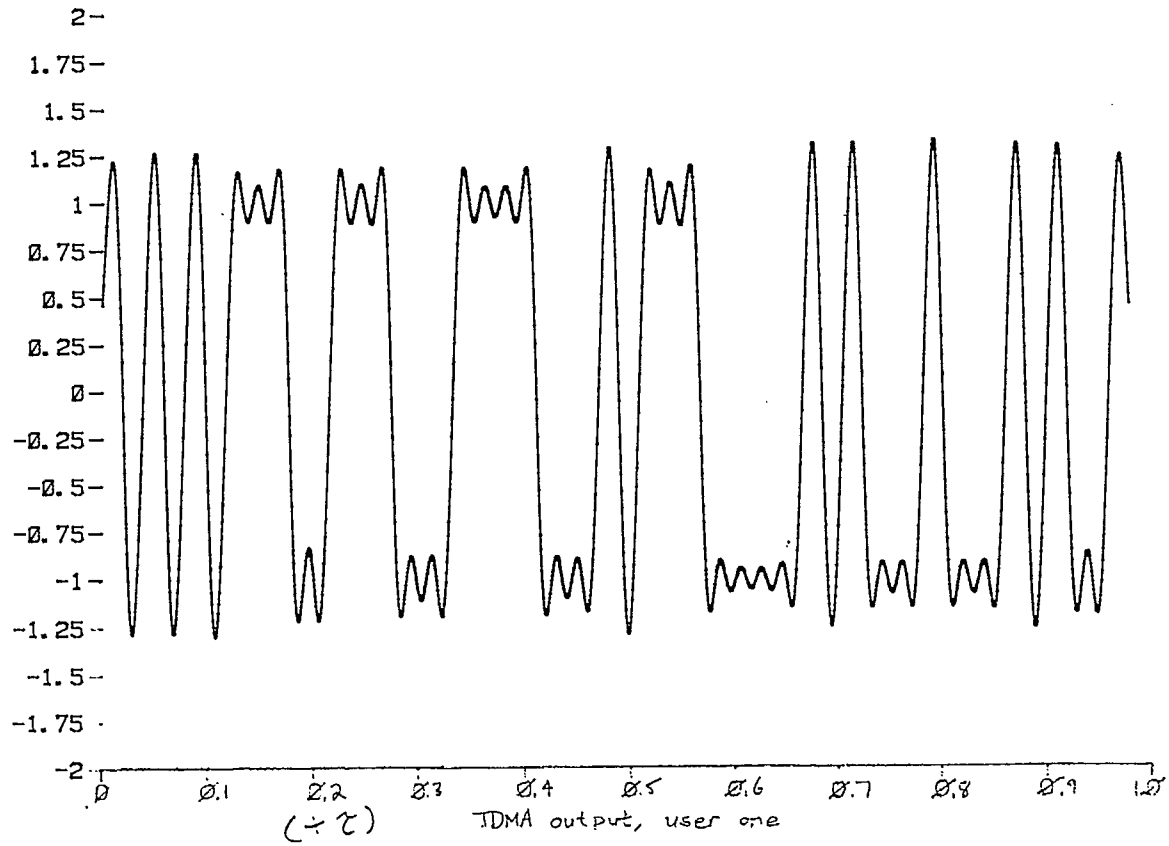


7a

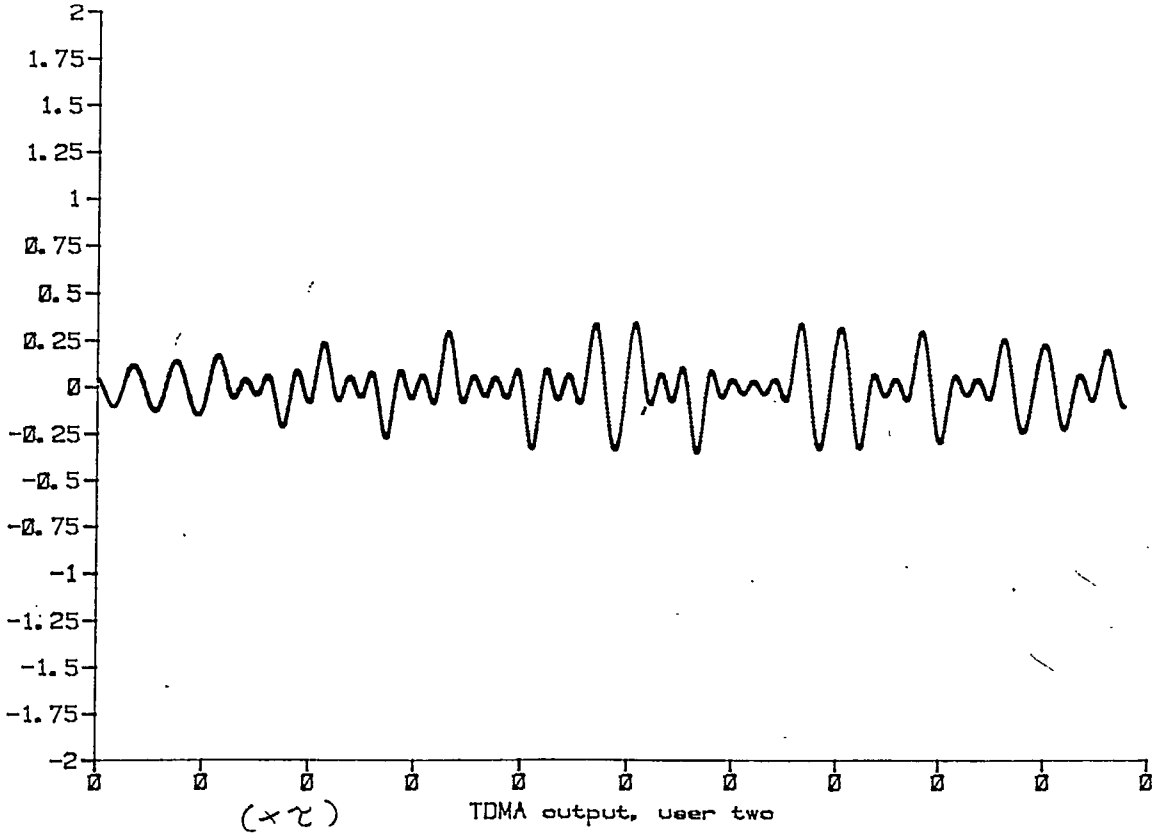


7b

Figure 8 (a) Spectral output for two users with $\Delta f = 2/T$

(b) Time domain output for the case in (a) but the window of Fig. 4(a) is applied

(c) The case for (b) but now the interfering user is 9dB more powerful than the reference user

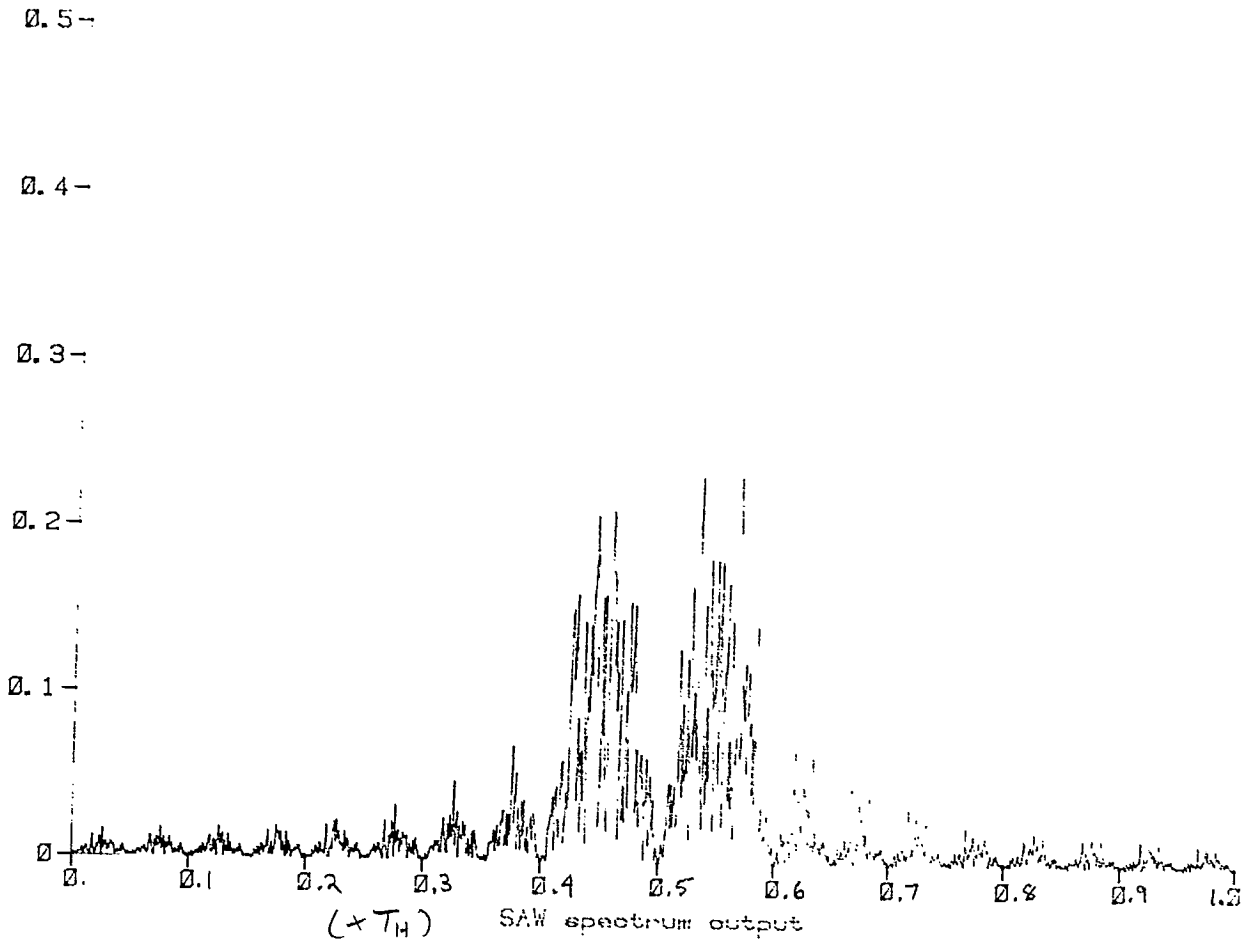

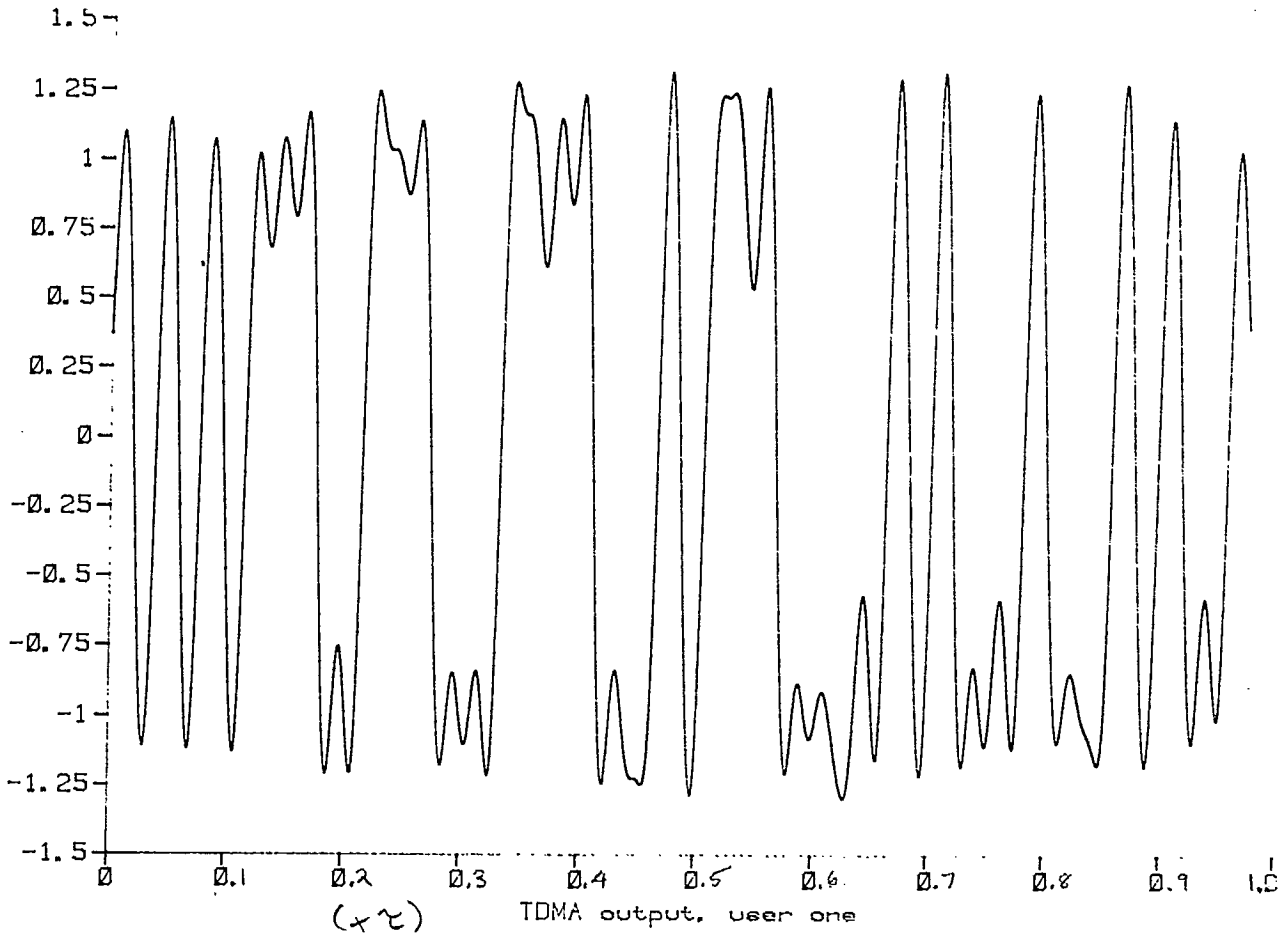
1.5
1.25
1
Ø.75
Ø.5
Ø.25
Ø
-Ø.25
-Ø.5
-Ø.75
-1
-1.25
-1.5
Ø
Ø.1
Ø.2
Ø.3
Ø.4
Ø.5
Ø.6
Ø.7
Ø.8
Ø.9
1.Ø
(×τ)
TDMA output, user one

8b

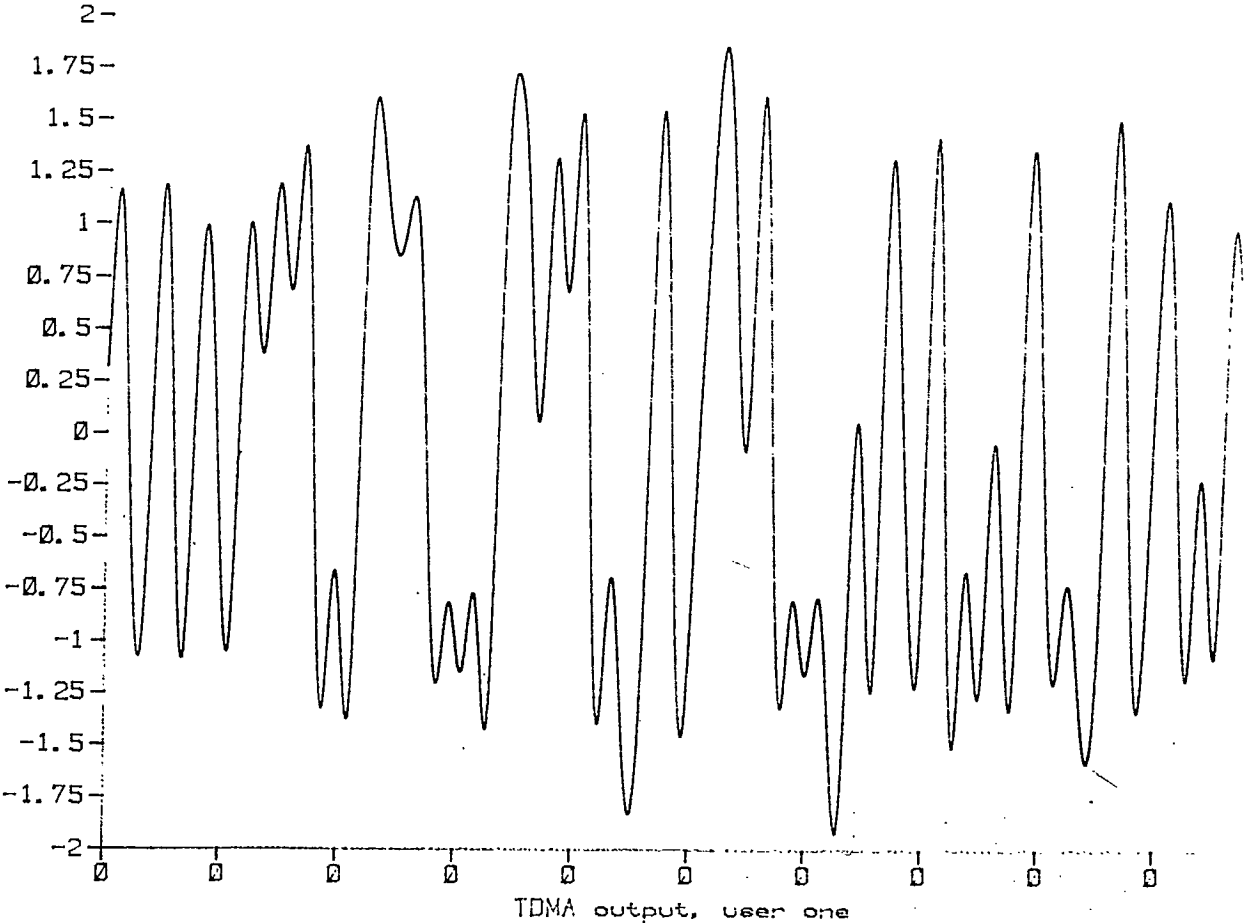
2
1.75
1.5
1.25
1
Ø.75
Ø.5
Ø.25
Ø
-Ø.25
-Ø.5
-Ø.75
-1
-1.25
-1.5
-1.75
-2
TDMA output, user one

8c

Figure 9: The situation of Fig. 8 but now the window of Fig. 4(c) ($\alpha = 1.0$) is used

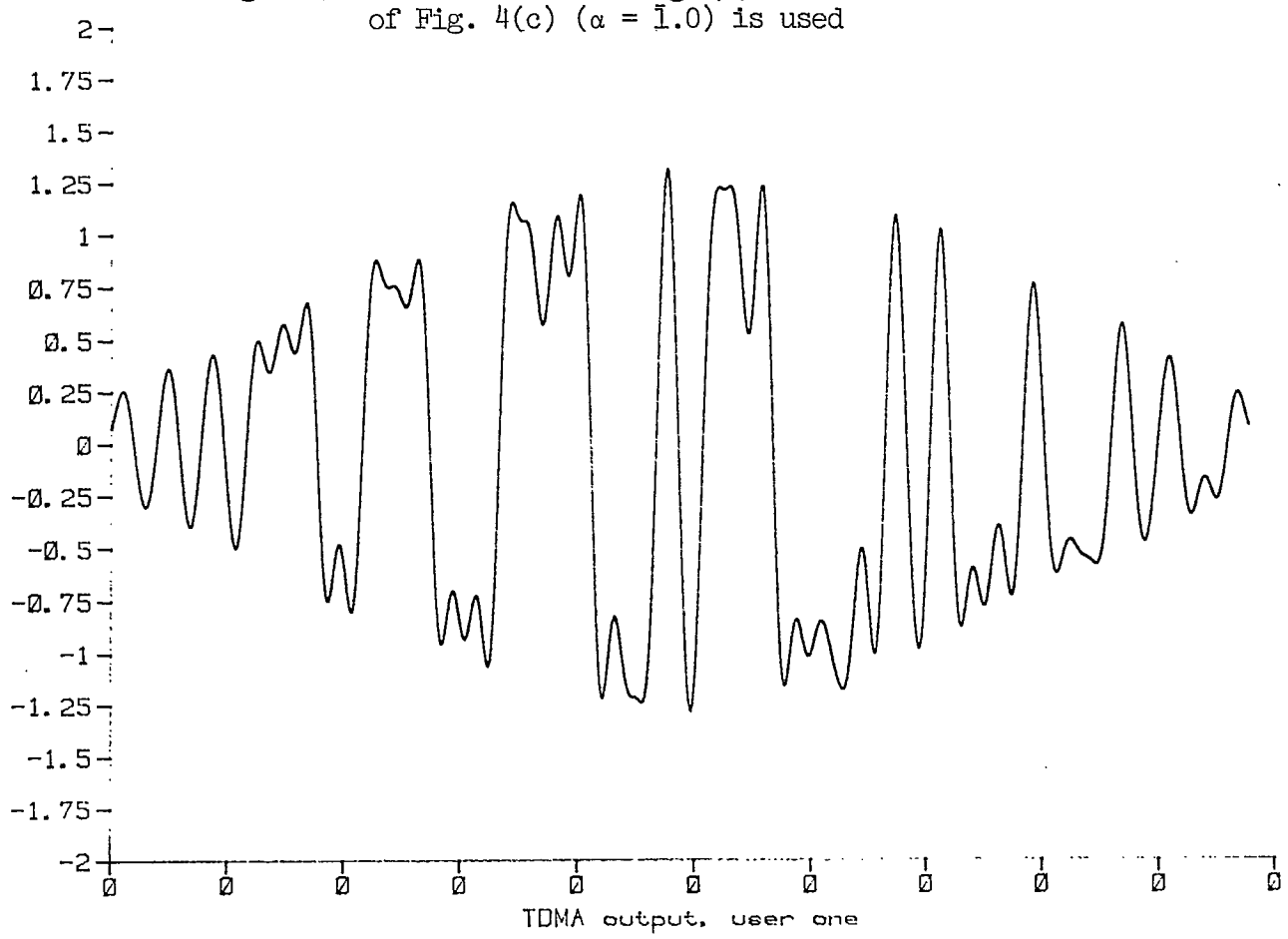


9a

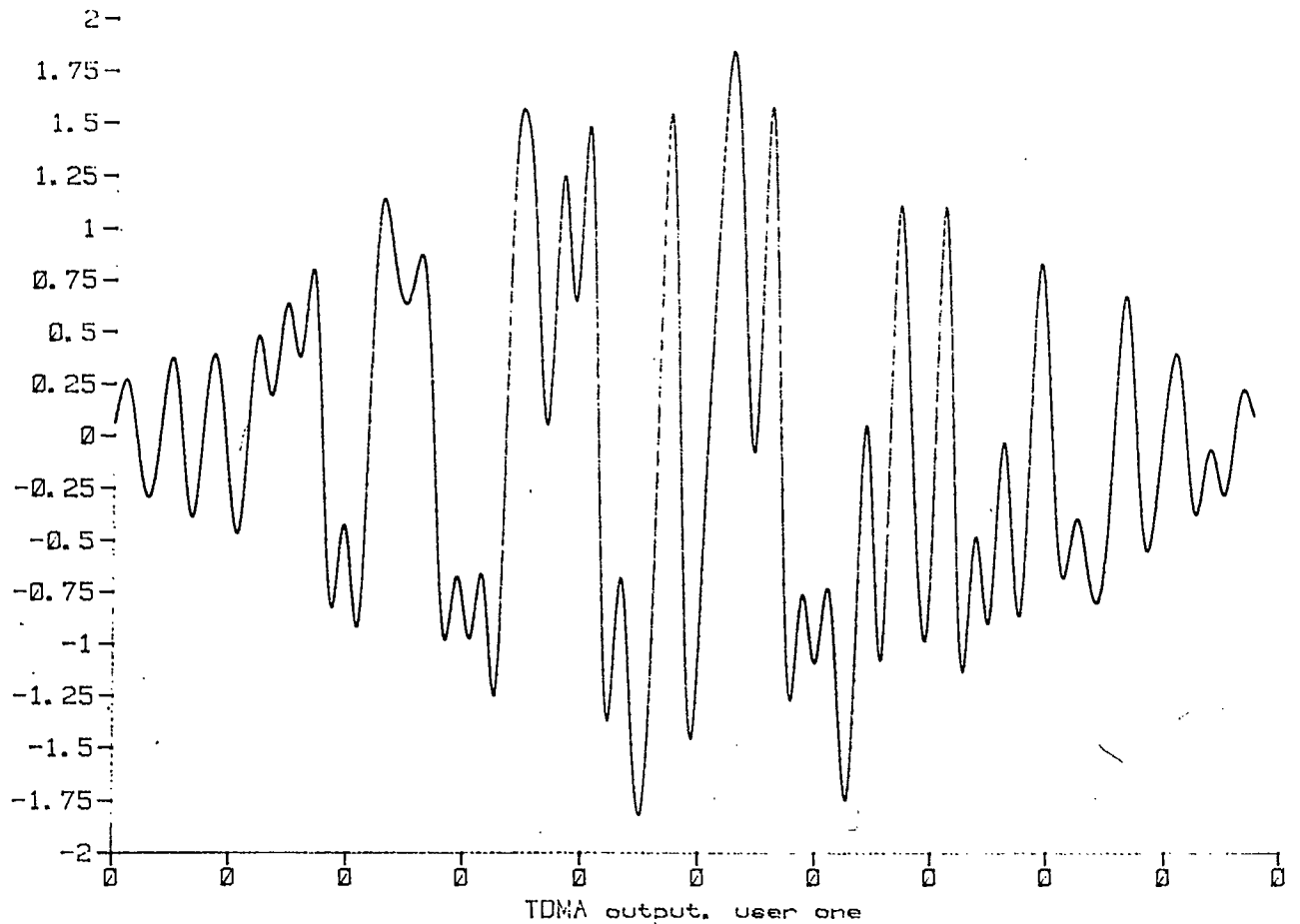


9b

Figure 10: The equal power reference user and interfering user signal for the situation in Fig. 9

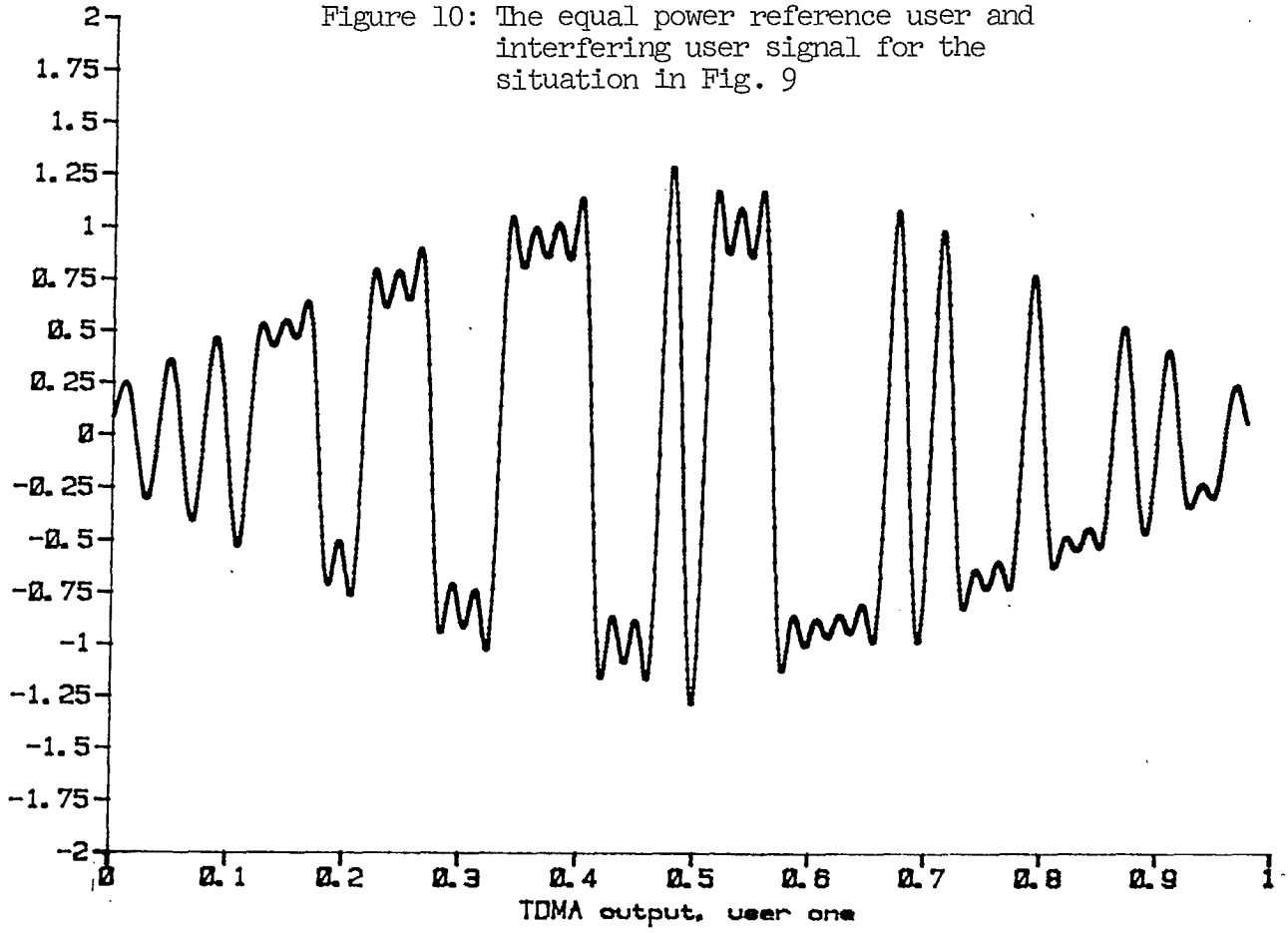


10a

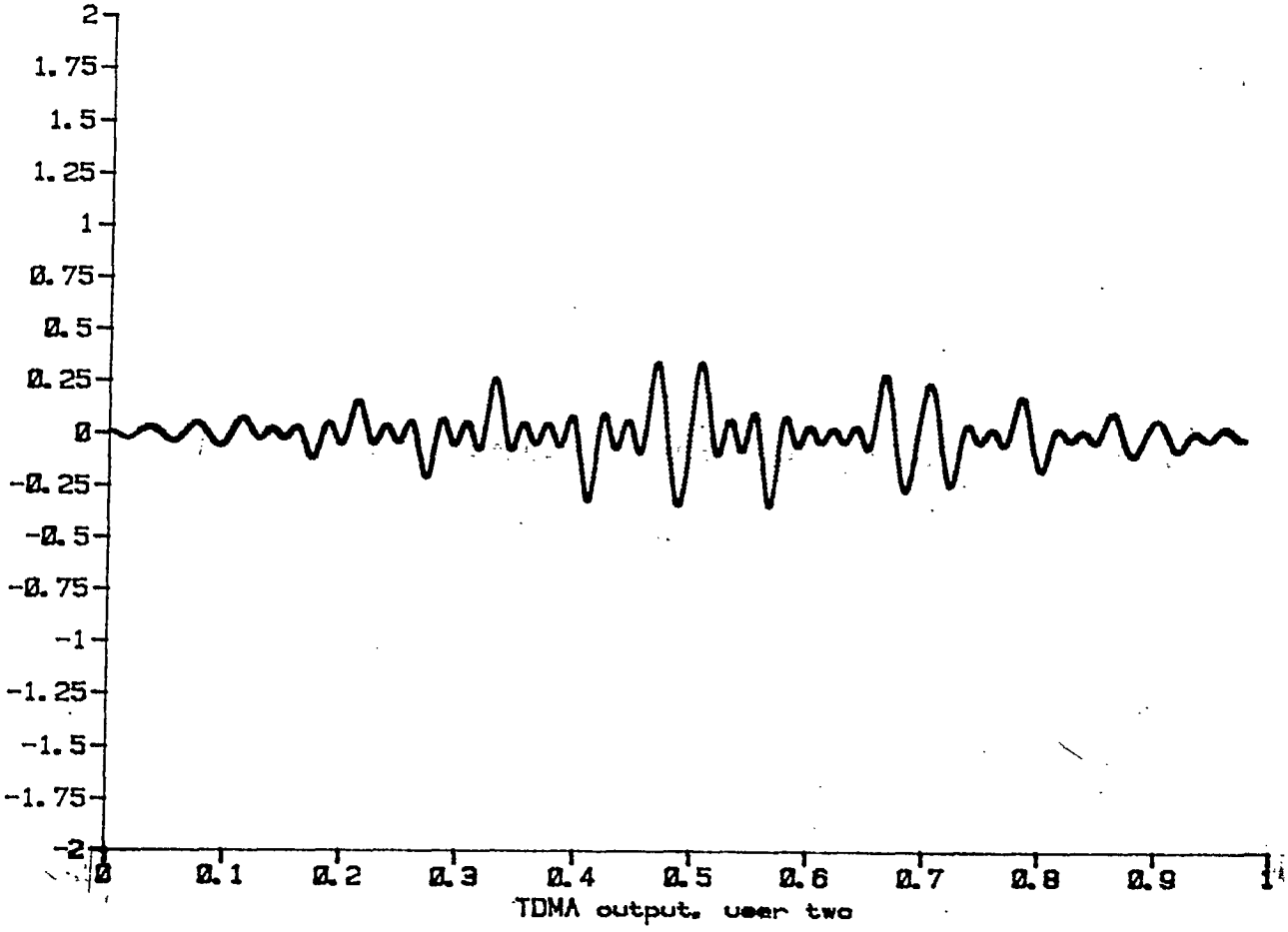


10b

Figure 11: Comparative spectral for a DBPSK data signal and a hop based $\alpha = 1.0$ window function

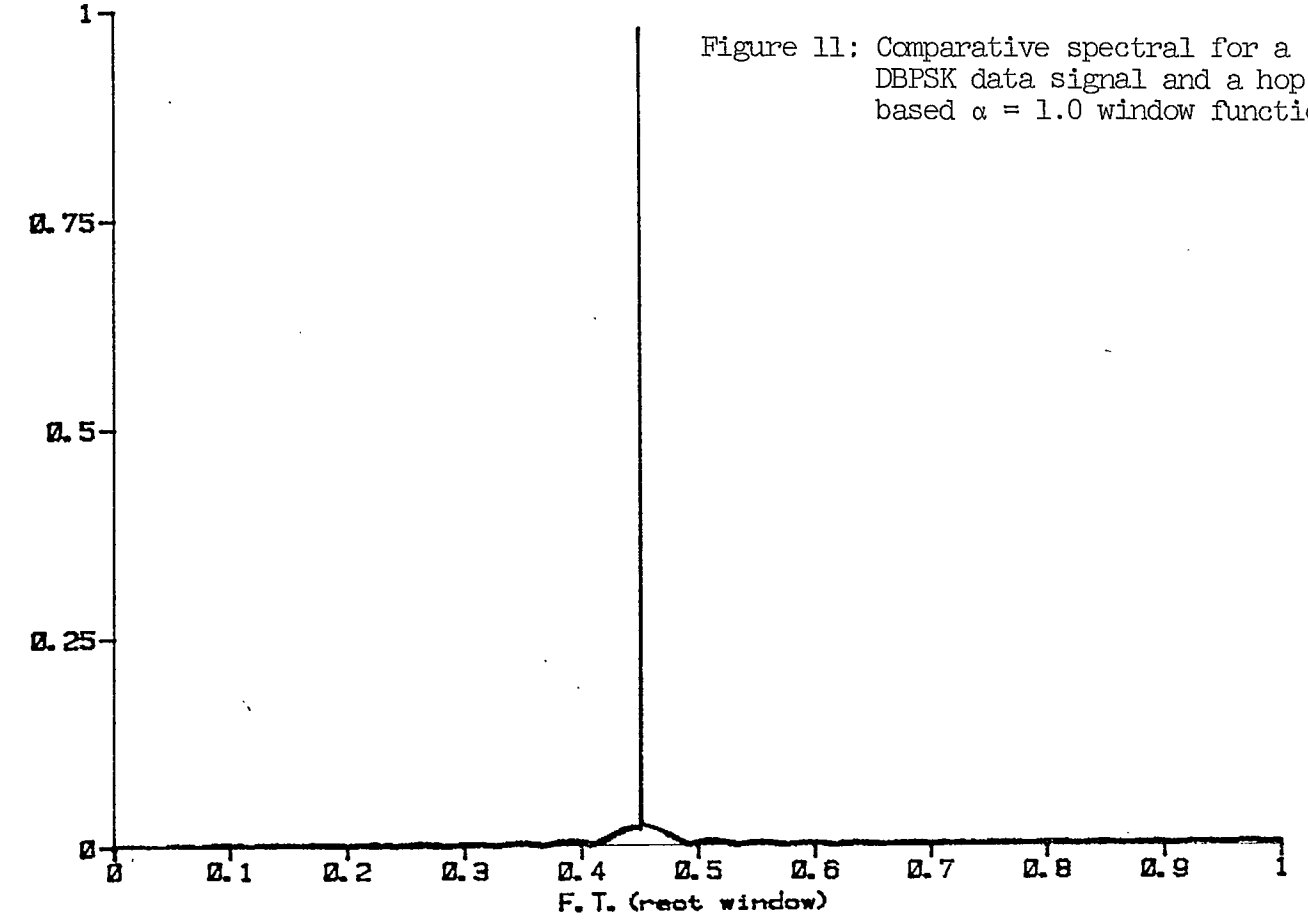


11a

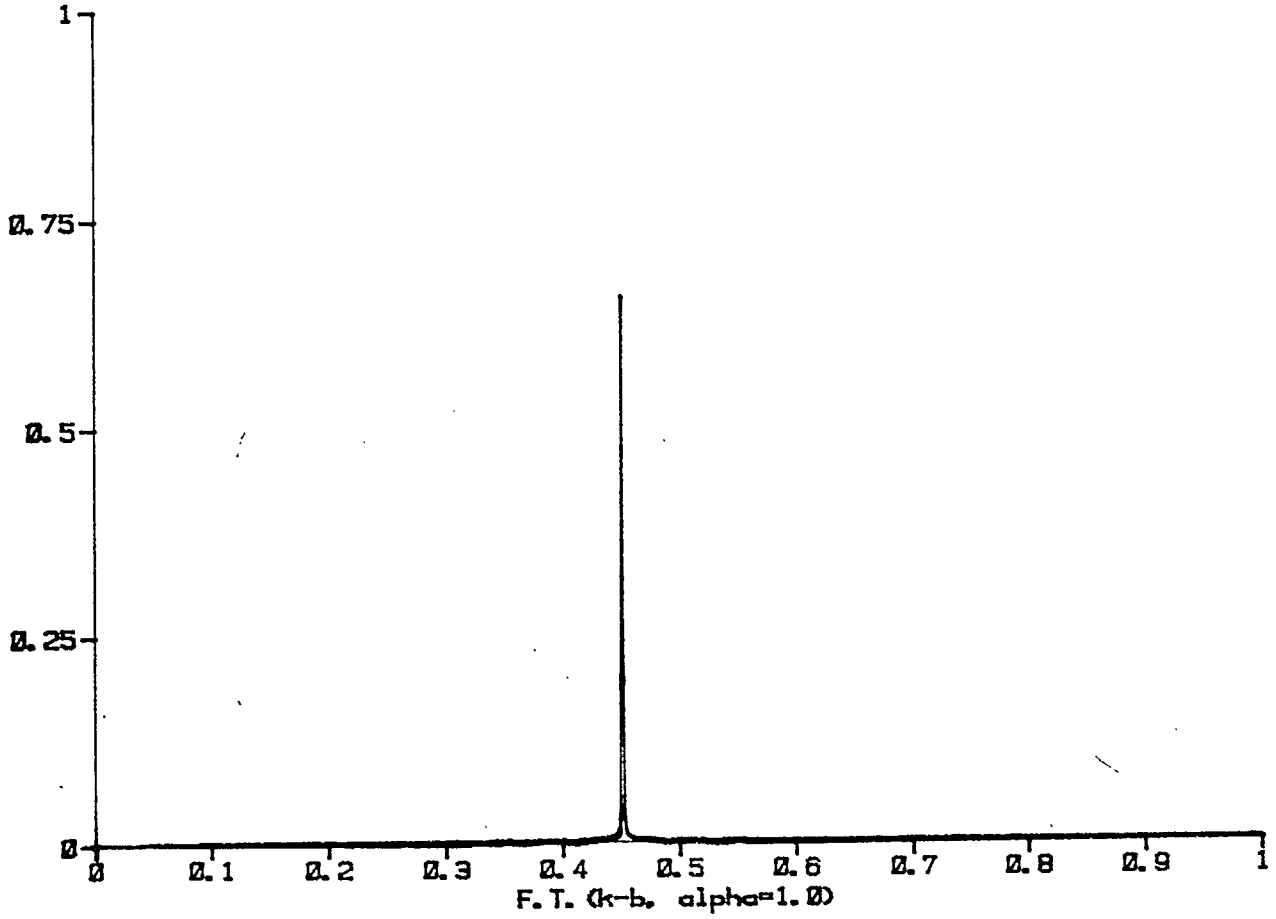


11b

# A STUDY OF SPACE COMMUNICATIONS SPREAD-SPECTRUM SYSTEMS

(Phases 5 and 6)

Part 2 Coding and Moduation

INTERIM PROGRESS REPORT

Y.M. Lam

and

P.H. Wittke

Report No. 89-1

March 1989

Prepared for

The Department of Communications

Under DSS Contract No. 36001-8-3528/01-ST

Department of Electrical Engineering

Queen's University

Kingston, Ontario, Canada

A STUDY OF SPACE COMMUNICATIONS SPREAD-SPECTRUM SYSTEMS

Part 2 - Coding and Modulation


## SUMMARY

In previous coding and modulation work under the DSS Contract, trellis codes were obtained for use with noncoherent m-ary FSK. These codes gave improved performance in additive noise but they do not require an increased bandwidth. The current task under Part B. of the work statement - Coding and Modulation, is to investigate trellis-like codes to improve immunity to the three types of jamming: partial-band noise, tone and pulse jamming. This part, Part 2 of the Interim Report, reports the progress achieved in this area since the work was started in October 1988.

Our goal in the current work is to find the performance of trellis-coded noncoherent frequency-shift keying (NCFSK) as would be used in a hopped spread spectrum system, in the presence of jamming and with a range of possible detection metrics or schemes that will be effective in a jamming environment. In particular, in our trellis coding, we expand the signal set for noncoherently orthogonal M-ary FSK to 2M-ary noncoherent FSK. The tones are uniformly spaced, but to avoid significant bandwidth expansion, nonorthogonal tone spacing is permitted. For example, the tone spacing is reduced from the usual spacing of 1/T Hz to 1/2T, 1/3T or 2/3T Hz. For simplicity in analysis, the performance of 4-FSK with 2-state and 4-state trellis coding is evaluated and the effects of tone spacing on error performance is investigated. The soft decision decoding metric employed is the simple energy metric. Performance in the presence of noise is analyzed and it is concluded that coding gain can be achieved without significant bandwidth expansion.

For partial band noise jamming, a noncoherent receiver which is able to detect the presence of jamming in the band, is considered. The performance analysis is based on the union Chernoff bound on the probability of bit error. A transfer function bound is derived for the present case of trellis coding and noncoherent detection, and used to obtain the union bound. Very substantial performance improvements are indicated by use of trellis coding in worst case partial band noise jamming. It is planned to investigate performance for other decoding situations and other forms of jamming, in the remaining period of the contract.

A STUDY OF SPACE COMMUNICATIONS SPREAD-SPECTRUM SYSTEMS

Part 2 - Coding and Modulation

Statement of Work:

A previous contract identified possible issues to be investigated in three areas:

A. Uplink Synchronization

B. Coding and Modulation

C. Surface-acoustic Wave Block Demodulation.

In particular, previous coding and modulation work obtained trellis codes for use with noncoherent m-ary FSK, that give improved performance in additive noise and do not require an increased bandwidth. The current task under Part B. Coding and Modulation, is to investigate trellis-like codes to improve immunity to the three types of jamming: partial-band noise, tone and pulse jamming. The purpose of Part 2 of the Interim Report is to report the progress achieved in this area since the work was started in October 1988.

## I. INTRODUCTION

The use of spread spectrum communications to combat jamming is well-known and much of the ongoing research in military satellite communications (MILSATCOM) has been focused on frequency-hopped systems [1-16]. Hopping the carrier frequency over a wide band results in an improved error performance against a simple jammer which must distribute its power thinly over a wide band in order to jam the signal. However, it is well-known [1, vol.II, pp.73-94; 2, pp.574-582 and pp.597-602] that the performance of uncoded frequency-hopped systems can suffer degradations of the order of 30 - 50 dB at typical operating points when confronted with more sophisticated jammers such as, for example, a partial band noise jammer which jams a fraction of the bandwidth and brings greater degradation to the communications system. Worst-case partial band noise jamming involves balancing the probability of jamming a given hop against the effective strength of jamming power for a fixed total jammer power.

Under worst case partial band noise jamming, the choice of modulation alone makes little difference in error performance [3, 4, 5 p.173]. The use of coding is extremely important when considering the worst case performance against an intelligent jammer. Evaluation of the coded error probabilities for antijam communications systems shows that gains of the order of 30-40 dB can be obtained over uncoded systems [6-9]. Besides error correcting coding [6-14], diversity [4,8,13,14] and interleaving [13] have also been utilized to enhance the protection against partial band or pulsed jammers. When coding is employed, various decoding metrics [8,15] for use in a jamming environment have been devised. The most popular decoding metrics under study are: the hard decision metric with and without side information [8,10], and Viterbi ratio threshold techniques with erasure and quality bits [11]. More recently, a robust metric called the square-law self-normalized energy metric [8,9,16] has also received attention.

The ability to detect or correct errors can only be provided by the transmission of additional redundant bits and thus by lowering the effective information rate per transmission bandwidth. Conventional hard decision encoders and decoders for error correction operate on binary, or more generally m-ary, code symbols transmitted over a discrete channel. However, when modulation and error-correcting coding are performed in the classical independent manner, disappointing results are obtained. The reason has been pointed out to be irreversible loss of information in the receiver due to independent hard symbol decisions made prior to decoding [17]. When coherent detection is utilized another problem is that mapping of code symbols of a code optimized for hamming distance into nonbinary modulation signals does not guarantee that a good Euclidean distance structure is obtained [17].

Massey [18] was the first to show that considerable performance improvement could be obtained by treating coding and modulation as a single entity. Trellis-coded modulations, so named by Ungerboeck [17,19,20], then evolved as a combined coding and modulation technique for digital transmission over band-limited channels. It can be shown that, in order to get a significant coding gain, it is sufficient that k bits be coded into $2^{k+1}$ channel signals. The number of channel signals for uncoded modulation is then doubled. Redundancy is provided by the signal-set expansion and in

the case of coherent transmission, more bandwidth is not required than for the equivalent uncoded scheme. Coding gains can be obtained with moderate additional complexity.

Early work on trellis-coded modulation [17-22] was primarily on multilevel and multiphase modulations, in order to achieve coding gain without the accompanied sacrifice in band efficiency. Coherent detection was the primary detection scheme considered throughout the development of Ungerboeck's trellis-coded modulation. In the context of frequency hopped systems in MILSATCOM, noncoherent detection is required due to difficulty of maintaining coherent carrier phase through frequency hopping and dehopping processes. In an earlier report [23], work on frequency-hopped FSK with trellis coding by using convolutional encoder and transmitting combinations of orthogonal FSK tones to avoid any bandwidth expansion, was reported. Significant coding gains were obtained for transmission in additive noise. Results reported were obtained by simulation with only a few analytical results, as the signals were correlated multiple tones for which there are not explicit detection expressions. Our goal in the current work is to find the performance of trellis-coded noncoherent frequency-shift keying (NCFSK) as would be used in a hopped spread spectrum system, in the presence of jamming and with a range of possible detection metrics or schemes, as mentioned above. We wish to avoid exhaustive simulation in the search for good codes and in the examination of a range of techniques for decoding in a jamming environment. Thus we have chosen to examine trellis coding for the single-tone NCFSK modulation format, which is much easier to analyse. As well, this is the modulation commonly proposed for hopped spread spectrum systems.

In this report we consider expanding noncoherently orthogonal M-ary FSK to 2M-ary noncoherent FSK. Nonorthogonal tone spacing is considered to avoid significant bandwidth expansion, and the tones are uniformly spaced. For example, in one case the tone spacing is reduced from the usual spacing of 1/T to 1/2T Hz, and 2 subsets of orthogonal FSK signals are obtained. The bandwidth expansion is small, tending to zero as M increases. For simplicity in analysis, the performance of 4-FSK with 2-state and 4-state trellis coding will be evaluated. The effects of tone spacing on error performance is investigated. The soft decision decoding metric employed is

the simple energy metric. For partial band noise jamming analysis, a decoder with perfect side information is considered. The performance analysis is based on the union Chernoff bound on the probability of bit error. The well-known transfer function bound [24-26] is derived and used to obtain the union bound. Performance improvement by the use of trellis coding under the usual additive white Gaussian noise will presented first. Performance under worst case partial band noise jamming will then be presented. It is planned to invesitigate performance for other decoding situations and other forms of jamming, in the coming contract year.

## II. SYSTEM DESCRIPTION

The frequency-hopped system under consideration employs noncoherent frequency-shift-keying (NCFSK) with trellis coding. A system block diagram is shown in Fig. 1. The binary bit stream goes into a rate k/k+1 trellis encoder. The trellis-coded symbols are mapped in groups of (k+1) bits, into an $m=2^{k+1}$ level NCFSK signal set according to the set partitioning method [19]. The carrier frequency of the NCFSK signal is hopped pseudorandomly by the frequency hopper and transmitted. In the receiver, the received signal is dehopped by the frequency dehopper to its original signaling frequency. We consider the hopping rate to be the same as the symbol transmission rate, in this report. Time diversity is not considered here. For NCFSK, the optimum detector is a bank of envelope detectors (or energy detectors which give the square of the envelope) matched to each of the NCFSK signaling frequencies. The energy detector outputs together with any side information about the jamming go to the trellis decoder, which is simply a maximum metric decoder (e.g. Viterbi decoder). The transmitted data is decoded according to the decision rule employed.

It should be noted that based upon a new description of trellis codes by Calderbank and Mazo [21], the two step processes of specifying an underlying trellis code and mapping the output code symbols into the signal constellation based on the set partitioning rule, can be combined into a single step [22]. The trellis-coded NCFSK signal can be easily produced by a voltage-controlled oscillator (VCO) with the control voltage being a trellis-coded m-ary level signal. The FSK tone spacing is set by the

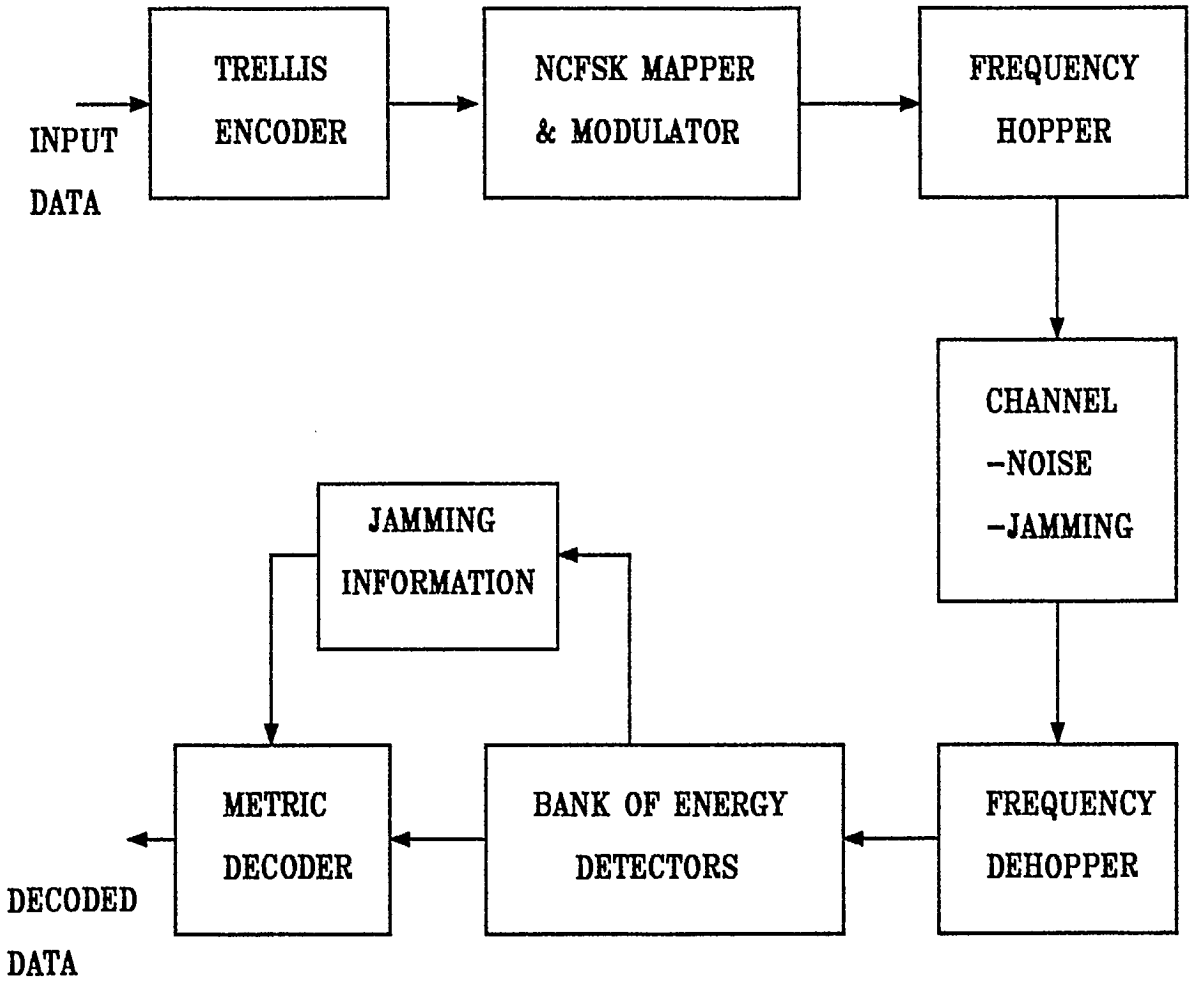


Figure 1: Frequency - hopped trellis - coded noncoherent FSK system block diagram.

amplitude of the trellis-coded modulating signal and the frequency sensitivity of the VCO.

Consider an m-ary NCFSK signal set with uniform tone spacing of $\Delta$ Hz. For convenience let $S_1$ to $S_m$ denote the m NCFSK signals as shown in Fig. 2. During any signaling interval, one of the NCFSK signals in the signal set is transmitted. The signals are given by

$$S_i = \sqrt{2P} \cos [2\pi f_i t + \theta_i] \qquad 1 \leq i \leq m , \; 0 < t < T \tag{1}$$

where P is the signal power, $f_i$ is the $i^{th}$ signalling frequency and $\theta_i$ is the noncoherent carrier phase of the $i^{th}$ signal. With the signals ordered in the way shown in Fig. 2, the frequency separation between two signals $S_i$ and $S_j$ denoted by $\Delta_{ij}$ is given by

$$\Delta_{ij} = |i-j| \, \Delta \tag{2}$$

The cross-correlation coefficient $\rho_{ij}$ of $S_i$ and $S_j$ is given by [27, p.148].

$$\rho_{ij} = \frac{\sin \pi T \Delta_{ij}}{\pi T \Delta_{ij}} \; e^{-j\pi T \Delta_{ij}} \tag{3}$$

Its magnitude is

$$|\rho_{ij}| = \left| \frac{\sin \pi T \Delta_{ij}}{\pi T \Delta_{ij}} \right| = \frac{\sin \pi T \Delta \, |i-j|}{\pi T \Delta \, |i-j|} \tag{4}$$

When the tone spacing $\Delta = \frac{1}{T}$, $|\rho_{ij}| = 0$ for all $i \neq j$, all NCFSK tones are mutually orthogonal. This gives an expanded signal set with the best error performance. However, the bandwidth occupancy of this orthogonal NCFSK signal set is approximately twice that of the uncoded case. To avoid bandwidth expansion, we consider expanding the uncoded (m/2)-ary NCFSK signals to m-ary NCFSK signals with nonorthogonal tone spacing. According to the set partitioning rule [19], the m-ary signal set is successively partitioned into subsets of signals. The frequency separation between signals is doubled after each level of partitioning as shown in Fig. 2 for m=8.

At the $\ell^{th}$ level of set partitioning, the frequency spacing of signals in each subset is $2^{\ell} \Delta$ Hz. In particular, if $\Delta = 1/2^{\ell}T$ all signals in each

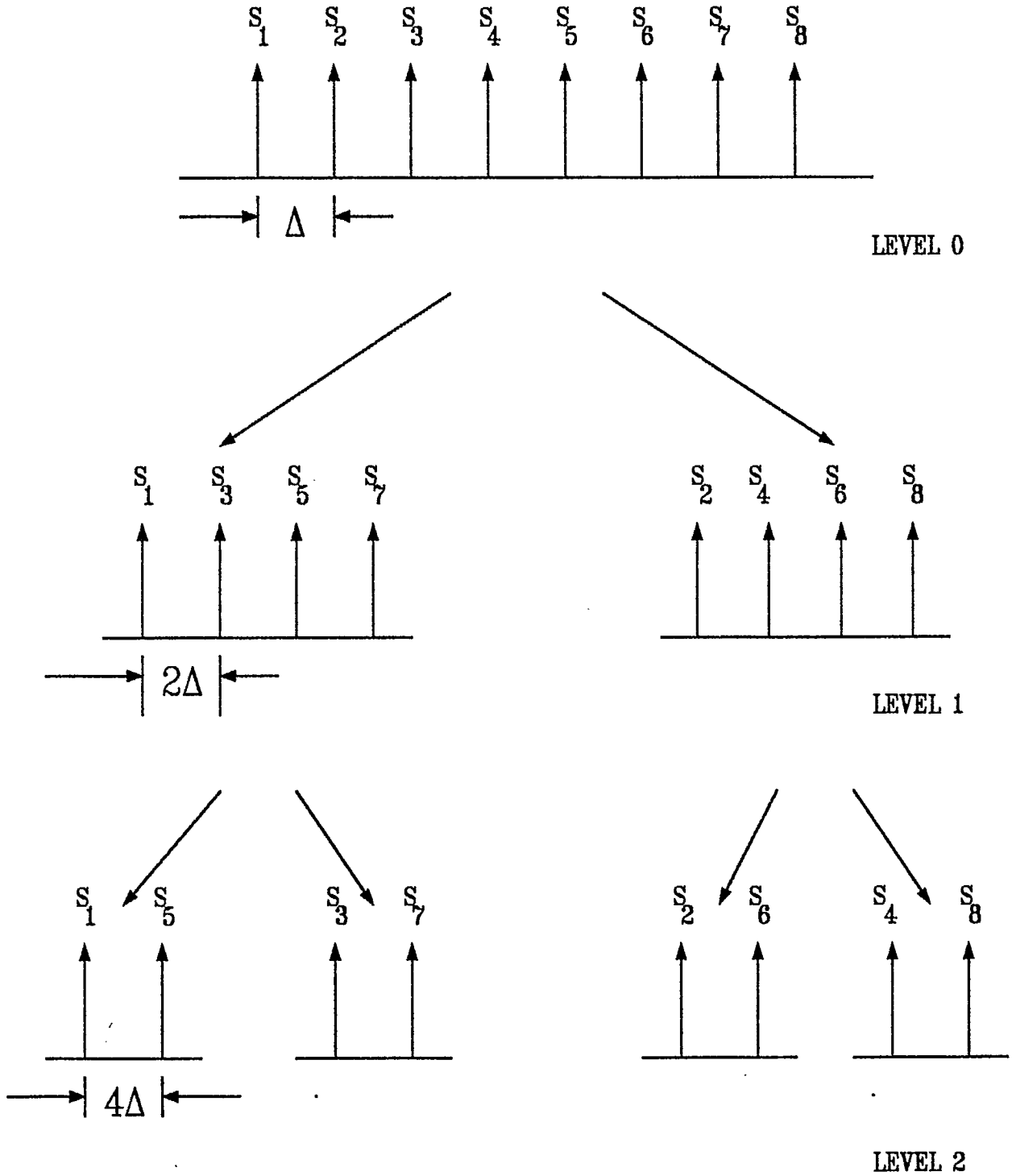


Figure 2: Set partitioning of 8-NCFSK.

subset are orthogonal and there is no advantage in partitioning the signals any further.

For m-ary NCFSK in additive white Gaussian noise, the optimum noncoherent detector is a bank of m envelope or energy detectors. The square of the $j^{th}$ envelope detector output is the energy of the received signal at the $j^{th}$ signalling frequency. Let $U_1, \ldots U_m$ be the outputs of the envelope detectors. Given $S_i$ was transmitted, the output of the $j^{th}$ envelope detector is [27, p. 206]

$$U_j = \left| \rho_{ij} \sqrt{E} + \eta_j \right|, \quad j \neq i, \quad i,j \in [1,m]$$

$$U_i = \left| \sqrt{E} + \eta_i \right| \tag{5}$$

where $\rho_{ij}$ is the complex cross-correlation coefficient of $S_i$ and $S_j$, E is the signal energy and $\eta_j$ are complex-valued Gaussian random variables with zero mean and variance $N_o/2$.

The probability density function of the output for the $j^{th}$ envelope detector given $S_i$ was sent, is a Rician-distributed random variable. If $U_i$ is normalized by $(2/N_o)^{1/2}$, the density is given by [27, p.206].

$$p(U_j|S_i) = U_j \exp\{-[U_j^2/2 + |\rho_{ij}|^2 E/N_o]\} I_o(U_j [2E \left|\rho_{ij}\right|^2/N_o]^{1/2}); \quad u_j>0$$
$$= 0; \quad u_j < 0 \tag{6}$$

where $I_o$ is the zeroth order modified Bessel function of the first kind. For the $i^{th}$ envelope detector, the probability density function is given by

$$p(U_i|S_i) = U_i \exp\{-[U_i^2/2 + E/N_o]\} I_o(U_i\{2E/N_o\}^{1/2}); \quad u_i > 0$$
$$= 0; \quad u_i < 0. \tag{7}$$

To avoid the irreversible loss of information caused by hard decisions made in the demodulator prior to final decoding, soft-decision decoding is employed. (If results for the simpler case of hard-decisioning are required, they can be obtained as well.) The maximum-likelihood decision

rule for noncoherent detection and coding, requires a metric that includes a zeroth order modified Bessel function and also the noise spectral density which must be known by the decoder. A more practical decoding metric is the energy metric, which is the square of the envelope detector output. This energy metric is the most commonly used metric for coded noncoherent MFSK systems [1, vol.I.p.211] and it approximates the optimum metric for high signal-to-noise ratio.

An effective jammer against an uncoded frequency-hopped spread spectrum system is an average-power-limited partial band jammer [6]. We consider a jammer with power J that transmits Gaussian noise with constant power spectral density over a fraction $\alpha$ of the system bandwidth W. We define an equivalent broadband noise spectral density

$$N_J = \frac{J}{W} \tag{8}$$

The jamming noise power spectral density over the jammed bandwidth of $\alpha W$ Hz is then

$$N_J' = \frac{N_J}{\alpha} \tag{9}$$

and zero for the rest of the system bandwidth.

Assume that each hop is independent of other hops and equally likely to be in any part of the total spread spectrum bandwidth. The probability of a hopped signal being jammed is $\alpha$. Also, assume that during any hop interval the whole set of m NCFSK tones is either totally in the jammed band or not.

Define a binary jammer state random variable Z, where Z=1 indicates that the transmitted tone hopped into the jammed band, while Z=0 indicates that it hopped outside the jammed band.

$$P[Z=1] = \alpha$$
$$P[Z=0] = 1 - \alpha \tag{10}$$

This is the jammer state information that may be available at the receiver.

We will assume that the receiver knows with certainty whether each hop is jammed or not. Possible methods for deriving this information include implementing automatic gain control in the receiver, which may be monitored to determine whether jamming power is corrupting a given hop [1, vol.II p.97]. Another method suggested by Trumpis [29] for orthogonal noncoherent FSK is to declare a hopped signal to be jammed when more than one energy

detector output goes high. When nonorthogonal FSK tone spacing is employed the Trumpis approach may not be as reliable, since nonorthogonal energy detectors will also have output. However, if $\Delta = 1/2T$, two sets of orthogonal tones are obtained, in which case, there is always at least one other tone orthogonal to each transmitted tone. A hopped signal is declared to be jammed when two or more orthogonal energy detectors have high output.

The metric considered here is the suboptimum energy metric with perfect side information [1, VolI, p.216]. For an input X and channel output Y, it is given by

$$m(Y,X;Z) = c(Z)\, e_X \qquad (11)$$

where c(Z) is a weighting function depending on the jammer state variable Z. For example, the function can simply take on one value for Z=0 and another value for Z=1. $e_X = U_X^2$ is the energy detector output (or the square of the envelope detector) corresponding to input X.

## III. PERFORMANCE ANALYSIS

For trellis-coded coherent multilevel and multiphase modulations, the error performance at high signal-to-noise ratio is specified by the minimum Euclidean distance between any pair of paths through the trellis. An asymptotic coding gain is usually defined as the ratio of the minimum Euclidean distance of the trellis code to the minimum distance between signals in the uncoded situation [17,19,22]. For the trellis-coded noncoherent FSK modulation with the soft energy metric and decision rule considered here, the union Chernoff bound on bit error probability is evaluated.

The Chernoff bound is known to be not particularly tight and can be 1 dB to several dB off, depending on the code and the number of channel symbols used in the modulation. However, it has the advantage of being relatively easy to compute and of decoupling the channel influence from the code itself [8]. It is widely used to obtain an upper bound on error probabilities for convolutional codes and block error-correcting codes with a maximum metric decoder (eg. a Viterbi decoder) using an arbitrary metric. This method has been shown to provide useful and reliable information [30]. Usual coded systems use orthogonal signals and the Chernoff bound on the

pairwise error probability then depends on only one parameter. When nonorthogonal signals are employed, we will see that the Chernoff bound will depend on a number of parameters with each parameter corresponding to a pair of signals with a different cross-correlation coefficient.

## 3.1 Chernoff Bound on Pairwise Error Probability

Let $\underline{X} = (X_1, X_2, \ldots, X_N)$ be the transmitted code sequence of length N. The channel output sequence is denoted by $\underline{Y} = (Y_1, Y_2, \ldots, Y_N)$. In addition, a corresponding jammer state information sequence is denoted by $\underline{Z} = (Z_1, Z_2, \ldots, Z_N)$.

The metric used for decoding is denoted by $m(\underline{Y}, \underline{X}; \underline{Z})$. The maximum metric decoder chooses $\hat{\underline{X}} = (\hat{X}_1, \hat{X}_2, \ldots, \hat{X}_N)$ which corresponds to the maximum metric among all possible coded sequences. Error occurs whenever $\hat{\underline{X}} \neq \underline{X}$ with probability given by

$$P(\underline{X} \to \hat{\underline{X}}) = \Pr \{ \sum_{n=1}^{N} m(Y_n, \hat{X}_n; Z_n) \geq \sum_{n=1}^{N} m(Y_n, X_n; Z_n) \mid \underline{X} \}$$

$$= \Pr \{ \sum_{n=1}^{N} [m(Y_n, \hat{X}_n; Z_n) - m(Y_n, X_n; Z_n)] \geq 0 \mid \underline{X} \}$$

The pairwise error probability for this symbol-by-symbol noncoherent detection with soft decision metric decoding, cannot be evaluated except for the case when all the m NCFSK signals are orthogonal. Consequently, we have to resort to the Chernoff bound [1,Vol.I, App. 4A] on the pairwise error probability, as commonly utilized in performance analysis of coded systems.

Applying the Chernoff bound [1,Vol.I, App. 4A], we have

$$P(\underline{X} \to \hat{\underline{X}}) \leq E\left\{\exp\left(\lambda \sum_{n=1}^{N} [m(Y_n,\hat{X}_n;Z_n) - m(Y_n,X_n;Z_n)]\right) \mid \underline{X}\right\}$$

$$= E\left\{\prod_{n=1}^{M} \exp\left(\lambda\,[m(Y_n,\hat{X}_n;Z_n) - m(Y_n,X_n;Z_n)]\right) \mid \underline{X}\right\}$$

$$= \prod_{n=1}^{M} E\left\{\exp\left(\lambda\,[m(Y_n,\hat{X}_n;Z_n) - m(Y_n,X_n;Z_n)]\right) \mid \underline{X}\right\} \tag{12}$$

for any $\lambda \geq 0$.

For $\hat{X}_n = X_n$ it is clear that

$$E\left\{\exp\left(\lambda\,[m(Y_n,\hat{X}_n;Z_n) - m(Y_n,X_n;Z_n)]\right) \mid \underline{X}\right\} = 1$$

For $\hat{X}_n \neq X_n$ the expected value depends on both $\hat{X}_n$ and $X_n$ when nonorthogonal signals are employed.

Let $\hat{X}_n = j$ and $X_n = i$, and let $\rho$ be the crosscorrelation coefficient of the corresponding signals $S_j$ and $S_i$.

For the energy metric given by (11) we have

$$D(\alpha,\lambda,\rho) = E\left\{e^{\lambda[m(Y_n,\hat{X}_n;Z_n) - m(Y_n,X_n;Z_n)]}\Big|_{\underline{X}}\right\} \quad \hat{X}_n \neq X_n$$

$$= E\left\{e^{\lambda c(z)[e_j - e_i]}\Big|_{i}\right\} \quad j \neq i$$

$$= \alpha\, E\left\{e^{\lambda c(1)[e_j - e_i]}\Big|_{i,\ Z=1}\right\} + (1-\alpha)\, E\left\{e^{\lambda c(0)[e_j - e_i]}\Big|_{i,\ Z=0}\right\} \quad j \neq i \tag{13}$$

$$E\left\{e^{\lambda c(1)[e_j - e_i]}\Big|_{i,\ Z=1}\right\} \quad j \neq i$$

$$= E\left\{e^{\lambda c(1)\, e_j}\Big|_{i}\right\}_{j\neq i} E\left\{e^{\lambda c(1)\, e_i}\Big|_{i}\right\} \tag{14}$$

Using the probability density function (6) with the change of variable $U = \{e_j\}^{1/2}$, we have

$$E\left\{ e^{\lambda c(1)\, e_j}\Big|_i \right\} \quad j \neq i$$

$$= \int_0^\infty e^{\lambda c(1)\, U^2}\, U\, e^{-U^2/2}\, e^{-\alpha|\rho|^2 E/N_J}\, I_o(U\,[\,2\alpha|\rho|^2 E/N_j\,]^{1/2})\, dU$$

$$= \int_0^\infty U\, e^{-[1-2\,\lambda\, c(1)]\, U^2/2}\, e^{-\alpha|\rho|^2 E/N_J}\, I_o(U\,[\,2\alpha|\rho|^2\, E/N_j\,]^{1/2})\, dU \quad (15)$$

By change of variable $\beta = [\,1-2\,\lambda\, c(1)\,]^{1/2} u$ , this becomes

$$\frac{1}{1-2\,\lambda\, c(1)} \exp\{-\,\alpha E|\rho|^2[1 - 1/(1-2\lambda c(1))]/N_J\}$$

$$\int_0^\infty \beta\, e^{-\beta^2/2} \exp\{-\,\alpha\,|\rho|^2\, \frac{E}{N_J}\, \frac{1}{1\, -\, 2\lambda c(1)}\,\}\; I_o\left(\beta\,\left[\frac{2\alpha|\rho|^2 E}{(1-2\lambda c(1))N_J}\right]^{1/2}\right) d\beta$$

The integral is equal to 1 since it is the integration of the probability density function of a Rician random variable over its entire range. Hence (15) becomes

$$E\left\{ e^{\lambda c(1)\, e_j}\Big|_i \right\}_{j\neq i} = \frac{1}{1-2\lambda c(1)}\, e^{-\alpha|\rho|^2\, \frac{E}{N_J}\, (1-\, \frac{1}{1-2\lambda c(1)})} \quad (16)$$

Similarly,

$$E\{e^{\lambda c(1) e_i}\Big|_i\} = \frac{1}{1+2\lambda c(1)}\, e^{-\alpha\, \frac{E}{N_J}\;\; \frac{2\lambda c(1)}{1+2\lambda c(1)}} \quad (17)$$

Substituting (16) and (17) into (14), we have

$$E\{e^{\lambda c(1)[e_j - e_i]}\Big|_{i,\, Z=1}\}_{\, j\, \neq\, i}$$

$$= \frac{1}{1-(2\lambda c(1))^2}\, e^{-\alpha\, \frac{E}{N_J}\, [\, \frac{2\lambda c(1)}{1+2\lambda c(1)} \,-\, \frac{2\lambda c(1)}{1-2\lambda c(1)}\; |\rho|^2]} \quad (18)$$

for $0 \leq 2\lambda c(1) < 1$.

For the expected value when Z=0, that is the signal is not jammed, in (13) we simply have $e_j = |\rho|^2 E$ and $e_i = E$ when thermal background noise is neglected. Hence,

$$E\left\{e^{\lambda c(0)\,[e_j-e_i]}\Big|_{i}\,,\ Z=0\right\}_{j\neq i}$$

$$= E\left\{e^{\lambda c(0)[|\rho|^2 E-E]}\right\}$$

$$= \exp\{-\lambda c(0)E(1-|\rho|^2) \tag{19}$$

Substituting (18) and (19) into (13), we obtain

$$D(\alpha,\lambda,\rho) = \frac{\alpha}{1-(2\lambda c(1))^2}\, e^{-\alpha \frac{E}{N_J}\left[\frac{2\lambda c(1)}{1+2\lambda c(1)} - \frac{2\lambda c(1)}{1-2\lambda c(1)}|\rho|^2\right]}$$

$$+(1-\alpha)\, e^{-\lambda c(0)\, E\, (1-|\rho|^2)} \tag{20}$$

for $0 \leq 2\lambda c(1) < 1$.

When perfect side information is available, the metric can be chosen with c(0) large enough so that the second term in the above equation is negligible and c(1) = 1/2 chosen for normalization [1,Vol.I, p.216]. Then $D(\alpha,\lambda,\rho)$ becomes

$$D(\alpha,\lambda,\rho) = \frac{\alpha}{1-\lambda^2}\, e^{-\alpha \frac{E}{N_J}\left[\frac{\lambda}{1+\lambda} - \frac{\lambda}{1-\lambda}|\rho|^2\right]} \tag{21}$$

for $0 \leq \lambda < 1$.

For m-ary NCFSK with uniform tone spacing of $\Delta$ Hz, there are (m-1) different frequency separations between the various pairs of tones. When orthogonal tone spacing is used ($\Delta$ is an integer multiple of 1/T) $|\rho| = 0$ for all tone pairs. There is only one parameter $D(\alpha,\lambda)$ for orthogonal signaling. When nonorthogonal tone spacing is employed there are (m-1) different values of $|\rho|$ resulting in (m-1) different $D(\alpha,\lambda,\rho)$. Define

$$D_k(\alpha) = \min_{0\leq\lambda<1} D(\alpha,\lambda,\rho)$$

$$= \min_{0\leq\lambda<1} \frac{\alpha}{1-\lambda^2}\, e^{-\alpha \frac{E}{N_J}\left[\frac{\lambda}{1+\lambda} - \frac{\lambda}{1-\lambda}|\rho_k|^2\right]} \tag{22}$$

where

$$|\rho_k| = \left|\frac{\sin \pi T k \Delta}{\pi T k \Delta}\right| \tag{23}$$

The Chernoff bound on pairwise error probability can be rewritten as

$$p(\underline{X} \to \hat{\underline{X}}) \le \prod_{k=1}^{m-1} [D_k(\alpha)]^{W_k(\underline{X},\hat{\underline{X}})} \tag{24}$$

where $W_k(\underline{X},\hat{\underline{X}})$ is the number of places where $|\hat{X}_n - X_n| = k \neq 0$, $n = 1,2,..,N$.

## 3.2 Union Chernoff Bound

These pairwise error probabilities are the basis of bit error bounds for our trellis-coded NCFSK systems. A union bound is used to upper bound all the error events that can occur. Let $a(\underline{X},\hat{\underline{X}})$ denote the number of bit errors occurring when $\underline{X}$ is transmitted and $\hat{\underline{X}}$ is chosen by the receiver. If $p(\underline{X})$ is the probability of transmitting $\underline{X}$, then the coded bit error bound has the form

$$\begin{aligned} p_b &\le \sum_{\underline{X}} \sum_{\hat{\underline{X}} \in \zeta} a(\underline{X},\hat{\underline{X}})\, p(\underline{X})\, p(\underline{X} \to \hat{\underline{X}}) \\ &\le \sum_{\underline{X}} \sum_{\hat{\underline{X}} \in \zeta} a(\underline{X},\hat{\underline{X}})\, p(\underline{X}) \prod_{k=1}^{m-1} [D_k(\alpha)]^{W_k(\underline{X},\hat{\underline{X}})} \end{aligned} \tag{25}$$

where $\zeta$ is the set of all coded sequences.

An efficient method for evaluating the union bound is the transfer function technique [24,26]. Since the output of the trellis encoder is determined by the input bit sequence and the state of the trellis encoder, a state diagram is a more compact representation of the code than the trellis diagram. For the performance evaluation of our trellis-coded NCFSK, the state transition branches are labeled with $L^{\ell} I^{i} D_k$. L and I are just dummy variables and $D_k$ denotes the parameter given by (22) when the incorrect and correct channel signals associated with the state transition are separated by $k\Delta$ Hz. The exponents $\ell$ and i denote the number of channel symbols and the bit error corresponding to the state transition.

Let $\underline{D}$ denote the (m-1)-tuple of $D_k(\alpha)$ given by (22). The transfer function denoted by $T(L,I,\underline{D})$ derived from the state diagram, enumerates all possible pairwise error probabilities in a closed form.

For trellis codes which are in general nonlinear, the probability of error for deciding an incorrect path is dependent on the correct path. Consequently, one cannot assume the all-zeros code sequence to be the transmitted code sequence, as is usually done for linear codes. Biglieri's method [25] of pairwise states or product states involves a generalized state diagram defined over an expanded set of product states. The generalized transfer function so derived enumerates all possible incorrect paths for all possible correct paths. For an $\eta$-state trellis this method requires a product state diagram of $\eta^2$ states or equivalently a $\eta^2 x \eta^2$ state transition matrix for computing the transfer function. Consequently, this method is useful for trellis codes with only a small number of states.

Another method suitable for trellis codes having certain symmetries such as the Ungerboeck codes and other codes based on set partitioning, has been derived by Zehavi and Wolf [26]. This method requires a modified state diagram consisting of $\eta$ states for a $\eta$-state trellis code. It is therefore more computationally efficient than the product state method and is employed here.

The union Chernoff bound on bit error probability is then given by

$$p_b \leq \frac{1}{2} \frac{1}{k} \frac{\partial}{\partial I} T(L,I,\underline{D}) \Big|_{\substack{L=2^{-k} \\ I=1}} \tag{26}$$

with a factor of 1/2 added to improve the Chernoff bound [1,Vol.I. App.4B]. The worst case partial band noise jamming performance is then obtained by maximizing $p_b$ over $0<\alpha\leq 1$ as

$$p_{b\ WC} \leq \max_{0<\alpha\leq 1} \frac{1}{2} \frac{1}{k} \frac{\partial}{\partial I} T(L,I,\underline{D}) \Big|_{\substack{L=2^{-k} \\ I=1}} \tag{27}$$

It should be noted that the maximizing value of $\alpha$ is not necessarily equal to the worst case $\alpha$, because a bound rather than an equality is maximized.

## IV. SYSTEM EVALUATION

In this section the performance of frequency-hopped trellis-coded 4-ary noncoherent frequency-shift-keying is evaluated. Trellis coding with 2-state trellis and 4-state trellis has been used. Nonorthogonal NCFSK tone spacing of 1/3T, 1/2T and 2/3T have been considered together with orthogonal spacing of 1/T. Union Chernoff bounds on bit error probability

are computed when the system is under thermal noise (full band jamming) and worst case partial band noise jamming.

### 4.1 4-NCFSK with 2-state trellis coding

The binary input sequence is coded into a 4-NCFSK signal by a rate 1/2 2-state trellis encoder. Fig. 3 depicts the signal set partitioning, the signal assignments to the state transitions and the modified state diagram. From the state diagram the following state equations are obtained.

$$T(L,I,\underline{D}) = 2\,L\,D_1\,\chi_1 \tag{28}$$

$$\chi_1 = L\,I\,(D_1+D_3)\,\chi_1 + 2\,L\,I\,D_2 \tag{29}$$

Solving (28) and (29), we obtain the transfer function given by

$$T(L,I,\underline{D}) = \frac{4L^2\,ID_1D_2}{1-L\,I(D_1+D_3)} \tag{30}$$

for this 2-state trellis coding.

### 4.2 4-NCFSK with 4-state trellis coding

The set partitioning of the 4-ary NCFSK signals remains the same as for 2-state trellis coding. With a 4-state trellis, there are more state transition branches and Ungerboeck's rules 2) and 3) given in [19] can now be simultaneously satisfied. The signal set partitioning, assignment of signals to transition branches and the modified state diagram for this 4-state trellis coding, are shown in Fig.4.

From the state diagram, we get the following state equations

$$T(L,I,\underline{D}) = 2\,L\,D_2\chi_c \tag{31}$$

$$\chi_a = 2\,L\,I\,D_2 + 2\,L\,I\,\chi_c \tag{32}$$

$$\chi_b = L\,I\,(D_1+D_3)\,\chi_a + 2\,L\,I\,D_1\chi_b \tag{33}$$

$$\chi_c = 2\,L\,D_1\chi_a + L\,(D_1+D_3)\,\chi_b \tag{34}$$

Solving (31) to (34) yields

$$T(L,I,\underline{D}) = \frac{2\,L\,D_2[2\,L^3I^2D_2(D_1+D_3)^2 + 4\,L^2I\,D_1D_2(1-2\,L\,I\,D_1)]}{1 - 2\,L^3I^2(D_1+D_3)^2 + 4\,L^2I\,D_1(1 - 2\,L\,I\,D)} \tag{35}$$

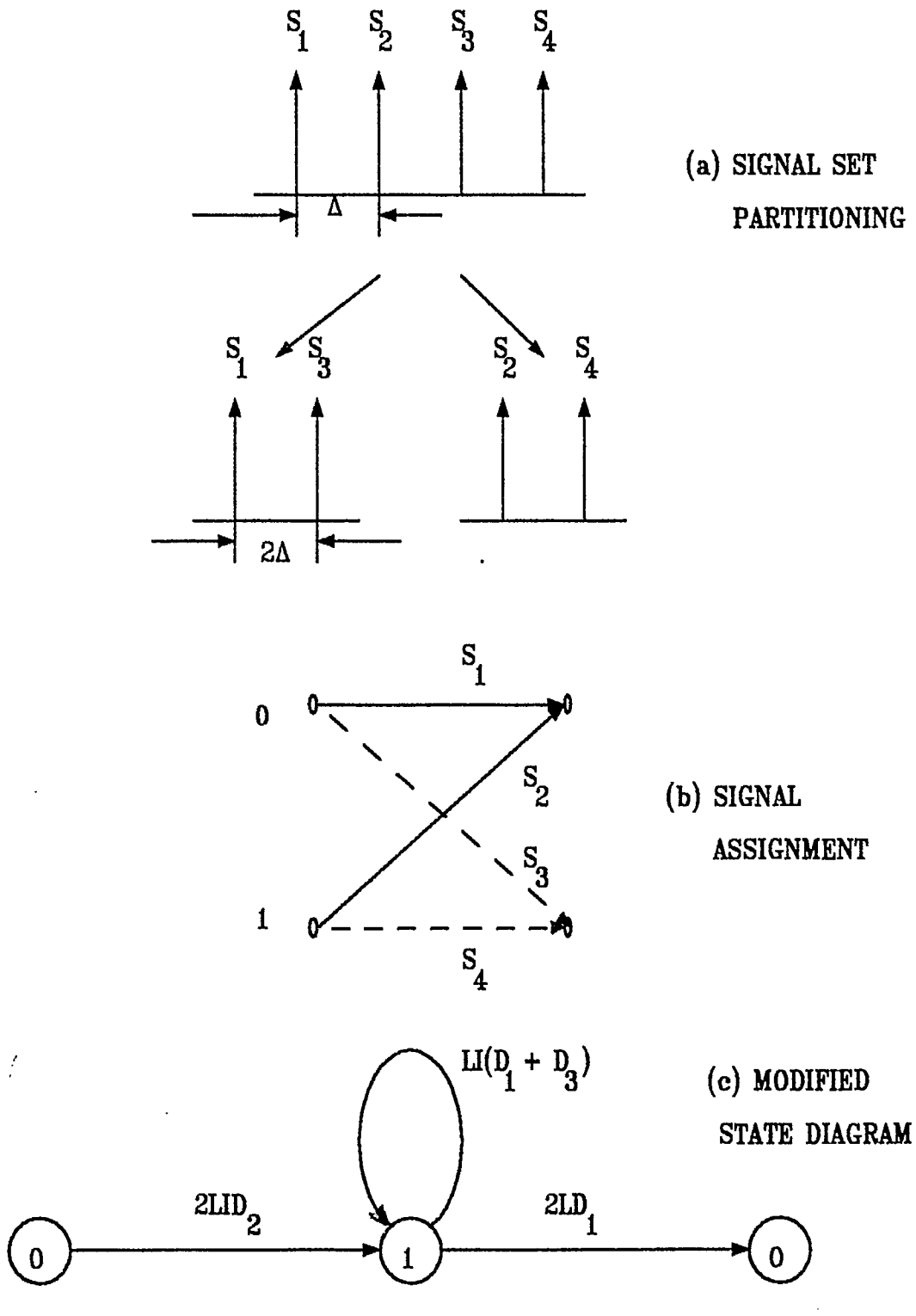


Figure 3: 4-NCFSK with 2-state trellis coding.

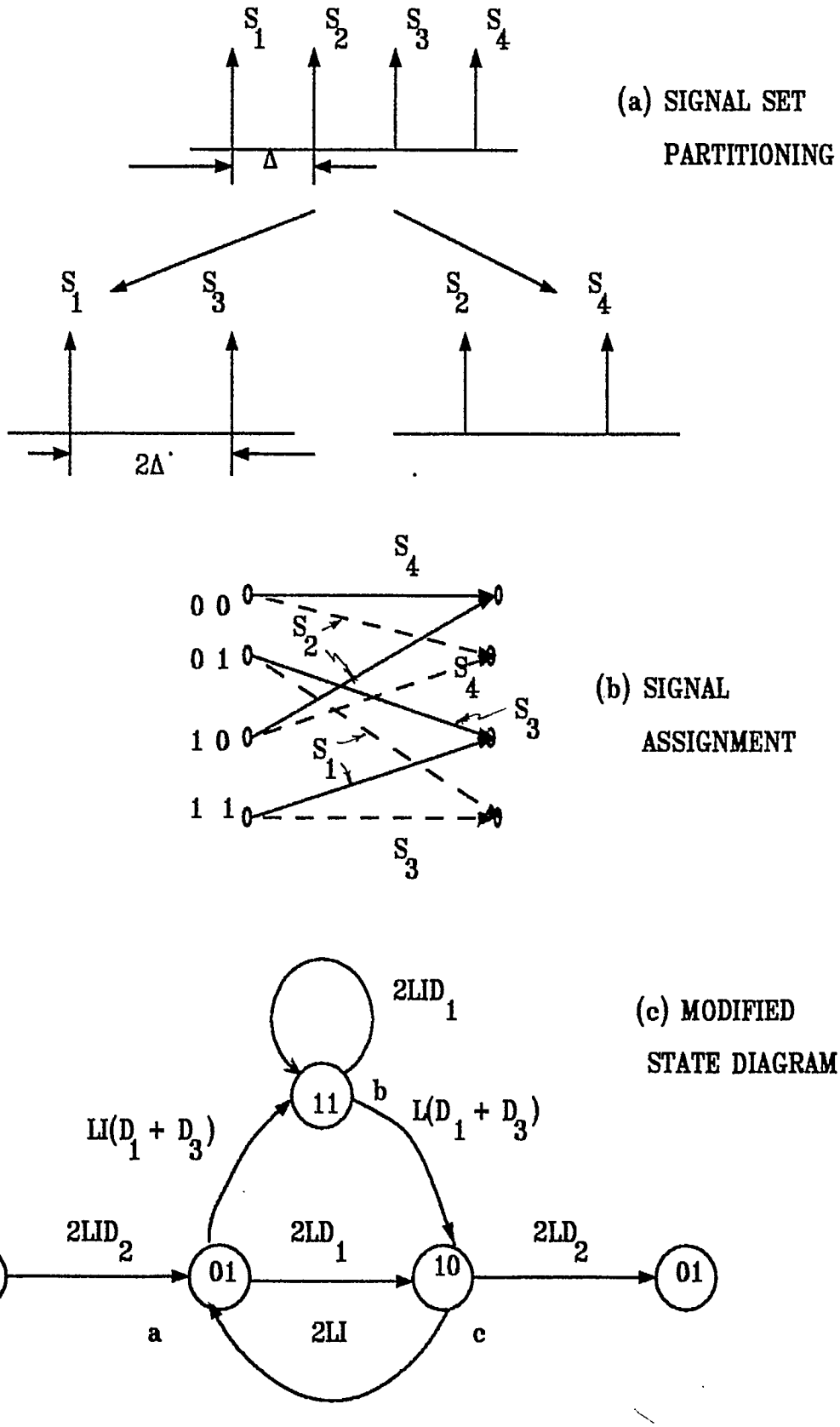


Figure 4: 4-NCFSK with 4-state trellis coding.

## 4.3 Results

We first examine the performance for the additive Gaussian noise channel. The union Chernoff bounds on bit error probability for 4-NCFSK with 2-state trellis coding with tone spacing $\Delta$ = 1/3T, 1/2T, 2/3T and 1/T were evaluated and are plotted in Fig. 5. The best performance is obtained when all the tones are orthogonal with $\Delta$ = 1/T, as expected.

To avoid large bandwidth expansion, the use of nonorthogonal tone spacing has been investigated. For $\Delta$ = 1/3T, the bandwidth occupancy of the coded 4-NCFSK is the same as that of the uncoded orthogonal binary NCFSK but the performance is not nearly as favourable. Using a tone spacing of 1/2T Hz such that two sets of orthogonal tones are obtained, the performance is worse than the best performance with orthogonal signals by about 2 dB. If the tone spacing is increased to 2/3T Hz, the performance actually degrades from that for a tone spacing of 1/2T Hz. This indicates 1/2T to be the best nonorthogonal tone spacing. The exact bit error probability for uncoded orthogonal binary NCFSK is also plotted in Fig. 5. Bear in mind that the uncoded performance is evaluated exactly while the coded system performance is obtained by using a union Chernoff bound.

The performance of 4-NCFSK with 4-state trellis coding in Gaussian noise, is presented in Fig. 6. Again, results for $\Delta$ = 1/3T 1/2T and 2/3T show that the best nonorthogonal spacing is 1/2T. We can see that the degradation in performance is less than 1 dB by using tone spacing of 1/2T Hz instead of orthogonal tone spacing. Large saving in band-occupancy is obtained with small degradation in performance by using tone spacing of 1/2T Hz.

Performance of 4-ary NCFSK in Gaussian noise with different tone spacings and codings are plotted in Fig. 7. For a given tone separation the 4-state code always yields better performance than the simpler 2-state code. As the tone spacing is increased from 1/3T Hz to 1/T Hz the performance improvement gained by using the 4-state code over the 2-state code decreases.

Performance in worst case partial band noise jamming for the systems considered above, is shown in Fig. 8. The performance of the uncoded orthogonal binary NCFSK is also plotted as a reference in Fig. 8. We can see that the use of trellis coding brings large coding gain under worst case

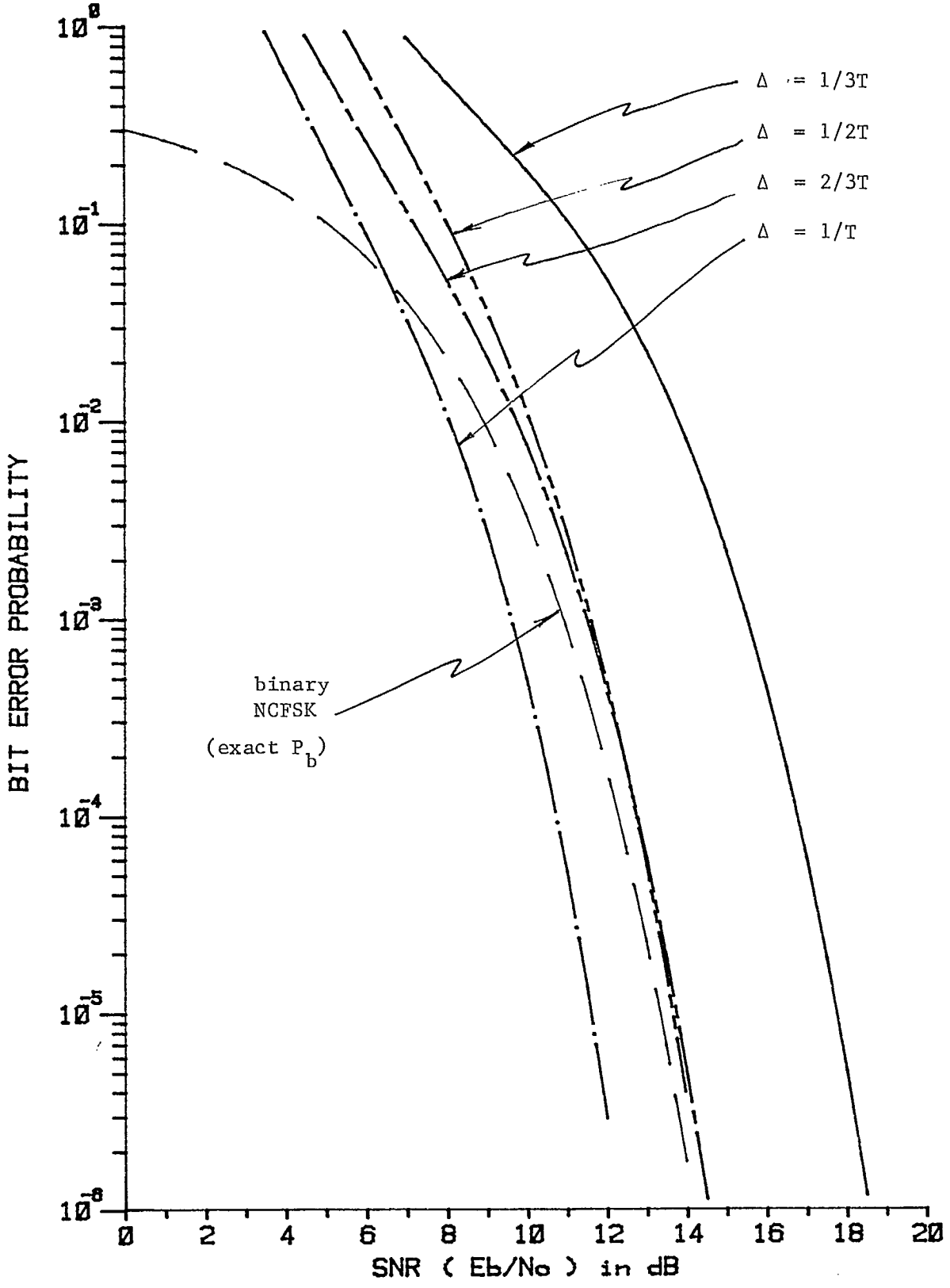


Figure 5: Performance of 4-ary NCFSK with 2-state trellis coding in additive white Gaussian noise.

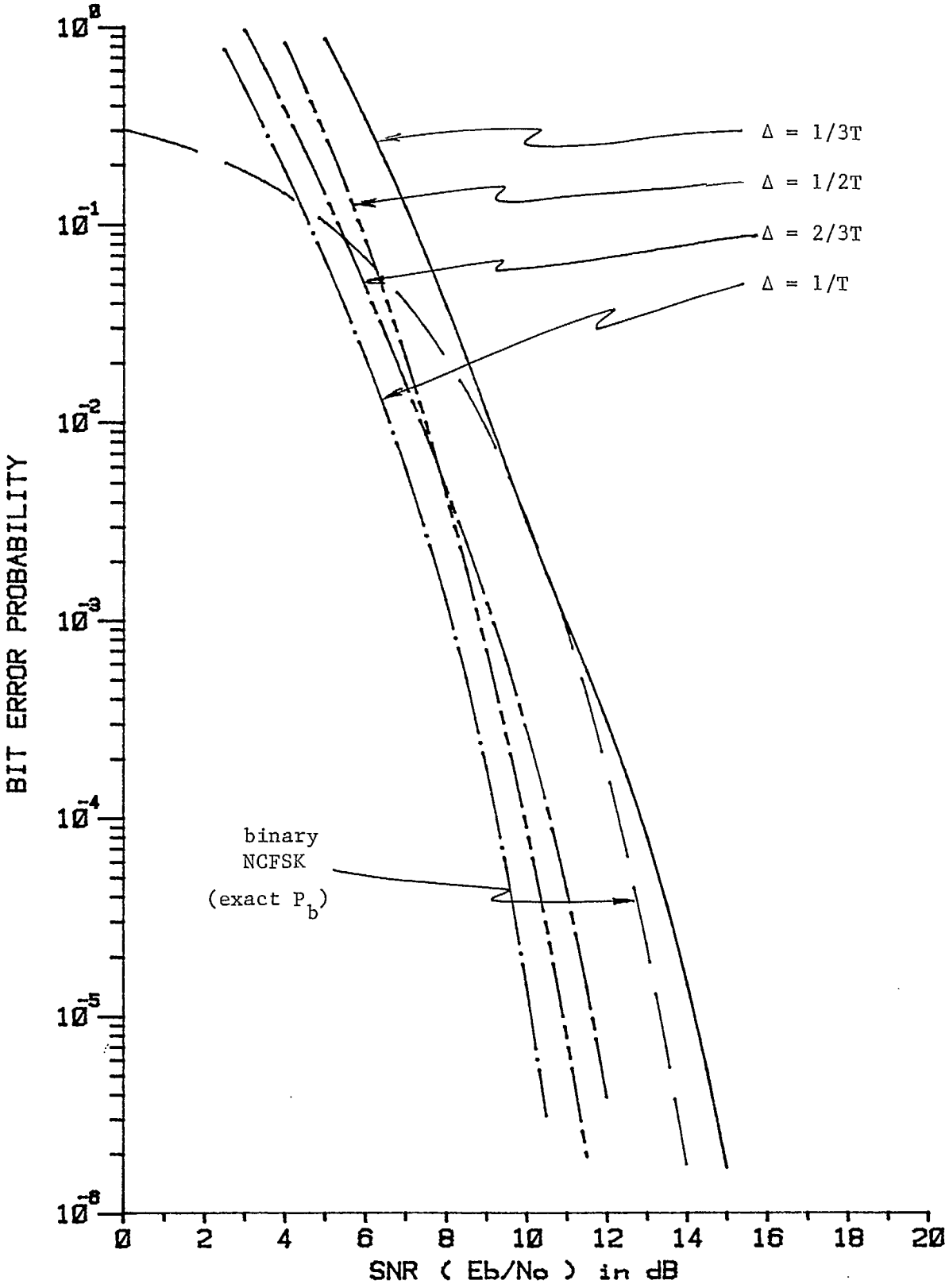


Figure 6: Performance of 4-ary NCFSK with 4-state trellis coding in additive white Gaussian noise.

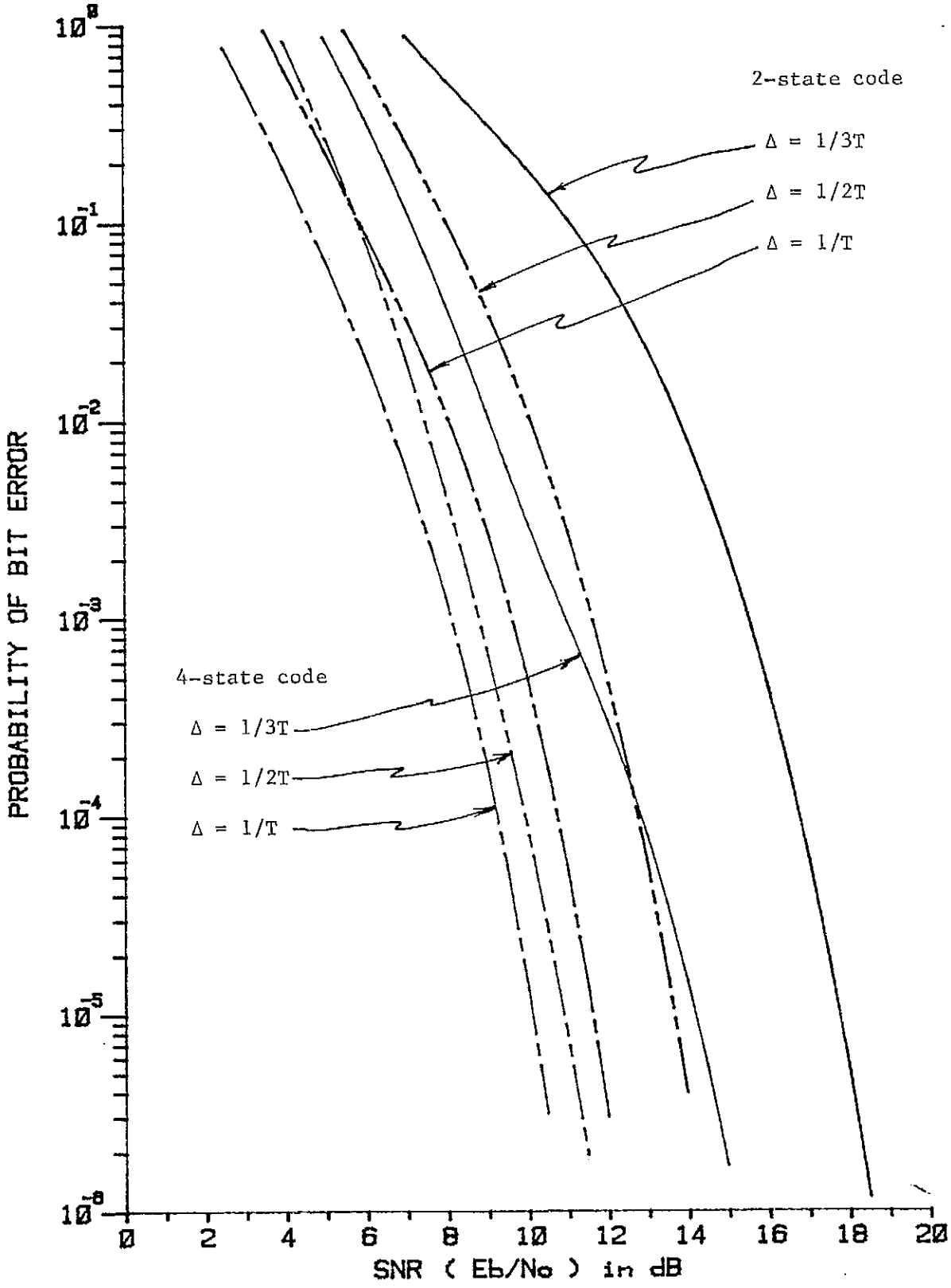


Figure 7: Performance of 4-ary NCFSK with 2-state code and 4-state code in additive white Gaussian noise.

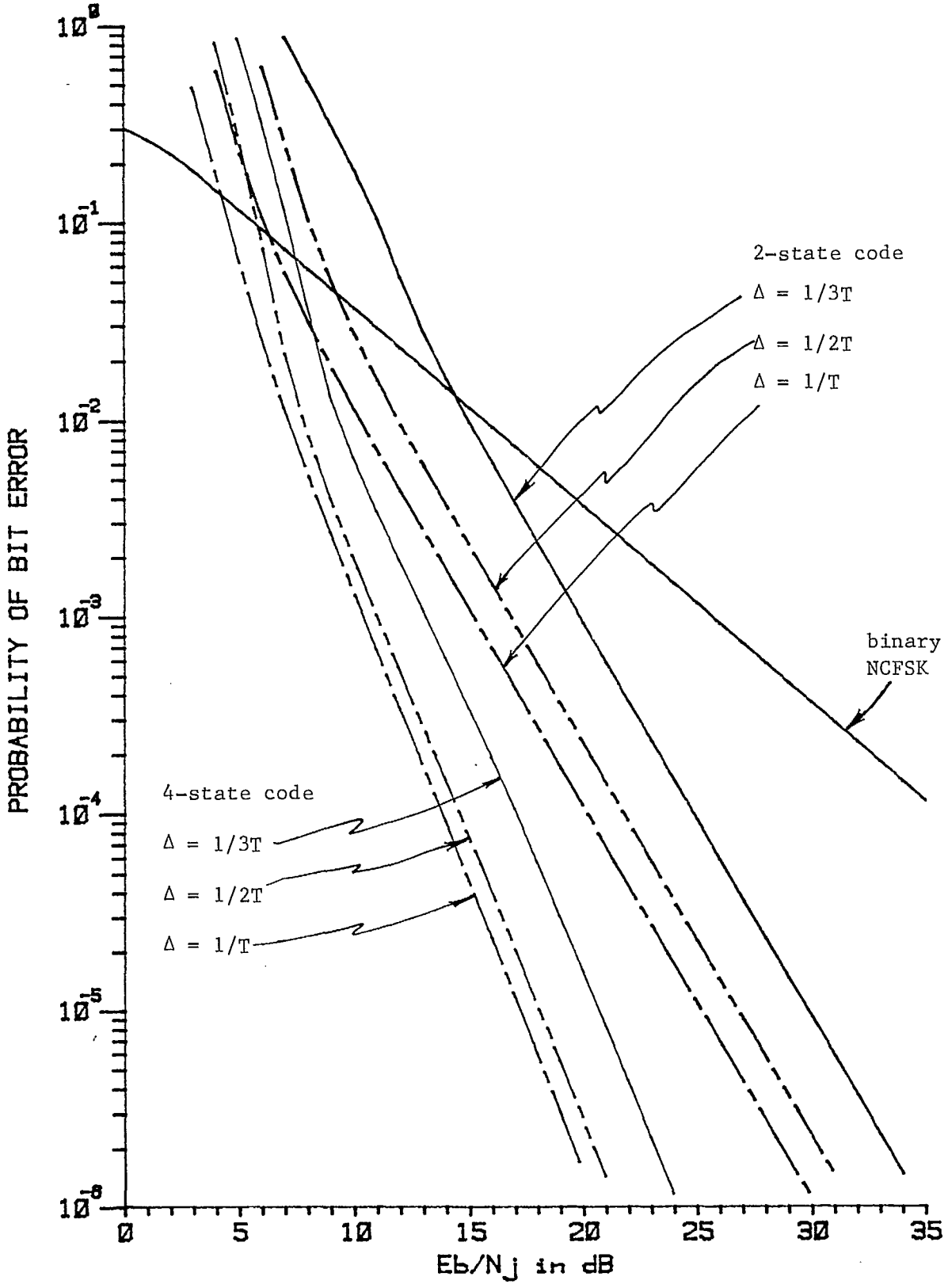


Figure 8: Performance in worst case partial band noise jamming.

partial band noise jamming. The 4-state code performs much better than the 2-state code. With either code, best performance is achieved by using orthogonal signals. However, the degradation in bit error rate is small in using nonorthogonal NCFSK signals separated by 1/2T Hz, rather than the orthogonal signal set.

Table 1 summarizes the coded performance under worst case partial band noise jamming, by tabulating the required signal to jamming noise ratio in dB to achieve a bit error rate of $10^{-5}$. The corresponding worst case fraction of the band jammed, $\alpha^*$, which maximized the bit error rate is also listed. The use of nonorthogonal signals with tone spacing of 1/2T Hz rather than 1/T Hz for orthogonal signaling, increases the required signal to noise ratio by only 1.6 dB and 0.85 dB respectively for the 2-state code and 4-state code.

## V. CONCLUSIONS

In this report a frequency-hopped system with trellis-coded noncoherent frequency-shift-keying is presented. It is proposed that k bits per baud be encoded into a set of $m = 2^{k+1}$ NCFSK signals. Nonorthogonal tone spacing is considered to avoid bandwidth expansion. Following Ungerboeck's signal set partitioning method, the m-ary signals are partitioned into subsets. When the tone spacing is chosen such that at some level of signal set partitioning the frequency separation between signals within a subset is equal to 1/T Hz, we obtain subsets of orthogonal signals. Soft decision decoding with a maximum metric decoder is employed. The metric considered in this report is the energy metric with perfect information as to the presence or absence of jamming in the band.

Performance analysis of the system under partial band noise jamming is presented. The analysis is based on the Chernoff bound on pairwise error probability. The union Chernoff bound on bit error probability is derived utilizing the transfer function bounding technique. For an m-ary nonorthogonal signal set, there are (m-1) parameters $D_k$ in the union Chernoff bound. The parameters $D_k$ are formulated for partial band noise jamming and are used in the derivation of the transfer function bound on

error performance, in place of the usual parameter D with squared distance exponent, which arises for coherent coded systems. For the codes under study, dramatic improvement in immunity to partial-band jamming is seen.

System performance is evaluated for 2-state and 4-state trellis codes with tone spacings of 1/3T, 1/2T and 1/T Hz. Results are presented for a system both in additive white Gaussian noise and in a worst case partial band noise jamming environment. The use of 1/2T Hz tone spacing instead of orthogonal tone spacing of 1/T Hz, brings little degradation in error performance. Large saving in bandwidth occupancy is obtained by using nonorthogonal NCFSK with 1/2T Hz tone spacing accompanied by a small sacrifice of 1 or 2 dB in signal-to-noise degradation.

## REFERENCES


1. M.K. Simon, J.K. Omura, R.A. Scholtz and B.K. Levitt, Spread Spectrum Communications, Vol. I, II and III, Computer Science Press, Inc., 1985.
2. R.E. Ziemer and R.L. Peterson, Digital Communications and Spread Spectrum Systems, Macmillan Publishing Company, Inc., 1985.
3. T.C. Huang and L. Yen, "Error Probability of a Noncoherent MFSK/FH Receiver in the Presence of Interference and Gaussian Noise," Proc. MILCOM'82, Boston, Mass., pp. 14.3.1-14.3.7, Oct. 17-20, 1982.
4. B.K. Levitt, "Use of Diversity to Improve FH/MFSK Performance in Worst Case Partial Band Noise and Multitone Jamming," Proc. MILCOM'82, Boston, Mass., pp. 28.2.1 - 28.2.5, Oct. 18-20, 1982.
5. Y.M. Lam, "High Data Rate Spread Spectrum Systems with Band-Efficient Modulations," Doctoral Dissertation, Department of Electrical Engineering, Queen's University, Kingston, Ontario, Canada, July 1988.
6. H.H. Ma and M.A. Poole, "Error-Correcting Codes Against the Worst-Case Partial-Band Jammer," IEEE Trans. on Commun., Vol. COM-32, No.2, pp.124-133, Feb. 1984.
7. W.E. Stark, "Coding for Frequency-Hopped Spread-Spectrum Communication with Partial-Band Interference - Part II : Coded Performance," IEEE Trans. on Commun., Vol. COM-33, No. 10, pp. 1045-1057, Oct. 1985.
8. K. Cheun and W.E. Stark, "Performance of Convolutional Codes with Diversity under Worst Case Partial-Band Noise Jamming," ICC'88 Proceedings, Philadelphia, PA., pp. 43.1.1-43.1.5, June 12-15, 1988.

9. L.E. Miller, J.S. Lee and A.P. Kadrichu, "Probability of Error Analyses of a BFSK Frequency-Hopping System with Diversity under Partial-Band Jamming Interference - Part III : Performance of a Square-Law Self-Normalizing Soft Decision Receiver," IEEE Trans. on Commun., Vol. COM-34, pp. 669-675, July 1986.

10. D.T. Torrieri, "Frequency Hopping with Multiple Frequency-Shift Keying and Hard Decisions," IEEE Trans. on Commun., Vol. COM-32, No. 5, pp.574-582, May 1984.

11. A.J. Viterbi, "A Robust Ratio-Threshold Technique to Mitigate Tone and Partial Band Jamming in Coded MFSK Systems," Proc. MILCOM'82, Boston, Mass., pp. 22.4.1 - 22.4.5, Oct. 18-20, 1982.

12. M.B. Pursley and W.E. Stark, "Performance of Reed-Solomon Coded Frequency Hop Spread-Spectrum Communications in Partial Band Interference," IEEE Trans. on Commun., Vol. COM-33, No.8, pp. 767-774, Aug. 1985.

13. S. Laufer and A. Reichman, "Analysis Of Frequency-Hopping Systems with Combined Convolutional and Diversity Encoding And Non-Ideal Interleaving in Worst Case Partial Band Jamming," ICC'88 Proceedings, Philadelphia, PA., pp. 43.2.1-43.2.5, June 12-15, 1988.

14. J.S. Lee, L.E. Miller and R.H. French, "Coded and Uncoded Performance of L-Hops/Symbol Frequency-Hopping Random MFSK Using a Nonlinear Diversity Combining Soft-Decision Schemes," ICC'87 Proceedings, Seatle, Washington, pp. 26.3.1-26.3.6, June 7-10, 1987.

15. D. Torrieri, "The Performance of Five Different Metrics Against Pulsed Jamming," IEEE Trans. on Commun., Vol. COM-34, No. 2, pp. 200-204, Feb. 1986.

16. P.J. Lee, "Performance of a Normalized Energy Metric without Jammer State Information for an FH/MFSK System in Worst Case Partial Band Jamming," IEEE Trans. on Commun., Vol. COM-33, No.8, pp. 869-877, Aug. 1985.

17. G. Ungerboeck, "Trellis-coded Modulation with Redundant Signal Sets - Part I : Introduction," IEEE Communication Magazine, Vol. 25, No. 2, pp.5-11, Feb. 1987.

18. J.L. Massey, "Coding and Modulation in Digital Communications," Proc. 1974 International Zurich Seminar on Digital Communications, Zurich, Switzerland, pp.E2(1)-(4), March 1974.

19. G. Ungerboeck, "Channel Coding with Multilevel/phase Signals," IEEE Trans. on Information Theory, Vol. IT-28, pp.55-67, Jan. 1982.

20. G. Ungerboeck, "Trellis-coded Modulation with Redundant Signal Sets - Part II : State of The Art," IEEE Communication Magazine, Vol. 25, No. 2, pp.12-21, Feb. 1987.

21. A.R. Calderbank and J.E. Mazo, "A New Description of Trellis Codes," IEEE Trans. on Information Theory, Vol. IT-30, pp. 784-791, Nov. 1984.

22. M.K. Simon and D. Divsalar, "A New Description of Combined Trellis Coding With Asymmetric Modulations," JPL Pulbication 85-45, July 15, 1985.

23. P.H. Wittke, P.J. McLane, S.J. Simmons, M.G. Wearring, Y.M. Lam and W. Hopkins, "The Study of Space Communications Spread Spectrum Systems (Phase IV )," Dept. of Elect. Eng., Queen's University, Research Report No.87-1, June 1987.

24. A.J. Viterbi and J.K. Omura, Principles of Digital Communication and Coding, New York : McGraw-Hill, 1979.

25. E. Biglieri, "High-Level Modulation and Coding for Nonlinear Satellite Channels," IEEE Trans. on Commun., Vol. COM-32, No.5, pp. 616-626, May 1984.

26. E. Zehavi and J.K. Wolf, "On the Performance Evaluation of Trellis Codes," IEEE Trans. on Information Theory, Vol. IT-33, No. 2, pp. 196 - 201, March 1987.

27. J.G. Proakis, Digital Communications, New York, McGraw-Hill, 1983.

28. M. Schwartz, W.R. Bennett and S. Stein, Communication Systems and Techiques, McGraw-Hill, 1966.

29. B.D. Trumpis, "On the Optimum Detection of Fast Frequency Hopped MFSK Signals in Worst Case Jamming," TRW Internal Memorandum, June 1981.

30. Q. Wang, T.A. Gulliver, V.K. Bhargava and D.W. Little, "Coding for Frequency Hopped Spread Spectrum Satellite Communications," Technical Report ECE-88-2, Dept. of Electrical and Computer Engineering, University of Victoria, April 1988.

INTERIM REPORT Part III
DSS Contract 36001-8-3528/01-SS

# A Study of Space Communications Spread Spectrum Systems Phases 5 & 6 UPLINK SYNCHRONIZATION

S.J. Simmons

Contents

## 1.0 Introduction

The system has been defined for the purposes of this study in the previous contract report [1] - PART III Synchronization of a Frequency-hopped Spread Spectrum Space Communications System. It is principally a point-to-point communications system based on circuit switching. Users communicate through a signal-processing satellite that dehops uplink transmissions from the group of users, separates individual user signals by frequency (uplink FDMA Fig. 1), and (after appropriate buffering) creates suitably formatted TDM frames for downlink transmission (Fig. 2). Call setup is performed by some central controller which may be satellite or ground based. In addition, there may be demand assignment of uplink and downlink channels to serve a large number of users with low duty-cycle access requirements.

Users transmit one of M tones every $T_s$ seconds to send $\log_2 M$ bits per symbol. We will confine our attention to the class of users whose data symbol rate is less than or equal to the hopping rate $R_h = 1/T_h$ such that there are $T_s/T_h = L$ hops per user data symbol, where $L \geq 1$.

Uplink synchronization refers to the process of a user adjusting his frequency hopping pattern, hop transition times, and nominal carrier center frequency in order that the satellite can detect the user transmissions. For this study, we are concerned only with coarse acquisition, that is, discovery of both the correct position in the long pseudo-random hopping sequence, and coarse carrier frequency, such that a second phase of fine adjustments may then be entered into to bring the transmissions into nominal alignment (strategies for fine sync are investigated in [4]). The distinction between coarse and fine synchronization here is partly a matter of degree in how much loss is encountered due to remaining misalignment, but more importantly, coarse acquisition brings the user from the point of having no (or virtually no) signal energy detected by the satellite in the user's normal channel to having some significant energy detected; it is at this point that we wish to declare coarse acquisition.

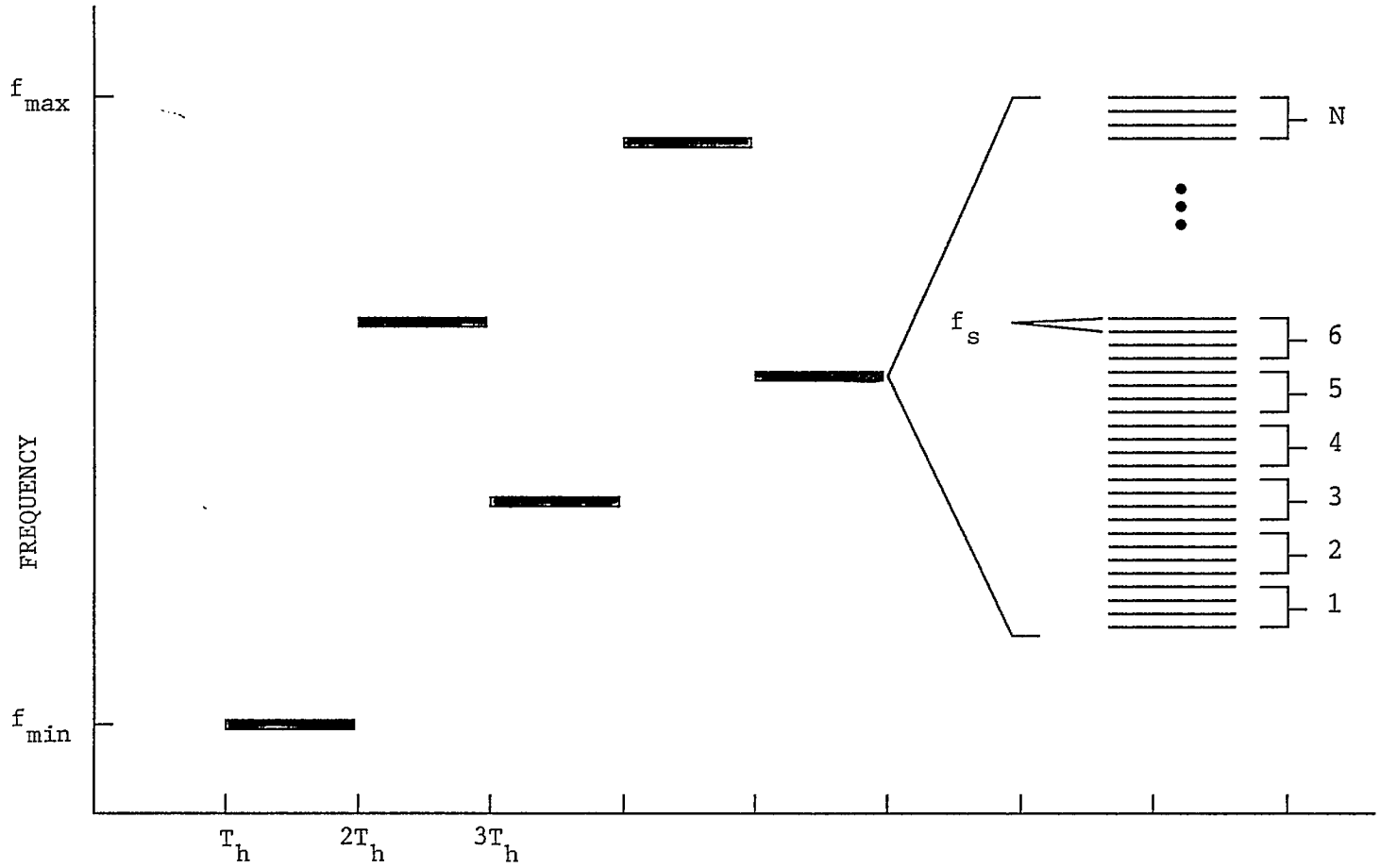


Figure 1: Uplink format for a group of N users employing 4-ary FSK.

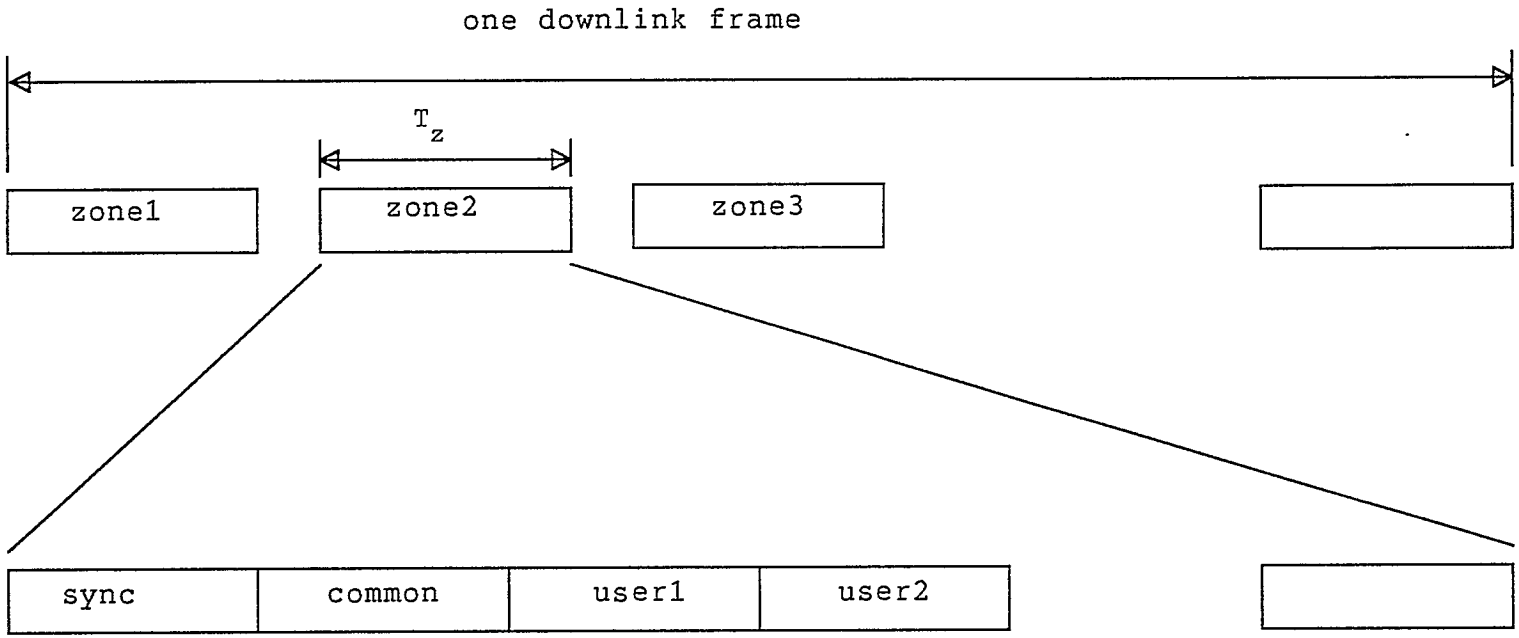


Figure 2: Downlink TDM format

Feedback from the satellite is necessary for synchronization. We assume that when user A is not actively engaged in a call, the network controller assumes user A to be in an unsynchronized state, and configures the satellite to direct all detections from user A's uplink slot to user A's downlink slot (a default "loopback mode"). Alternatively, these "loopback" resources may be separate from the user's normal slots, and shared on a round-robin or random-access basis with other users in a demand-assigned system. The important point is that some (even if very small) fraction of satellite resources must be dedicated to every possible user in a feedback mode so that they may attempt to synchronize at a-priori unknown (random) times.

We assume throughout that downlink synchronization is a given, so that users can read the downlink data. It should be kept in mind that basic uplink synchronization must be achieved in the absence of any knowledge about the formatting of data into blocks or messages, that is, before any higher-level protocol synchronization is achieved. This implies that the synchronization process must rely on only raw symbol detection data being placed at (approximately) known positions in the downlink frames. One resulting problem is that a user first attempting to synchronize will generally not yet know his propagation delay to the satellite, and therefore cannot immediately define a one-to-one correspondence between sync probe tones sent on the uplink hops and the corresponding data returned in the downlink frames. This is discussed in Section 10.0 below.

## 2.0 Objectives and Approach

It is the aim of this study to assess the expected time to acquire coarse synchronization $T_{acq}$ (a related but more difficult problem is determining the probability that sync time exceeds a given amount). This acquisition time of course depends on the SNR (signal to noise ratio) and SJR (signal to jamming ratio) at which the system is operating, on the jammer type, on the search strategy employed, on the format of the sync probe signals and the loopback downlink return data, and on the initial parameter uncertainties.

To restrict the large number of possibilities, we might look at one "low-end" and one "high-end" sync procedure, and produce a set of curves of average sync time vs. SJR and SNR for each. This will establish limits on what is possible. The low-end sync procedure will employ the simplest (most straightforward) search strategy and attempt to achieve maximum transparency, .i.e. to use signals and downlink returns identical to those employed for normal transmissions. The high-end procedure will employ a more powerful search strategy, and might relax the transparency requirement, all in the hope of a lower expected sync time. We intend to consider both partial band noise (PBN) jammers and multitone (MT) jammers.

Although the sync procedures are naturally attempting to distinguish between background jamming and the presence of user sync probe signals, we will not overtly incorporate any features that attempt to identify jammed hops. This may possibly lead to a longer expected time to sync, but the resulting procedures will be simple and robust. We expect to use an analytical approach to find performance of the low-end system, and simulations aided by analysis to find the performance of the high-end system.

Throughout it will be necessary to modify conventional frequency-hopping synchronization procedures to account for the special conditions imposed by the satellite-based receiver, namely, the large propagation delay before downlink returns can be seen, and the inability to directly access the output of the frequency dehopping receiver.

## 3.0 Initial Timing/Frequency Uncertainties

Conceptually, the whole synchronization problem arises as a result of timing and frequency differences between satellite and ground equipment occurring after satellite launch. More realistically, these differences will be due to the physically distant hardware never having been synchronized by physical connection, or by drifts between equipment over the interval between the last use (when synchronization was achieved) and the current use.

Timing uncertainty arises from differential drift between clocks on the satellite and those in the user equipment on the ground, as well as uncertainties in the propagation delay to the satellite, $t_{prop}$. When a user first attempts to transmit to the satellite, it is likely that his frequency-hopper will be several hops different from that of the satellite to which he must match, and that the timing of the hop transitions will be in error with a uniform distribution over $[0, T_h]$. Note that at sync, the user's transmissions must be adjusted so that the signal arrives properly aligned at the satellite after the propagation delay $t_{prop}$. In order to reduce the initial uncertainty in the hopping sequence phase, the following strategy has been proposed: users monitor a common slot in the downlink which contains data on the periodically-sampled internal state of the satellite's frequency hopper, and data which gives the time lag inside the satellite before that sample is added to the downlink data signal. If users load the sampled state into their replica sequencers, adjust for the delay from the sampling point and for downlink propagation delay, and run their sequencers ahead to adjust for uplink propagation delay, they should be in error by no more than the round-trip delay uncertainty. At a hopping rate of 20 kHz (50 usec per hop), a range error of 15 km tranlates into a hopping sequencer error of one hop. With geostationary satellites (positional drift on the order of 100 kM), and modest ground-positioning accuracy, this scheme should keep initial hopping sequence phase uncertainty to plus or minus a few hops. The range of hop phases that must be searched to acquire synchronization will be drastically reduced.

There is no need to protect this sequencer state information from discovery by an adversary. We can simply ensure that in addition to the sequencer state, users need to load a secret key that completes the true state of the sequencer. This secret key must be distributed by another secure means. The approach is described in more detail in [1].

The magnitude of the initial frequency uncertainty has not been specified. Presumably, it depends on the frequency synthesizers used. What is certain is that if the system is to operate at all, these synthesizers must be able to move the hopping carrier with an accuracy on the order of a few kilohertz

every $T_h$ seconds. Whether such ability implies that initial carrier accuracy will be comparable is uncertain. We will therefore assume that although the frequency synthesizers are capable of very accurate relative carrier motion, they must be closed-loop adjusted to achieve accurate nominal center frequency, and that the initial uncertainty in this nominal center frequency can be many times greater than the separation between users. If this is not the case, given the strategy outlined above for reducing initial hopping phase uncertainty to a few hops, there really is not much of a coarse synchronization "problem" to speak of (it would only require transmission attempts at each of the few possible hopping sequence phases to achieve successful detections at the satellite - elaborate search strategies would be unnecessary).

The presence of large initial frequency offsets in the FDMA group may require a user position "permutation" strategy to be employed to avoid a neighbour's synchronization attempts consistently interfering with an active user (or another user also attempting to synchronize). By permuting user positions within the group from hop to hop, users attempting to synchronize with large initial frequency offsets will appear as random tone jammers to the other active users. The unattractive alternative to this is to restrict synchronizing users to low duty-cycle transmissions.

If large initial frequency offsets are indeed a reality, it is frequency uncertainty that could greatly dominate the time to acquisition of sync. This being the case, it may be worthwhile contemplating dedication of a larger portion of satellite resources for synchronization purposes. An approach that uses a dedicated "sync" band that is shared on a random access basis is discussed in Section 11.0 below.

## 4.0 Misalignment Effects and Search Strategies

The search for synchronization occurs over a two-dimensional grid of cells having carrier frequencies separated by $\Delta F$, and hopping sequence phases separated by a fraction of (or possibly a whole) hop $\Delta T$ (see Fig. 3). The

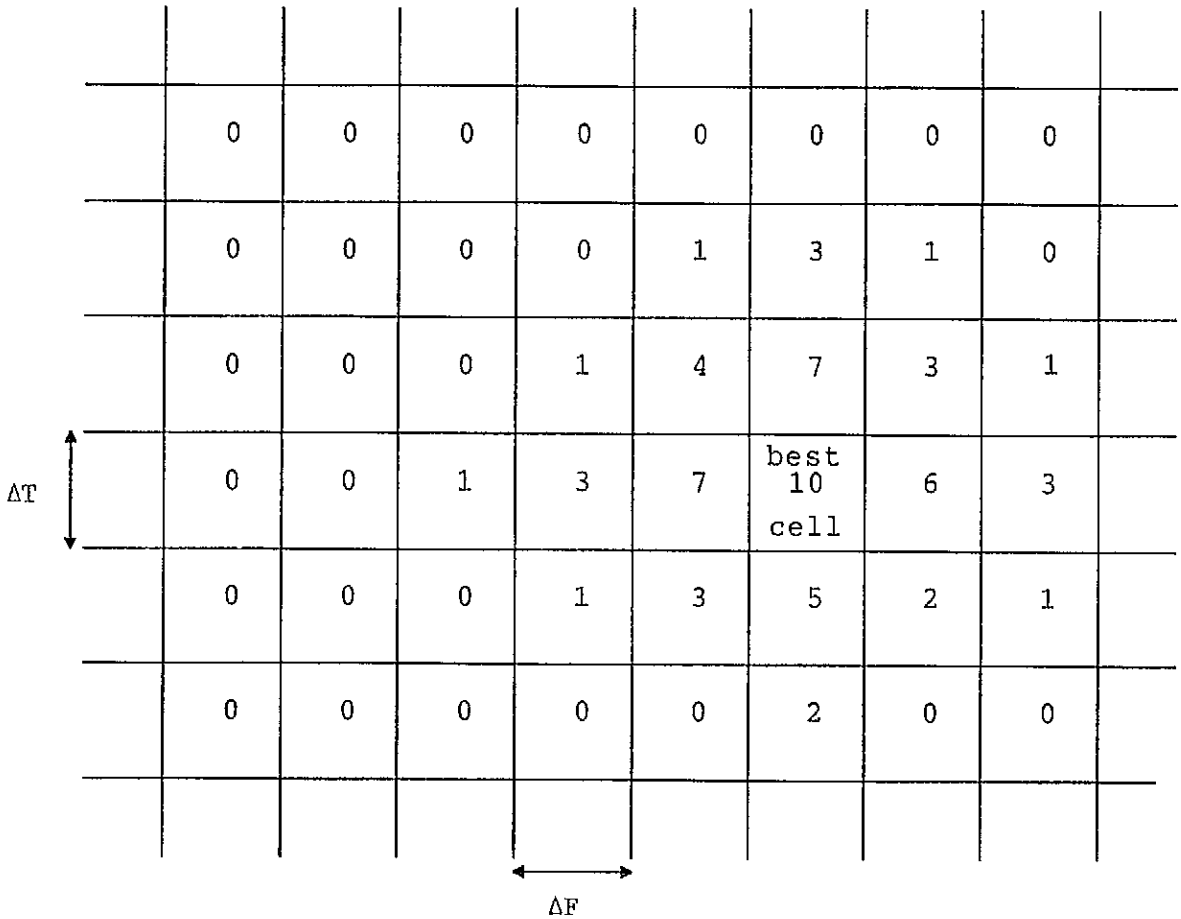


Note: Numbers indicate alignment quality in each cell.

Figure 3: Two-dimensional search grid for coarse synchronization.

number of cells is determined according to the maximum initial uncertainty in both parameters. To synchronize, users will dwell for some time within a cell (transmitting signals as sync probes) and check the downlink return for valid detections. A user may declare firm acquisition, no acquisition, or probable acquisition. If a strategy uses declarations of probable acquisition, once such a declaration is made, we enter into a verification phase with increased observation time in the cell being evaluated. If verification succeeds, we declare firm acquistion. If the initial declaration of probable acquisition is false, we incur the time for the failed verification phase as a penalty. The probability of false alarm must be tailored to this time penalty to achieve the lowest possible overall time-to-firm-declaration of coarse acquisition.
This final declaration must be made with great certainty as a very large time penalty will be incurred before any false synchronization is discovered.

The time spent in each cell and declarations made depend on the search strategy. There are a range of strategies from simple (count detections and compare to a fixed threshold, spending an equal amount of time in each cell) to complex (sequential probability ratio test giving variable dwell times on each cell). The coarseness of the grid quantization ($\Delta T$ and $\Delta F$) is subject to optimization: the larger these quantities, the greater the maximum signal loss due to worst-case residual misalignment (and the longer the expected dwell time needed), but the fewer the number of cells to be searched. The choice of the cell sizes is strongly tied to search strategy, and is something which will be investigated.

It is assumed that the user transmissions are detected by a SAW based receiver that in effect performs a Fourier Transform (with additional optional windowing) on the input signal over each hop duration, producing the energy in each of the M tone bins of each user. In the presence of misalignments, the signal presented to the detector after dehopping and IF filtering is as in Fig. 4 (assuming a single tone transmitted for the hop duration). After IF filtering, a portion of the sync tone will be absent with misaligned hop times (the entire tone is missing with incorrect hop

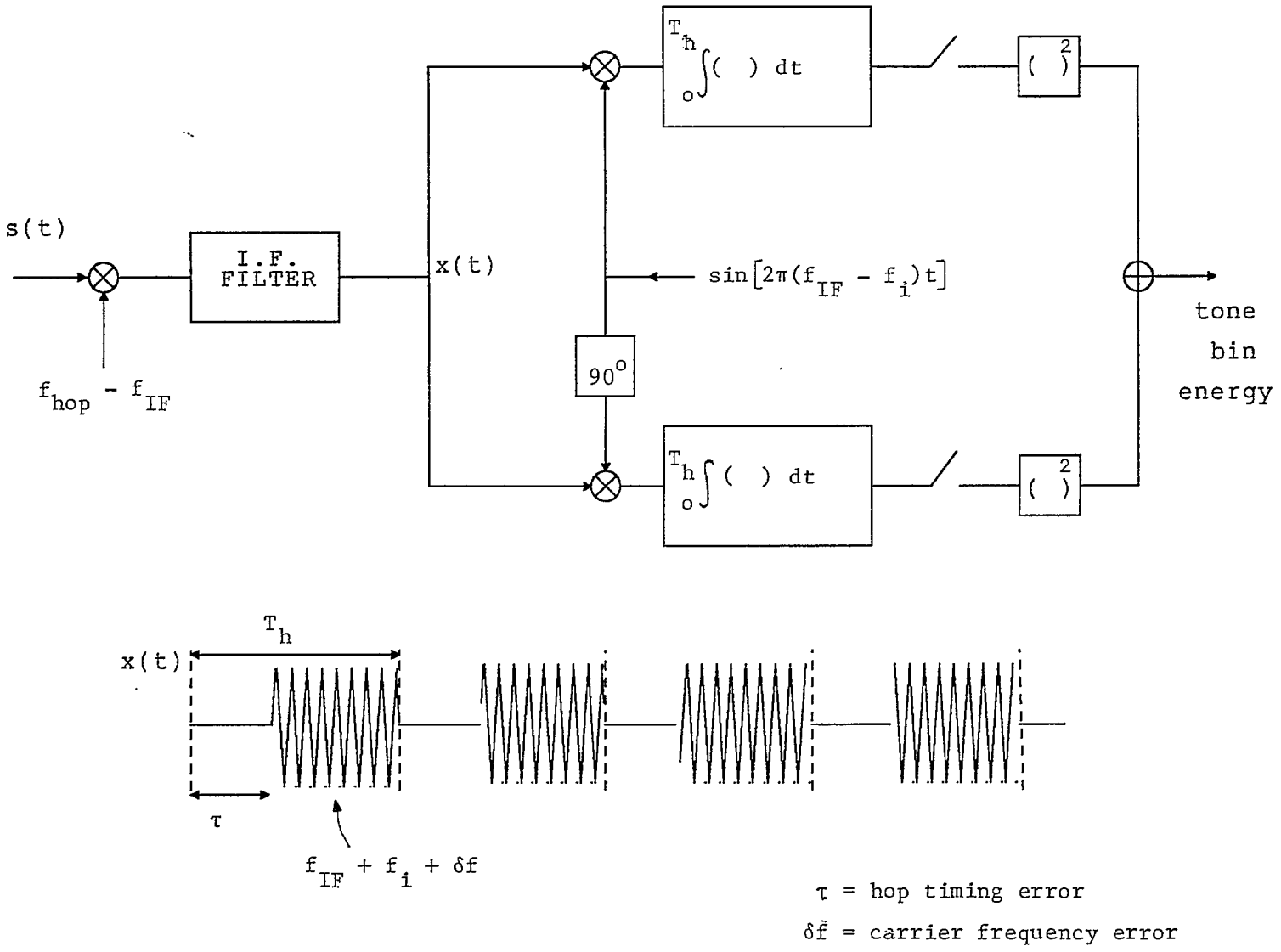


Figure 4: Detector structure and effect of alignment errors.

sequence phases), and the remaining portion contains a frequency error. Most cells will represent complete absence of synchronization, i.e. no (or virtually no) signal energy detected by the receiver. One cell will represent best alignment or full synchronization, and the rest of the cells will represent, to varying degrees, partial synchronization. The degree of alignment is represented by the numbers assigned to the cells of Fig. 3 . The time and frequency errors in these cells translate directly to a loss in signal energy (assuming matched filter reception with no additional windowing) according to the following equation [2]:

$$\text{fractional loss} = \frac{\sin^2 \Pi \delta f (T_h - |\tau|)}{(\pi \delta f T_h)^2} \quad ,$$

where $\delta f$ and $\tau$ are the residual frequency and time errors.

In actual operation, we can expect to sometimes declare sync in a cell even though a cell with better alignment exists. As part of the procedure, once a possible detection is declared, we will naturally step to adjacent cells to check for better alignment, and these "early" declarations will speed up synchronization. To simplify the analysis, and produce conservative results, we can ignore this help from cells adjacent to the one of best match. Furthermore, we can consider the worst case alignment at this best cell. For example, if the grid spacing is $\Delta F$, and adjacent cells are separated by one full hop ($\Delta T = T_h$), we would assume that only one cell exists with "correct" alignment and that this alignment has a residual frequency error of $\delta f = \Delta F/2$ and that half the tone is missing ($\tau = T_h/2$).

Propagation delay places unique constraints on the search procedure used. We are unable to see the feedback from a given test signal until the full round trip propagation delay, which for a geostationary satellite, is in excess of .2 seconds. There is also buffering delay on the satellite, but this will be negligible in comparison. Two tenths of a second at a hop rate of 20 KHz amounts to 4000 hops. This does not mean that we must dwell at every cell

for 4000 hops minimum. We can avoid this by "pipelining" the probe signals so that probes for evaluating many cells are issued without waiting for the return, as shown in Fig. 5 . By keeping a running history of the issued sync tones for each cell that is probed in turn, we can still match up the downlink returns that arrive over .2 seconds later and achieve a high search rate.

Our search strategy will determine how many hops we wish to dwell in each cell. If there are only C cells to be evaluated, we will have to spend at least 4000/C hops in each whether we need to or not. There is an incentive therefore to have a minimum C value that makes the search more efficient. Note that there are implications for multiple-dwell or variable-dwell searches. In these strategies, the amount of time we dwell in a cell depends on the observations made to date in that cell. The feedback delay clearly has a significant impact here. It will be necessary to break the total observation time into separate phases where these phases are separated in time by $2t_{prop}$. In each phase we send some multiple of the initial dwell time in hops, and there must be many of the same evaluations for other search cells in the pipeline for efficiency. In effect, we must be processing many search cells in parallel to avoid inefficiency due to the large $t_{prop}$. At the start of the search, we may be looking at a very large number of cells with a short dwell time of only tens of hops; towards the end of the search procedure we will be narrowing the search and looking at only a few cells with much longer dwell times. Clearly, the search strategy must be designed with propagation delay in mind.

## 5.0 Loopback Downlink Return Data

The downlink data returned in loopback mode depends on the type of sync probe signals we use, and the strategy we wish to detect these signals with. The number of bits we want to extract each hop depends on our detection strategy, for example, do we need access to the energy detections in many bins, or do we simply need a hard decision on one of M tone bins? The number

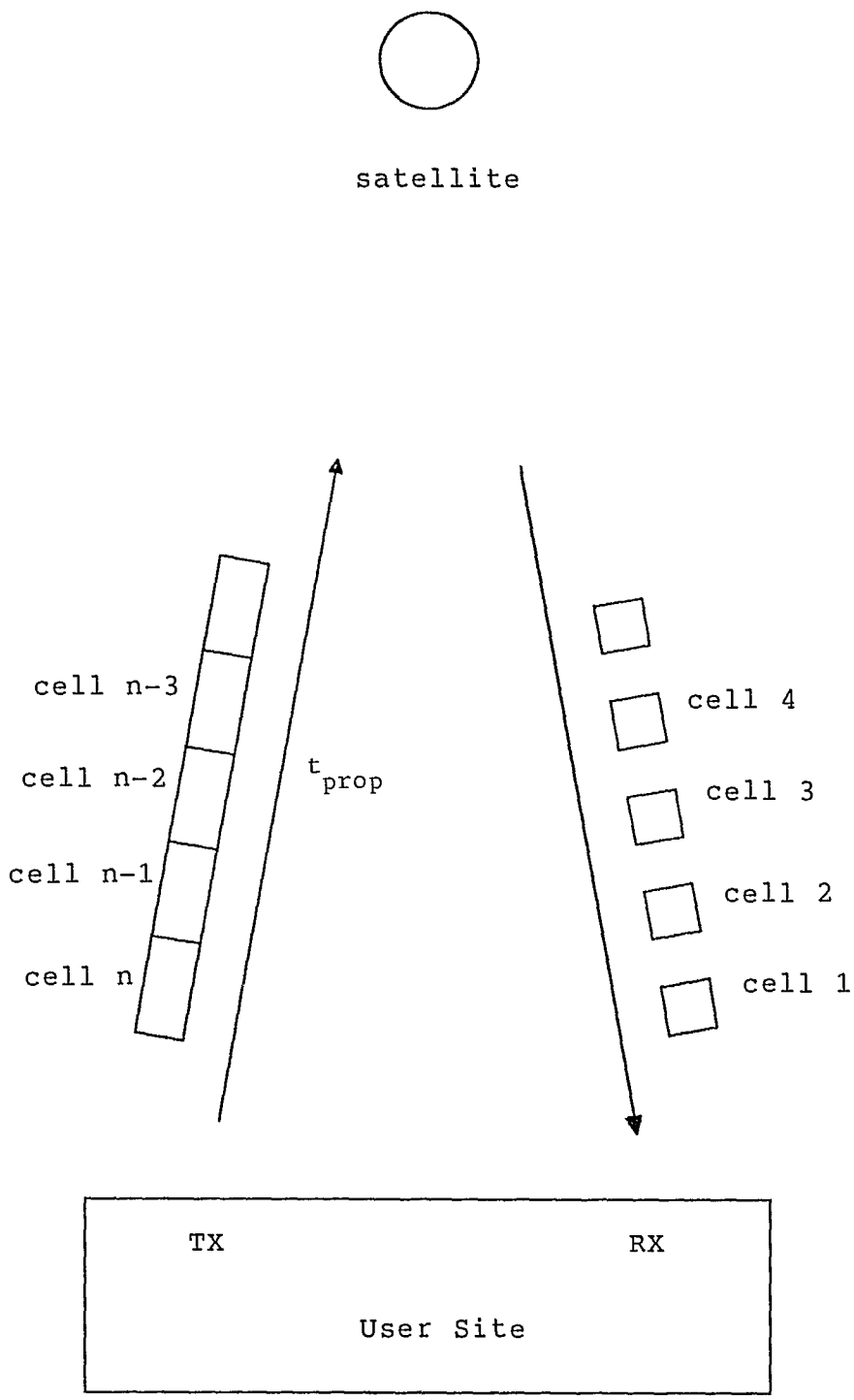


Figure 5: Pipelining the search

of bits we send on the downlink will also depend on how much processing we can apportion to the satellite, and how much must be done on the ground by the user attempting synchronization. Minimization of statellite processing hardware is important, but so too is the downlink data bandwidth required for sync purposes. In fact, in a demand-assigned system, the available downlink resources for sync might be only a fraction of what is available to users actively engaged in a call. This does not necessarily mean we are overly restricted in the types of information that we wish to extract from the receiver. For example, we can take multiple-bit samples of energy detector output from the SAW for each of the M user tone bins per hop, but we may need to average these over multiple hops, or only take this for every N'th hop to match to the available downlink data rate. This latter approach is clearly undesirable as it wastes available user signal power. It also seems important to aim for a good deal of transparency, that is, to avoid requiring separate hardware and different configurations for sync purposes as opposed to normal user-to-user transmissions.

## 6.0 Choice of Uplink Sync Probe Signals and Detection Strategy

A critical part of the specification of the sync procedure is the type of uplink signal used as a sync probe, and the strategy with which we intend to detect the presence of this signal. The obvious approach is to send one of the M tones as the sync probe signal. This keeps ths signal format identical to that needed for normal data transmissions. It is not at all obvious, however, that this is the best choice. What we are trying to do at synchronization is very different from what we are a trying to do during normal data transmission. During normal data transmission, we are attempting to send multiple bits every few hops. For synchronization, we are really only trying to discover one bit of information - whether the user signal energy is aligned or not in time and frequency - and we can take many hops to do this. In order to make this one-bit decision as quickly as possible, we would like to use a sync signal which is clearly differentiable from a background of noise and jamming, .i.e. it should look as different as possible from what we expect to see from noise and jamming (see Fig. 6).

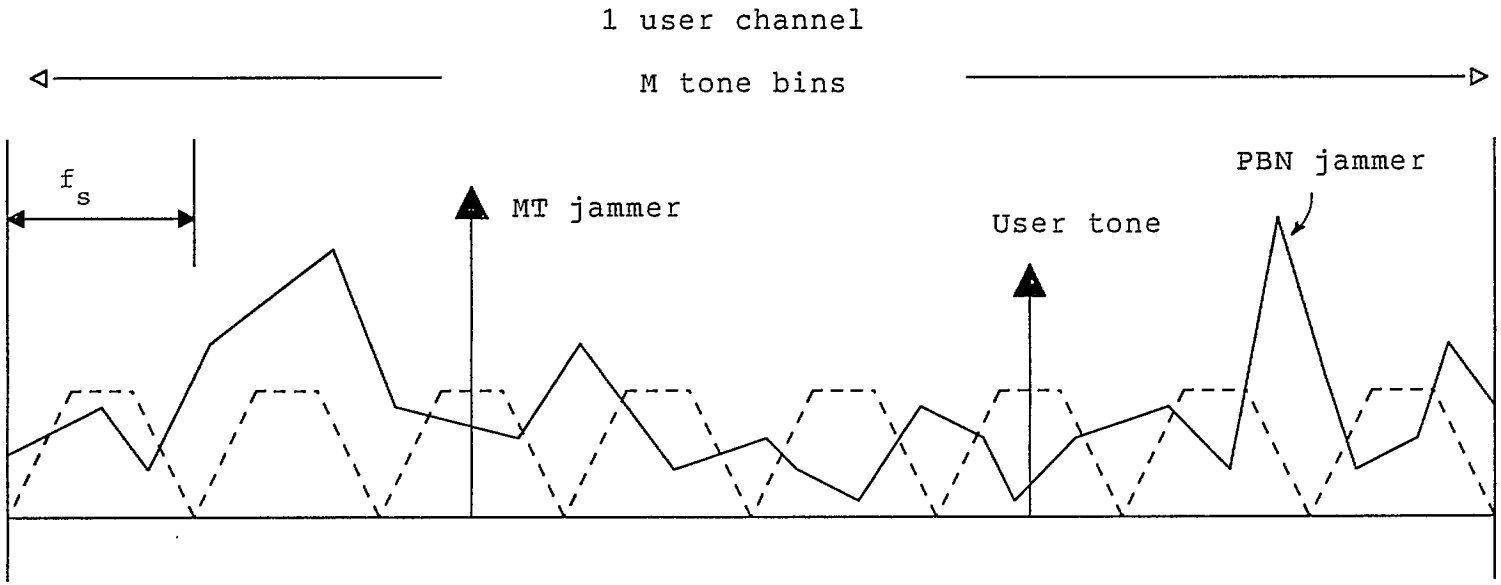


Figure 6: User sync probe signal with jamming background.

Ideally, we would like to concentrate the user signal energy in time and frequency, but we must still live within the constraints imposed by the M-ary FSK signal format, the need for frequency hopping, the limit on peak transmitter power, and the use of a SAW-based receiver. The single sync tone per hop seems to fit this bill. Spreading our available signal energy in frequency between multiple tones per hop does not appear to mesh with the objective of looking as different from jamming sources as possible. With the single tone sync probe, one precaution is necessary: the tone bin should be chosen randomly from hop to hop to thwart multi-tone jammers. Since the user is aiming for a particular bin and will be off the mark for all but the very last stages of sync acquisition, we avoid confusion by calling the bin that is being aimed for the "intended" sync tone bin.

Some sync procedures may require processing to be performed on board the satellite to avoid having to send too many bits on the downlink as loopback data. To do this, the satellite may need to know which is the intended sync tone bin. This can be accomplished by selecting the sync tone bin according to the $\log_2 M$ least significant bits of the K bits that select each of the $2^K$ hop frequencies. In this way, at correct sync alignment, both the satellite and user agree on the intended sync tone.

There are several alternatives for detection strategies. We might consider comparing detected energy in the intended tone bin to some threshold. This energy may optionally be averaged over some number of hops with some sort of hard limit on the energy detected in the sync tone bin each hop (to prevent the presence of heavily jammed hops from skewing the result and causing a high number of false detections). The threshold must be set to give reliable detection of the presence of the sync tone even with partial alignment, while reliably rejecting background noise and wide-band jamming. A very important consideration in such a threshold scheme is the uncertainty in received signal power level at the satellite. This uncertainty will arise from unknown signal fading levels and antenna pointing errors. If we don't know what to expect for received energy in the intended tone bin, it becomes very difficult to select a useful threshold. One possibility is to add the

antenna pointing angle as an additional search dimension, and set the threshold assuming some nominal fade level. This has its problems. If we are faded less than nominal, we won't be able to take full advantage of the extra signal level; if we are faded more than nominal, we may be making almost no use of the signal energy that is being received. And we still end up expanding and lengthening the search because of the additional antenna pointing-error dimension. It would be much better to avoid reliance on a threshold that does not allow for user signal power variation.

One way to accomplish this is to measure the average background jamming and noise per bin, and simply set a detection threshold equal to that level. When the user gets close to sync, the presence of user signal energy will put a positive bias on the average energy in the intended bin, and cause the detection threshold to be exceeded for a good percentage of the hops. There are two variations here. In the first, we average the background energy detected in bins known to be unoccupied by other users. This can be done using N bins from one hop, 1 bin from each of N hops, or something in between. The energy in the intended sync tone bin is then averaged over an equal number of hops, N, and if larger, tone detection is declared. Note that this is not the same as declaration of sync acquisition, which may require many such tone detections.

The other variation is to instead make the detection decison on a hop by hop basis, and then count up these detections over N hops. For each hop, we can simply compare detected energy in the intended sync bin to one other "unoccupied" bin, in effect picking the better of the two. It is not clear which of these two variations would be superior, but the latter provides an automatic hard limiting effect to prevent severely jammed hops from skewing the results, and appears to be more simple and robust than the energy-averaging scheme.

The detection scheme just outlined will produce some probability of correctly detecting the presence of the sync tone $P_d$ (which depends on the received user signal energy plus alignment errors in time and frequency) and a probability $P_{fd}$ of falsely detecting the presence of the sync tone

when it is in fact not present (no user sync). A threshold will be chosen for the number of sync tone detections that need to be seen over some number of N hops before declaration of sync tone presence (i.e. acquistion or possible acquisiton) can be reliably made. This threshold will be set to produce overall probabilities of detection and false alarm that are tailored to the searching strategy to be employed. The probability of false detection per hop $P_{fd}$ for this scheme is the probability that the energy in the intended sync tone bin exceeds the energy in one particular bin selected from the other M-1 tone bins when user energy is not present, and is clearly equal to 0.5. It may take many hops N to make a reliable declaration with a low enough false alarm probability. We can lower $P_{fd}$ very simply. Instead of comparing the energy in the intended sync bin to that in just one of the other bins, we could compare it to <u>all</u> M-1 other bins, in effect finding the bin of highest energy. This reduces $P_{fd}$ to 1/M while slightly reducing $P_d$. It is probable that by a judicious lowering of the detection count threshold, we can maintain a given probability of correctly declaring presence of the sync tone over the N hops observation while lowering the probability of false alarm, achieving an overall net benefit and lowering expected time-to-acquistion $T_{acq}$.

We can get any desired $P_{fd}$ by comparing to any number of other bins we want. For low M, these extra "unoccupied" bins can be readily provided as common sync resource located at the edge of the user group band. There is a small practical complication with choosing other than a best 1-of-M detection approach: to avoid sending on the downlink the energies for all M bins each hop, the satellite hardware would need to make the decision on board, and only relay the bits of that decision. This requires that the satellite know the intended sync tone bin each hop. This can be guaranteed as outlined earlier in Section 6.0 .

The number of other bins with which we compare, $M^*$ , is subject to optimization; there will be some point at which the decrease in $P_{fd}$ no

longer provides a net benefit because the drop in $P_d$ is too large. This optimum will be the subject of study.

## 7.0 Advantages of A Best 1-of-M* Approach

From the standpoint of maintaining transparency with hardware needed for normal data transmissions, the best 1-of-M* approach suggested in the previous section is attractive. There is no need for extra satellite hardware to perform averaging or combining operations. In addition, for $M^* = M$, it generates only $\log_2 M$ bits per hop, which depending on the system implementation, may be matched to the downlink return data rate during normal data transmissions. If diversity combining is done on board the satellite, $\log_2 M$ bits per hop would represent a downlink data rate expansion by a factor of L. We might, however, simply modify the best 1-of-M sync procedure to use these symbol decisons rather than the hop decisions, so there would be again no downlink data rate expansion. This may, however, lead to a degradation in performance. This is subject to investigation. The ramifications of on-board diversity combining are discussed below.

There are two other important benefits to a best 1-of-M* approach. The first is that the false alarm probability is fixed independently of jammer strategies, jamming levels, and noise levels. The resulting sync procedure is absolutely "bullet-proof" as far as false alarms go. Jammers cannot increase the probability of false tone detection given no sync. Secondly, analysis is greatly simplified. To evaluate $T_{acq}$, we can use a two-step procedure. Since $P_{fd}$ is fixed, we start by selecting $P_d$, and evaluate $T_{acq}$ given our candidate search strategy. Then to cast $T_{acq}$ as a function of SNR and SJR, we need only relate $P_d$ to SNR and SJR. But this is straightforward; we can translate worst case frequency and hop time alignment errors in the best search cell ($\Delta F/2$ and $\Delta T/2$) into equivalent energy losses and apply the

results of [3] to find $P_d$ at any SNR, SJR, and jamming strategy. This is a very clean two-step approach.

## 8.0 Effect of Jammers/Noise and Misalignments on Synchronization

Here the relative effect of jammers and background noise on the best 1-of-M* detection scheme is briefly discussed.

Figure 7 shows the situation with frequency alignment errors. If these alignment errors are less than $f_s$, we have approximate alignment. All randomly selected sync tones will fall into one of the bins in the user channel that the satellite defines; there will be an equal signal energy loss for each which depends on the residual alignment errors $\delta f$ and $\tau$ defined in Section 4.0. If the frequency errors are several times the bin spacing $f_s$, only a fraction of the randomly-selected user sync tones will fall into any of the bins at the satellite. Note that this actually has a beneficial effect in that it significantly reduces the probability of false detection $P_{fd}$ as we get within about M/2 bins of proper alignment. In that case, about half of the total time, the transmitted sync tones appear in the incorrect bins where they have a high probability of winning the best 1-of-M competition. The probability of seeing the intended tone bin win out is correspondingly reduced, lowering $P_{fd}$. We will ignore this helpful but minor effect in what follows, and also in analysing the performance of the best 1-of-M scheme.

It is also clear from Fig. 7 why we could not use a different approach based on looking for a consistent winner among <u>any</u> of the M bins in the hope of reducing the frequency search time. That would work for large frequency errors (such as depicted in the middle of Fig. 7) only if the location of the sync tone probe was fixed in a particular bin. But as discussed earlier, this should be avoided because of susceptibility to MT jamming.

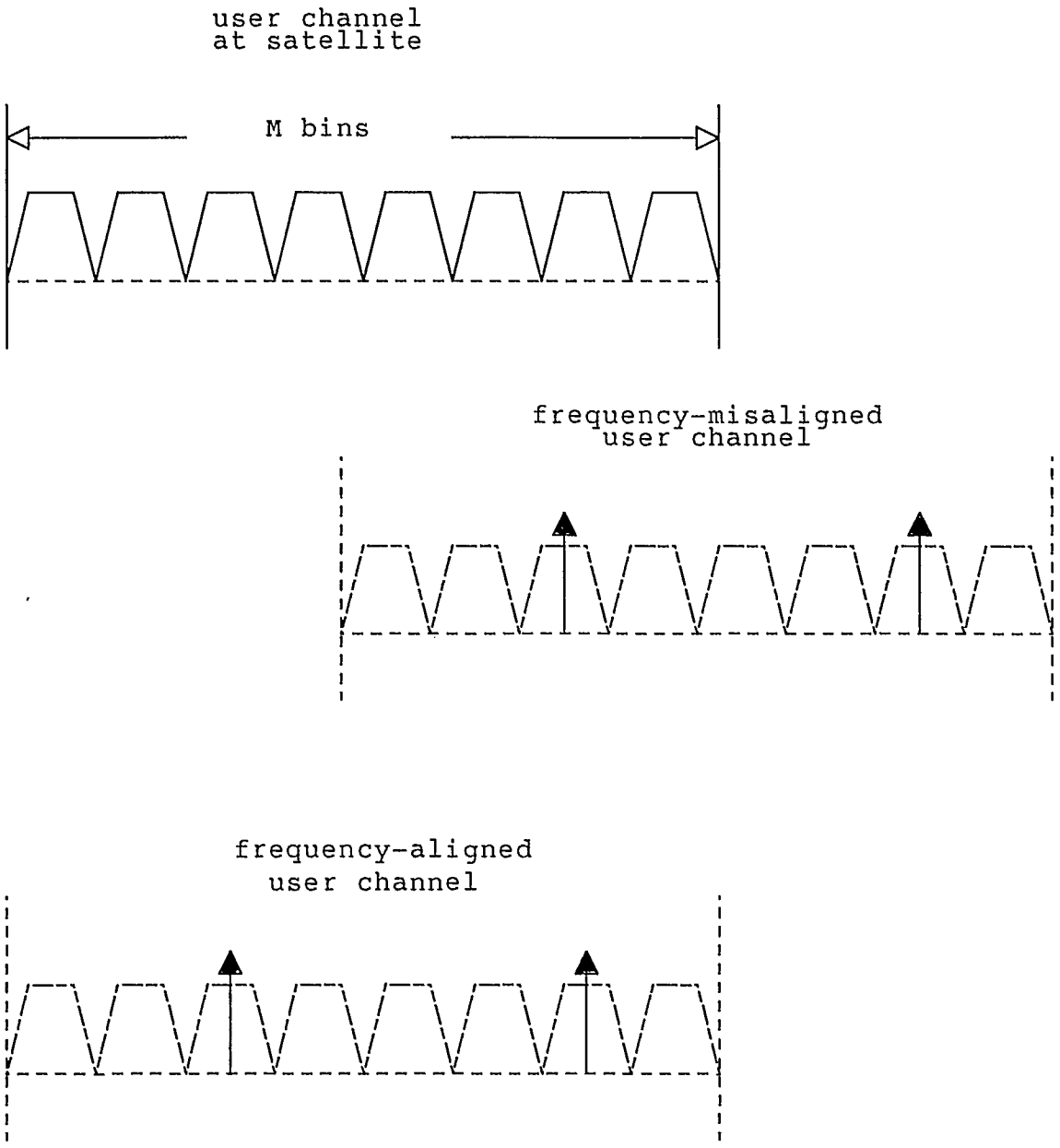


Figure 7: Frequency alignment errors with a best 1-of-M strategy.

Consider first the case of negligible background noise (SNR is high) and no diversity (L=1). The jammer is of any type with a fraction $\gamma$ of the hop band jammed. In order to effectively jam normal user data transmissions, $\gamma$ is typically a small fraction unless the jammer has very large power resources in which case he does better with a larger $\gamma$. For small $\gamma$, a large percentage of the hops during sync will be clear, and user signal energy will be reliably detected during these hops ($P_d$ is high). And independent of whether the hop is jammed or not, the probability of getting a false sync tone detection, $P_{fd}$, is only $1/M^*$.

Now consider the case of non-negligible background noise. For example, the SNR may be at a level to give a $10^{-3}$ probability of error on an unjammed hop for a fully synchronized user during normal data transmission (again no diversity; L=1). During sync acquisition, we must account for signal loss due to alignment errors even at best alignment, and this depends on the coarseness of our search grid ($\Delta F$ and $\Delta T$). But at this SNR we should not have to choose $\Delta T$ and$\Delta F$ overly small to still retain a modest probability of tone detection on an unjammed hop of, say, $P_d = 0.8$. For small $\gamma$, the presence of sync will still be readily distinguishable from the (no more than) one in $M^*$ false detections caused by jamming. For example, consider $M^* = M = 8$, $P_d = 0.80$, with counting of detections over 10 hops. With a threshold of five or more detections for declaring sync detection, the probability of false sync detection is only about .005, while the probability of correctly detecting sync is about .994 (from binomial distribution tables). Doubling the observation interval to 20 hops rapidly reduces the probability of false sync declaration. And because $P_{fd}$ is independent of jamming, even if $\gamma$=1 we can still reliably detect presence of sync as long as a modest $P_d$ can be maintained.

Now consider the case of high diversity (L large). The need for large L implies a low SJR. A "majority-vote" diversity of L=9 with M=8 can achieve a

symbol error rate (for synchronized users) of around $10^{-3}$ (after combining) starting from a $P_s = 1 - P_d$ (probability of missed tone detection on one hop) as large as 0.4. Now for an unsynchronized user, the alignment errors will cause a loss of signal energy, and a corresponding error probability $P_s$ that may rise toward 1-1/M. This corresponds to a probability of correct sync tone detection approaching 1/M, and it will take a very long time to distinguish this case from the unsynchronized false detection probability of 1/M. This implies the need for small enough $\Delta F$ and $\Delta T$ to keep alignment losses small. Of course, there will be tradeoffs of search cell size versus observation time as suggested earlier. This will be the subject of investigation.

The above discussion suggests that synchronization will be fast unless jammer power is sufficiently high that diversity needs to be employed during normal data transmission. The most detrimental form of jamming would appear to be MT jamming with a high $\gamma$ (implying high jammer power).

## 9.0 Diversity Considerations

Under low SJR conditions, diversity combining over L hops may be needed to achieve an acceptable error rate during normal data transmissions. A simple majority vote after best 1-of-M detection has been suggested in [3]. The issue arises as to whether the diversity L is fixed as part of the system specifications, or may be allowed to vary in response to changing user and/or jammer signal levels (clearly the latter is more efficient). A change in L means a change in data rate, and must be handled by appropriate protocols.

The complexity of varying L depends on whether the diversity combining is done on board the satellite or is handled by the user on the ground. Highest flexibility is achieved by leaving diversity combining to the ground user, but the cost is an expansion of downlink data rate by factor L. There are, however, problems for the synchronizing user if the combining is done on the

satellite. First, majority-vote combining, while good for estimating which of M symbols was sent during normal data transmissions, is information lossy for sync purposes. Because the satellite has no way of determining which value of L a user may need, L would have to be fixed ahead of time for sync purposes. If L were fixed at the maximum value, then with good signal levels, sync might be delayed by almost a factor of L. But with poor signal levels, the information loss may be so excessive as to make sync acquisition almost impossible. Secondly, an unsynchronized user would have to search over all L possible starting positions for the diversity combining in order to discover the particular L-grouping that the satellite was using. This can lengthen acquisition by up to a further factor of L. This suggests that no diversity (L=1) should be employed for sync purposes. The downlink data rate expansion in this case may be unacceptable (especially in a demand-assigned system) necessitating the use of only every L'th hop. This again lengthens the sync acquistion time, but not as much as if diversity were to be used.

## 10.0 The Initial Correspondence Problem

When first synchronizing, a user will be uncertain as to the exact propagation delay $t_{prop}$ to the satellite. As mentioned earlier, a range error of 15 km translates into 1 hop time uncertainty at $R_h$ = 20 KHz. With a geostationary satellite having a positional uncertainty of 100 km, even if the user knows his ground position very accurately, there would be a resulting delay uncertainty of plus or minus 3 hops. What this means is that the user does not know the exact correspondence between the signals he is sending on the uplink hops and the data the satellite is returning on the downlink. The problem is depicted in Fig. 8. The user transmits in one uplink frame, which the satellite detects and formats into a (delayed) downlink frame. Here we assume for clarity that the satellite is sending the user at least one bit per hop on the downlink in loopback mode. The unknown propagation delay error is represented by the horizontal offset of the frames. The user is forced to match up his uplink transmissions that

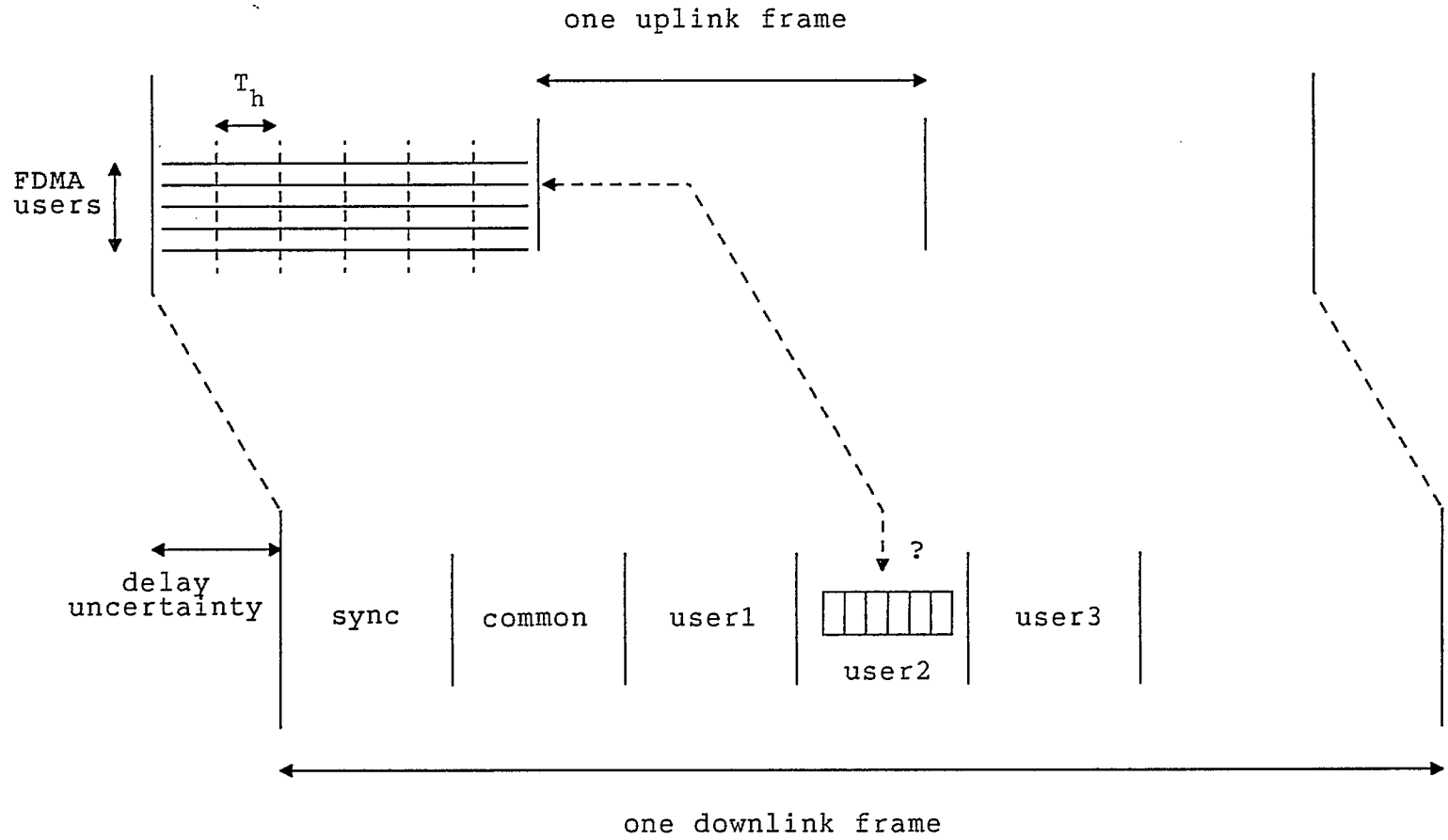


Figure 8: The initial correspondence problem.

occurred approximately $2t_{prop}$ seconds ago with each of Q possible correspondence positions in the downlink data.

Consider this example. We are using a best 1-of-M approach with a dwell time in each cell of 10 hops, and a propagation delay uncertainty of Q=6 hops. To check the results of probing a given cell, we attempt to match the ten intended sync tone bins (that were transmitted when probing that cell and have been stored in memory) to groups of ten contiguous detections in the downlink data, trying six different start positions for the group of ten, three of these positions delayed from nominal, and the other three advanced from nominal. Each of these Q=6 positions can, however, be tested in parallel, so this does not necessarily lengthen the acquisition procedure. This does have other implications however.

First, we will be forced to dwell at least several hops in each search cell so that there is a significant chunk of consistent data with which to match to. For example, if we only send two hops per search cell, it will be quite impossible to identify when the correct cell was probed even if the sync tone was correctly detected in both hops; there will just be too many other places in the downlink data where the detected tone agrees with the transmitted sync tone by random chance. This is related to $P_{fd}$. If $P_{fd}$ is 1/8 ($M^* = 8$), then spending at least ten hops in a row may be sufficient. If $P_{fd}$ is only 1/2 ($M^* = 2$), we clearly must spend a much larger number of hops at each cell. It could be argued that it would be easier to match up the data if the intended sync tone were fixed instead of being changed randomly from hop to hop, and if consecutively searched cells used a different sync tone bin. While this is quite true, the possibility of MT jamming may make the random selection of the sync tone bin a necessity. In any event, it will be necessary to consider the correspondence problem in analysing the performance of the sync procedure.

## 11.0 A "Sync-Band" Approach

The possibility of large initial uncertainty in nominal carrier frequency was alluded to earlier in Section 3.0. In this section, an approach that deals effectively with this possibility is proposed.

Consider dedicating a portion of the user group resources for sync purposes. A frequency band of bandwidth B may be located at the edge of the FDMA user group as shown in Fig. 9 . This band is shared on a random access arrangement by any user wishing to synchronize. To keep the overhead acceptable, the sync band might be chosen to be, say, 10 % of the user group bandwidth. With 1000 user channels for data transmission, this would create 100 noname "sync" channels. The SAW receiver will produce energy detector ouputs for each of the $B/f_s$ tone bins in this band, just as it does for the channels in the active message portion of the user band. A best 1-of-M detection can be applied to these $S = B/Mf_s$ noname sync channels, and these S decisions can be supplied as data in a common sync information slot in the downlink.

A user attempting to synchronize starts by aiming for the center of the sync band, and transmitting a randomly selected tone in this middle channel. The user dwells here for a number of hops, then randomly selects a new channel to aim for (from the S/2 channels centred in the sync band), and transmits again. This is repeated over a number of random jumps within the sync band. We specify aiming for the middle S/2 channels so that when aligned with an error of no more than plus or minus B/4, all random jumps are sure to fall inside the sync band. Note that the user sync probe tone will have alignment errors with the bins detected by the SAW, so the procedure should be modified to transmit the probe signals at each of several alignments centered on the newly selected random position in the sync band. These will be separated by a $\Delta F$ chosen to ensure an acceptable amount of energy loss in the event of worst-case alignment $\delta F/2$.

The downlink return is monitored for tone detections that are consistent with the random relative motions the user has selected within the sync band.

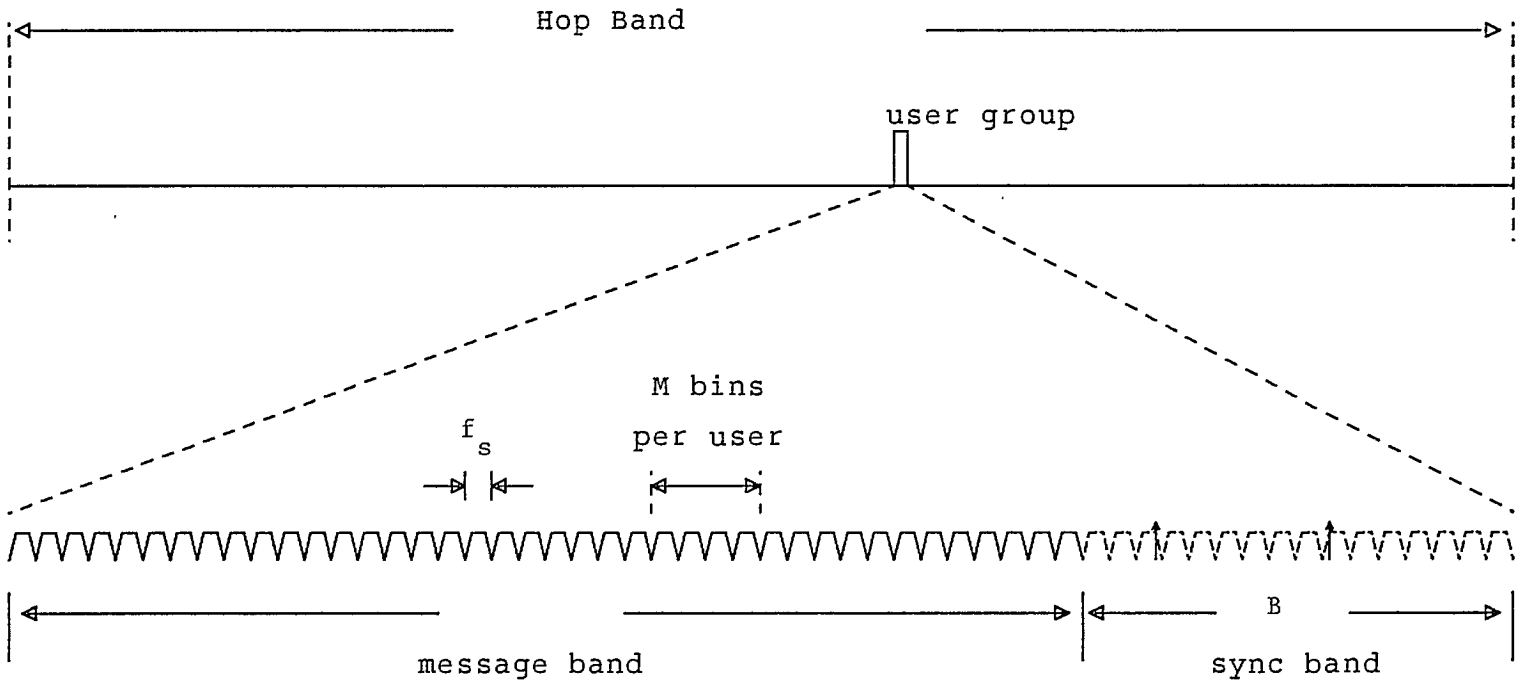


Figure 9: Sync - band approach

The user is not concerned that the satellite is dividing the sync band up into M-ary channels for its own detection purposes, and is not concerned about which particular tone bin he happens to land in. He is only concerned about hitting one of these bins with a reasonably good alignment. N o t e that the downlink return of the sync band channels will contain mostly random tone detections due to background noise and jamming, as well as some consistent detections due to other users who are attempting synchronization at that same moment. But each user will have his own unique randomly-selected jump pattern within the sync band, and so they will be clearly differentiable from one another, and from the random background detections. In addition, since synchronization will be a reasonably rare event, only a small fraction of the user population will be expected to be using the sync band at any one time.

If after a sufficient amount of observation time the user does not see the consistent detection pattern he is searching for, he steps his nominal carrier centre frequency by B/2 Hz, and repeats the procedure. This process is of course repeated over all possible hopping sequence phases to be searched. Once the consistent pattern is seen, the user immediately knows his carrier frequency error to an accuracy of plus or minus $f_s$, and adjusts his carrier relative offset to aim for his normal user uplink channel. In this way, large initial carrier frequency alignment errors can be quickly reduced using these large B/2 frequency steps. This contrasts to the situation without a sync band in which users can only use their own normal uplink channels with a frequency step size $\Delta F$ chosen to yield an acceptable loss due to alignment error when the best search cell is probed ( $\Delta F$ will be some fraction of the tone bin separation $f_s$).

The steps of sync-band approach are summarized as follows:

1) Aim for the center of the sync band and transmit a sync tone probe for a number of hops. Make small alignment adjustments (plus or minus $k\Delta F$, k a small integer) and repeat the transmissions at these alignments.

2) Aim for a new randomly selected location in the central 50 % of the sync band, and repeat 1). Repeat this step several times.

3) Monitor the downlink data returned for all channels in the sync band looking for relative motion of a detected tone that is consistent with the random motions selected in step 2). This is done with $(B/2)/f_s$ parallel hardware match detectors.

4) If no consistent pattern is seen, step the carrier frequency by half the size of the sync band, B/2, and go to 1).

5) If still no consistent pattern, step the hopping sequence phase by $\Delta T$ and go to 1).

6) Consistent pattern is seen; jump relative by your discovered frequency error to get to your normal uplink channel, and proceed to the verification phase.

Note that the procedure is amenable to pipelining as in Fig. 5. This sync band procedure clearly has the possiblity of greatly reducing search time in the face of large initial frequency offsets. The reduction factor will be at most $(B/2)/\ell f_s$ where $\ell$ is a factor that accounts for i) the extra observation time needed because of the random jumping within the sync band, and ii) the increased observation time needed to make the detection of a consistent pattern as compared to simply looking for a detection in one particular position (as is done when searching without a sync band).

Note that we can think of this reduction as being due to the ability to process many different possible frequency alignments simultaneously, a form of parallel processing. This is exactly what is being done in trying to match up the tone detections evident in the downlink sync-band data with the relative motions imposed on the sync probe. We will have to check all $(B/2)/f_s$ possible start positions simultaneously, searching for consistent relative motion of a detected tone. This is made possible by having access

to the detections to all $B/f_s$ bins provided in a common portion of the downlink frame. This does have implications for the downlink overhead created by adoption of this sync-band approach. This common slot must be repeated in each of the downlink beam zones (see Fig. 2). If each beam zone has only a fraction of the user population, this sync band data may represent a large overhead. One way to reduce the redundancy is to partition the sync-band into subbands, one for each user zone. Users in a particular zone use their own sync subband; the subband location and size can be specified in the common downlink slot. This can reduce the downlink overhead by a factor of $N_z$ , where $N_z$ is the number of downlink beam zones. This means, however, that the frequency adjustment steps must be reduced in size to match the reduced size of the subbands, and the sync time will be increased. This is simply a consequence of reduced parallelism.

Even if we are forced to make the size of the sync band (or subband) available to a user small to reduce the downlink overhead, we can still achieve useful reductions in the time-to-acquisition in the face of large initial carrier frequency errors.

Note that we cannot apply an analogous procedure in the hopes of reducing search time over the region of uncertainty in hopping sequence phases. That would require more than one frequency dehopper on the satellite.

## 12.0 Summary

Many of the issues involved with achieving coarse uplink synchronization have been addressed. Because of the nature of the satellite-based system and resulting uncertainties in received user signal levels, a traditional synchronization approach based on an energy detection threshold seems undesirable. A simple, robust, and transparent approach based on the use of a single sync tone per hop, and best 1-of-M tone detections at the satellite, has been proposed. The motivation for this approach and the effect of jamming have been discussed. The issues of diversity combining and the initial correspondence problem have been addressed. A sync-band approach

that promises to greatly reduce acquisition time in the face of large initial carrier frequency uncertainties has been presented.

It is proposed to concentrate almost exclusively on the best 1-of-$M^*$ detection strategy and to investigate the performance for different values of $M^*$. We propose to look at a matched-filter detector and avoid the complication that additional windowing would involve. In addition, the loss due to onboard majority-vote L-hop diversity combining will be investigated. A low-end approach based on fixed-dwell single serial search over the initial uncertainty region will be analysed for $T_{acq}$, the average time to acquisition. A high-end procedure will incorporate a variable-dwell search with a sync-band approach. Tradeoffs of search grid cell size vs. dwell time will be investigated. Results from [3] can be directly applied to determine the effects of different jammer types and signal-to-jammer ratios.

## References


[1] P.J. McLane, P.H. Wittke, and S.J. Simmons, "Final Report: A Study of Space Communications Spread Spectrum Systems: Part III Synchronization", D.S.S. Contract no. 36001-6-3530/0/ST, Feb. 1988.

[2] "Spread Spectrum Communications: Vol. III", M.K Simon, J.K. Omura, R.A. Scholtz, and B.K. Levitt, Computer Science Press, 1985.

[3] J.S. Bird and E.B. Felstead, "Antijam Performance of Fast Frequency Hopped M-ary NCFSK - An Overview", IEEE Journal on Selected Areas in Communications, vol. SAC-4, pp. 216- 233, March 1986.

[4] L.J. Mason, "A Method for the Precise Synchronization of a Frequency-Hopped Spread Spectrum System", Technical Memorandum DSAT #7/88, Nov. 1988.